SHEFFIELD HALLAM UNIVERSITY

Local Plastic Deformation in Pressure & Tensile Armour Layers of Flexible Risers

by

Shivaraj Alavandimath

The thesis is submitted in partial fulfilment of the requirements of Sheffield Hallam University for the degree of Doctor of Philosophy

January 2009

PAGE NUMBERING AS ORIGINAL

Any pages, tables, figures or photographs, missing from this digital copy, have been excluded at the request of the university.

Abstract

Flexible pipes are commonly used for connecting seabed flow-lines to floating production facilities. The general riser design consists of an internal carcass for collapse resistance, a polymer fluid barrier, carbon steel interlocked circumferential pressure armour layer for resisting internal pressure loads, helically wound carbon steel tensile armour layers to resist axial loads and a watertight external sheath. Much of the analytical work that has been carried out on flexible composite pipe is based on the early stress analyses of wire ropes, and this is primarily because of the helical geometry of many of the metallic elements such as pressure armour and tensile armour layers of a flexible riser. The general design philosophy of the layer is defined in API 17J (American Petroleum Institute) in terms of the stress "utilisation" factor that specifies the maximum allowable average hoop stress in the layer, which is conventionally produced by the elastic stress analysis.

The layers are subjected to severe cyclic bending and twisting deformation during manufacturing of the pipe which makes the material to exceed the yield point. Consequently, residual stresses are developed in the pipe material and variable amounts of non zero stresses exist in the metallic layers of the newly manufactured pipes. An attempt has been made to model the amount of residual stress evolved during manufacturing stage for two different metallic layers, namely; pressure armour and tensile armour layers and its effects on overall pipe's performance while in service.

The strategy is to apply the finite element (FE) method by creating a 3 dimensional wire model of the segment of pipe. Solid structural elements with plasticity were employed for the analyses. Kinematic hardening with Baushinger effect, contact and friction effects were also taken into account. Precise boundary conditions were applied to the model for elastic-plastic bending. The resulting residual stresses have been transferred to 3D axisymmetric model to investigate the internal and external pressure effects. This new procedure was carried out for both layers satisfying equilibrium and compatibility conditions for the pressure and tensile armours to find the common interface pressure and contact loading. FAT (Factory Acceptance Test) condition is simulated to investigate the level of residual stress variation. Experimental measurements of residual stress by X-Ray diffraction are in well agreement with FE results.

Contents

Notation

A_T = Tensile force acting on an arbitrary area

A_C = Tensile force acting on an arbitrary area

b = Width of the beam

E = Young's Modulus

$e = y/R$

F = Force

h = Height of the beam

I = Second moment of Inertia

L = Length of the beam

M = Bending Moment

M_E = Elastic Moment

M_p = Plastic Moment

NN = Neutral Axis

R = Radius of Curvature

W = Load

Y = Bending Stress

y = Distance from the neutral axis

v = Poisson's Ratio

σ = Stress

ϵ = Strain

δ_w = Deflection under the load W

Δ = Deflection

ΔE = Elastic Springback

ΔF = Final deflection

List of Figures

Declaration

This thesis is submitted in partial fulfilment of the requirements of Sheffield Hallam University for the degree of Doctor of Philosophy. It contains an account of research carried out between November 2004 to July 2008 in Materials Engineering and Research Institute, Sheffield Hallam University under the supervision of Dr Richard Crampton and Dr Mohammed Islam. Except where acknowledgement and reference is appropriately made, this work is, to the best of my knowledge, original and has been carried out independently. No part of this thesis has been, or is currently being submitted for any degree or diploma at this or any other University.

Shivaraj Alavandimath

November 2008

Acknowledgements

I would like to acknowledge the support and encouragement of my director of studies Dr Richard Crampton and Dr Mohammed Islam during the course of this research project. I also acknowledge the Materials Engineering and Research Institute and the Faculty of Arts Computing Engineering and Sciences at Sheffield Hallam University for the provision of laboratory and computing facilities.

I thank all the technical staff in the Materials Engineering and Research Institute for their help and assistance during the course of research work. Special thanks are extended to Professor Robert Akid, Dr Doug Cleaver, Dr Rosemary Booth and Rachael Ogden.

I would also like to thank Dr Upul Fernando, Professor John D Atkinson and Dr Terry Campbell for their Constructive criticisms and discussions. I am also indebted to Dr Terry Sheldrake and Richard Clements of Wellstream International Ltd for their technical data and test samples.

My special thanks goes to Ruminda Wimalasiri for his help in using X-Ray diffraction machine and Tim O' Hara, Roger Tingle, Brian Didsbury and Tony Earnshaw for their support in Mechanical testing workshop.

Thanks are also extended to my family and my dear friends Shivaprakash and Narasimha Raj for their unfailing support and encouragement. Special thanks are extended to my friends Anna Lasilla, Chandra Sekhar, Dawn Hughes, Gavin Tolan, Graham Lister, Janardhan Saithala, Jayne Wellings, Mark Jones, Pradeep Hegde, Russell Bailey, Thomas Scott, Tom Phol and Willie Brink. All have unknowingly inspired me to complete this thesis.

Dedicated to

My beloved Parents

Jagadeeshaiah Alavandimath

Annapoorna Alavandimath

Chapter 1

The Flexible Risers

1.1 Introduction

Unbonded flexible pipes are commonly used for connecting seabed flow lines to floating production facilities and have been in use for more than 20 years. Flexible risers are critical components because they provide the means of transporting the condensate from seabed to the FPSO (Floating Production, Storage and Offloading Vessel) and also the processed fluids from the structure. These are extensively used in the petroleum industry for a variety of applications, including static applications, such as pipelines or dynamic applications such as marine risers. They have served to tie satellite wells to central manifolds and to bring oil & gas to the surface. The general riser design consists of an internal carcass for collapse resistance, a polymer fluid barrier, carbon steel interlocked circumferential pressure armour layer for resisting internal pressure loads, helically wound carbon steel tensile armour layers to resist axial loads and a watertight external sheath as shown in Figures 1.1 to 1.3.

The advantages offered by the use of flexible pipe have resulted in it becoming an essential component in most offshore applications. Although it can be integrated successfully within an overall design by satisfying design limitations specified by

the manufacturers, there is comparatively little understanding within the engineering community of its detailed performance under loading. The riser consists of several metallic and non-metallic layers and two metallic viz., pressure armour and tensile armour layers which are responsible for overall performance and strength. These are subjected to severe plastic deformation during manufacturing of the pipe and factory acceptance test (FAT).

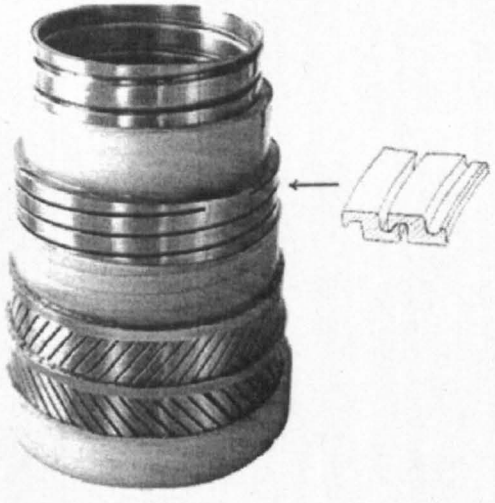

FIGURE 1.1: Typical riser showing pressure armour layer

Consequently, residual stresses are developed at various locations in the wires and variable amounts of non-zero stresses exist in the metallic layers of the newly manufactured pipes. A little work has been done to understand the magnitude of residual stress in pressure and tensile armour wires and the effect of interaction of the two layers on their local stress distribution. An accurate knowledge of local stress distribution in two layers under service conditions is imperative for the safe design and integrity assessment of the flexible pipes. Recent literature survey revealed that there is no validated method available to calculate local stresses in pressure and tensile armours by considering the residual stresses and the layer interactions. The present research work addresses this issue by developing an integrated stress analysis procedure for both pressure and tensile armour layers considering the layer interactions and residual stresses introduced by pipe manufacturing.

FIGURE 1.2: Metal & Non-metallic layers of a riser

The structural analysis of flexible pipes demands customized mathematical models, expert's interaction to interpret and optimize results, mechanical tests to adjust and validate the mathematical model and an extended data base of materials and geometries to gather information about different manufacturers and products. The substantial amount of money involved in a flexible line project and installation, the safety requirements of the design and the need of consolidating and sharing the technology through different sectors of the company, demands the integration of different knowledge sources of the domain into a system that must meet portability and efficiency.

Developments in the design of risers have made the exploitation of oil resources in deep waters with hostile environments economically viable. In deep water applications, because of the low bending stiffness when compared to axial and torsional stiffness, a flexible pipe can suffer large displacements and deformations which demand special nonlinear static and dynamic analysis. The composite internal structure of the pipe is custom built to meet design requirements. The manufacturing process, the material and the geometric shape of pipes may vary widely. Different layers of the pipe are designed to meet particular requirement. Four of them are summarized as follows:

- An inner collapse-proof steel carcass to resist external pressure and axial load confinement effect;
- A leak-proof polymer or a composite cord-reinforced rubber layer;
- Tension amour layers of steel wires applied contra helically to resist axial loads and internal pressure;
- An external impermeable plastic sheath that keeps armours together and protects them against external corrosion, abrasion or damage.

It is clearly evident that analysis of the strength and long term durability of complex risers requires some quantitative knowledge of the stresses and strains in the component parts of the cross-section and also of the ways in which these components interact. The work involves 3D FE analysis of pressure and tensile armours of the flexible pipe to simulate residual stress formation during pipe manufacturing. These are considered with service load conditions where it is subjected to internal and external fluid pressure to model local stress-strain behaviour of the material. The varying degree in sophistication level of the numerical model permits different problems to be effectively and efficiently analysed. This is the core section where the bulk of the current research is being devoted. More information on flexible risers and offshore installation is given in Appendix D.

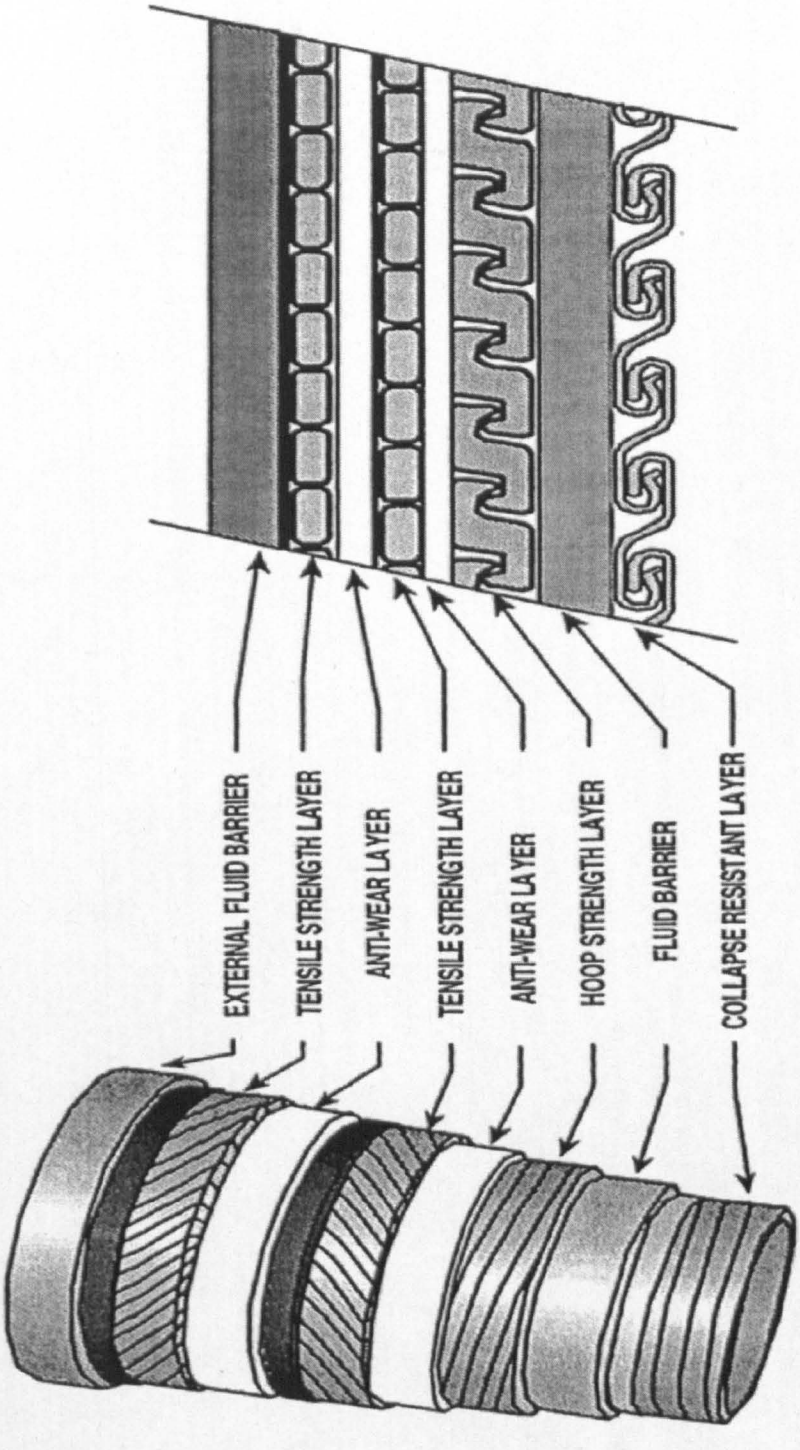

FIGURE 1.3: Different layers of a flexible pipe

Chapter 2

Literature Review

2.1 Flexible Risers

A floating production system is an attractive concept for production of oil and natural gas from deep water fields. The system will, in general, require flexible risers for production lines from wellheads and for export lines. The risers consist of several layers of metallic and non metallic materials, which constitute a leak-proof continuous umbilical between wellhead and floating production system. Stress analysis of flexible pipe has fascinated many researchers and engineers around globe for more than two decades. Helically wound wires constitute a wide class of important engineering components. The major advantages of such elements are their capacity to support axial loads with comparatively small bending or torsional stiffness [1]. Analytical methods have been attempted to model the stresses and strains in the layers of pipes and moderate success has been achieved [2]. The structural behaviour of flexible pipes is governed by the response of helical components to bending [3]. Love [4] developed a set of non linear equations to describe the equilibrium of helical rod under a general force and moment conditions. Costello [5] applied Love's equations to predict the bending stiffness of a single helical spring when subjected to large deflections. LeClare and Costello [6]

estimated the resultant moments and forces of a bent cable by substituting geometrical variables describing the bent helical configurations into Love's equations. Blanco & Costello [7] used Love's formulae to evaluate the contact stresses in twisted wire cable. The cable was divided into a set of individual helical rods and the corresponding equilibrium conditions were satisfied together with the continuity conditions of displacement and contact forces at the interfaces. In the analysis, the friction between wires was ignored and the rods were taken as inextensible in accordance with the assumption in Love's theory. Oliveira et al. [8] presented a set of linear equations for evaluating axial and torsional stiffness. They assumed that the helical armour strips experience only pure axial deformation. Goto et al. [9] followed a similar approach to predict mechanical strength of flexible pipes. In the paper presented by McNamara & Harte [10] these formulae were significantly improved by taking the constriction factor as an independent variable rather than an empirical co-efficient.

Feret & Bournazel [11] investigated the internal structural behaviour of flexible pipes. They stated that each component of pipe is taken as an individual element which satisfies equilibrium conditions as well as continuity conditions. Also, they mentioned that a reduction in bending stiffness of an unbonded flexible pipe occurs after slipping takes place. Unfortunately some important aspects still remain uncertain. Feret and Bournazel assume that the armour strips follow a geodesic path once slip takes place. No evidence is provided for this assumption.

Mathematical equations derived from Love's formulae are difficult to solve analytically. An alternate approach was suggested by Lutchansky [12] which directly calculates the deformation state of helical elements according to different geometrical configurations before and after flexure. A bent helical element is expected to exhibit a non uniform deformation state. Spillers et al. [13] followed a similar approach to investigate the mechanical behaviour of a helical tape on a bent cylinder. A bent helical element is expected to exhibit a non-uniform deformation state. In Lutchansky paper the axial strain state of the armour strips in a bent cable was investigated with and without the presence of internal friction which prevents slip caused by non uniform axial deformations. Twisting slip may occur

between individual helical wires. This mechanism was investigated by Vinogradov & Atatekin [14] when they considered the behaviour of a cantilever cable bent by transverse force. By considering the equilibrium of helical wires subject to friction in the twisting direction Vinogradov & Atatekin derived analytical expressions for the resultant slip propagation with respect to acting load. As a result of energy dissipation caused by overcoming internal friction Vinogradov & Atatekin demonstrated that the cable's bending stiffness was hysteric. Cardou & Jolicoeur [15] have considered only axial wire forces in the strand and the investigation is restricted to elastic behaviour under small deformations. Raoof & Kraincanic [16] developed a theoretical model to predict contact deformations in compliant layers on overall characteristics such as axial and torsional stiffness. In their paper, non-Hertzian contact formulations are used to obtain the interlayer compliances. Ramsay [17] reported that the friction is an inevitable phenomenon in multilayered cables and similar structures.

McIver [18] developed a method to predict the behaviour of bending under the sensitive values of coefficient of friction. Detailed material and contact stresses are provided in addition to slippage between layers. However, stresses developed during manufacturing were not considered. The McIver paper suggests that stresses built during manufacturing should be considered in any flexible pipe design. A 3D Finite element analysis by Fernando [19] et al., compared axisymmetric and 3D models subjected to pressure, which shows that conventional elastic 2D analysis could underestimate the local stresses, also FAT (Factory Acceptance Test) pressurization relaxes a significant amount of residual stresses. Cyclic bending deformation was considered in this analysis. Residual stresses measured by x-ray diffraction methods yielded considerably lower values of residual stresses compared to numerically derived stresses. [20] Jiang & Walton [21, 22] developed a concise finite element model to analyze complex nonlinear effects such as plastic deformation, trellis point of contact and non-uniform stress distribution. Huh & Kim's [23, 24] paper is concerned with evaluation of stress components in elasto-plastic bending for each increment step in the finite element analysis. It is noted that

conventional integration schemes cause inaccurate evaluation and oscillatory behaviour of stress components while a reduced integration scheme with hourglass control yields accurate evaluation. Residual stresses developed during manufacturing (deforming), was not considered in literature either by analytical methods or numerically.

Flexing deformations due to fluid pressures and other service loads, cause movement of layers resulting in fatigue fretting, commonly leading to the degradation in the fatigue properties of a material. The reduction in the fatigue strength of material due to fretting can be influenced in a complex manner by factors such as contact pressure, elastic and plastic properties of mating surfaces, the roughness of surfaces, amplitude of sliding displacement, environment, residual stresses etc. Fretting acts as a catalyst in the fatigue process leading to early crack initiation, imparting more damage to material than fatigue alone [25]. The normal fatigue crack initiation may occur at 90% of life but in fretting fatigue, crack initiation may start at 5% of fatigue life. Previous experimental work has established a sound understanding of the fretting phenomenon as Mindlin analysis [25] shows in sphere and plate contact case, as the tangential force is increased, the size of locked region decreases and total slip occurs giving way to fretting crack initiation. The tangential force depends on the amplitude of movement. Possibility of crack initiation diminishes as the total slip occurs, resulting in wear. Further continuation of slip facilitates the glide and constantly removes the material from contact region which eliminates further crack growth.

Failure or damage to flexible pipe can occur in many ways; largely they can be classified as accidental damage and system failure. Damages caused to the flexible pipe by an accidental source, external to the pipe system is termed as accidental damage. Examples of such damage include installation damage, dropped object damage or trawl-board damage [26, 27]. For the vast majority of these incidents, the pipe was repaired and continued in service. In some cases, particularly for the risers, the damage occurred during installation and the damaged riser was replaced with a new one. An incident that occurs while the pipe is in service that results in failure of the flexible pipe system is termed as system failure. If the failure occurs

for the pipe itself, this means that the pipe has failed to contain its fluids, that is, it leaks [28, 29]. This can be either catastrophic, or it can be small leak depending on the failure mode.

FIGURE 2.1: Damage during Installation Vs Operation [26]

If an ancillary device fails, this is also included as a system failure and is categorized as ancillary device failure in the upcoming statistical analysis. Figure 2.1 shows that under the accidental damage category, 76% of these have occurred during installation.

An analysis of accidental damage by damage modes is given Figure 2.2. External sheath damage is by far the most damage mode at 61% and vast majority of this occurs [26] during installation. Figure 2.3 splits the failure into various failure mode categories. Internal sheath aging is the most common failure mode (31%) and that is all degradation of PA11 sheath. Next is PVDF sheath pull-out from its end fitting at 25% followed by ancillary device failure at 12%.

2.2 Residual Stresses

The lifetime of a structural component is dependent on the interaction between the defects within the components and the stress, which it is subjected to during

FIGURE 2.3: System Failure mechanisms [26]

their service life. The stresses could be a combination of those that are encountered in service and those that develop during manufacturing processes. The latter referred to as residual stress. The stresses that are introduced during manufacturing or processing either may be beneficial or may be detrimental as encountered in fatigue analysis of materials. The applied stresses are more predictable in nature and can be incorporated in the design stage itself. With certainty the same

cannot be said about residual stresses. In the current study, there are two stages where residual stresses have crept into wire material: first, at the manufacturing stage, due to rolling of the wire, where compressive residual stresses have risen, secondly during winding on bobbins in both lateral directions [19]. Consequently, the magnitude and direction of total residual stress becomes unclear. Bending on bobbins accumulates more compressive stresses at inner radius and relieves the existing compressive stresses on outer radius. However the wire is bent on rollers cyclically six to seven times before it is wound onto the pipe, developing unknown magnitude of residual stress in the material.

Although stresses in rolling (manufacturing stage) can be eliminated by heat treatment, they cannot be ignored, as the resultant magnitude and direction of residual stress at any section may create a best site for fretting fatigue crack initiation. This accounts to be 30–180 MPa all around the section [20]. In fact, some cases in the rail industry have reported that residual stresses alone were the cause of crack initiation and propagation [27 - 29]. The scale over which they are significant may classify residual stresses, and hence the type of measurement technique used to study them. Macroscopic residual stresses exist over large distances whilst microscopic residual stresses operate over the grain scale or the atomic scale of the material. Residual stresses are sometimes classified according to their origin (e.g., thermal or elastic mismatch). Residual stresses originate from a variety of sources. Macroscopic stresses can arise from heat treatment, machining, secondary processing and assembly. Micro-structural stresses often result from the CTE (Coefficient of Thermal Expansion) mismatch between phases and constituents or from phase transformations. Both types may be present at any one time in a material or component. The importance of residual stresses depends on the particular material, component and application. No single answer can be given. Residual stresses can be beneficial or detrimental to performance; they may be critical or insignificant. Each case must be examined on its own merits. It is unlikely that any component will be entirely free from residual stresses induced during manufacturing and processing. Residual stresses may be present in engineered components, thin films and coatings, composites and multiphase materials. Depending on the manufacturing

process, the type of material and the component criticality, the levels of residual stress may or may not be significant.

In manufactured materials, the processing implicit in fabrication more often than not introduces residual stresses. Inhomogeneous heating and cooling phase transformations during heat treatment, and localized plasticity during machining are all processes that can introduce residual stresses. In extreme cases, these processes can substantially alter the strength available for an application. Thus durability, fatigue, fracture toughness, and strength are all affected. Consequently, the ability to measure (and predict) the presence of residual stress is a critical technology for material processing, stress relief, heat treatment, lifetime prediction, and alloy design. Because a residual stress is locked inside an object, it may only become apparent long after fabrication, perhaps when a failure occurs at a significantly lower stress than anticipated resulting from a design that did not account for it. In metallic objects where residual stresses may be a fraction of a millimetre or many centimetres from a free surface, a measuring tool that probes the interior is needed. Because they have no electric charge, neutrons penetrate many centimetres into most materials (with less attenuation than X-rays), making them ideal for examining, in a non-destructive manner, the interior of polycrystalline materials.

Components may fail during the service in many different ways [30]. The important aspects are, onset of plastic deformation or exceeding of allowable plastic deformation, crack initiation or exceeding of allowable crack length, unstable crack propagation that results in fracture of component, instability such as buckling, which result in elastic or plastic collapse and hence catastrophic failure.

In practice, failure of a component is almost always determined by the interaction of several external parameters, such as unexpected high static and or cyclic loads, friction, thermal energy, oxidation corrosion and so on [31]. On the other hand, the component itself may contribute to premature failure, if there is confusion of the component material, wrong heat treatment, and surface decarburization.

The residual stress state in a component may be one of the most important parameters influencing it service behaviour, particularly regarding high-strength materials states. Residual stresses may reduce yield or elastic collapse loads and may promote corrosion cracking. With respect to fatigue, the residual stresses may alter the cyclic deformation behaviour, promote or retard crack initiation, accelerate or decelerate crack propagation, and may be beneficial or detrimental to finite fatigue life and endurance limit. It is important to realize that in a component, locally very high amount of residual stresses may exist. For example, in a spring steel up to 200 MPa compressive residual stresses may be produced by a combined warm and stress peening process [32].

In practice, no component is free of micro residual stresses. Almost all components have macro residual stresses to a certain extent. Only a small number of components exist where macro residual stresses are negligible, for example, after a suitable stress relaxation heat treatment. The most important ones are various manufacturing processes. The fundamental mechanisms of residual stress formation are inhomogeneous plastic deformation caused by the mechanical, thermo mechanical or thermal attack and development of constrain between different constituents of a components such as phases during the formation of the constituents, for example, during the casting process and the cooling from high process temperature.

Manufacturing processes not only result in the formation of definite macro residual stress states but may also effect other changes of the components close to the surface: Formation of specific topography, work-hardening (in very hard materials) or work-softening processes and hence alteration of the micro residual stress state, phase transformation, crack initiation.

All these processes may change the fatigue behaviour of the given component. It is hardly possible to completely separate these influences, even though this is very important for the understanding of the existing relationships.

It is shown that the micro residual stress state is more stable against the mechanically and thermally induced relaxation than the macro residual stress state. On

FIGURE 2.4: Coupling of temperature, stress and microstructure [33]

the other hand, it is also proved that during the fatigue the micro residual stress state of given steel may be changed by the cyclic hardening or cyclic softening processes, which are closely related to the cyclic plastic deformation. Hence during fatigue loading of the component with locally varying macro as well as micro residual stress states, complex interactions of the macro residual stress state with cyclic loading stress and the micro residual stress state with the work-hardening and/or work-softening process occur. In both cases, the amount of the cyclic plastic deformation is the most important parameter. Since during the fatigue loadings that result in technically relevant lifetimes or infinite life, the cyclic plastic deformations decreases with increasing the hardness, it is generally expected that the influence of macro residual stress is lower in low-strength steel than in high-strength steel.

Residual stresses are results of interactions [33] among the time, temperature, deformation and lastly microstructure as briefly illustrated in Figure 2.4. Material or material related characteristics that influence the development of residual stress include thermal conductivity, heat capacity, thermal expansion, elastic modulus and Poisson's ratio, plasticity, thermodynamics and kinetics of transformations,

mechanisms of transformations and transformation plasticity. The manufacturing process of the risers introduces residual stresses in the wire material which can affect its performance during service when deployed for transporting hydrocarbons. The permanent deformation and material characteristics can change due to time, temperature, the rolling diameter, elastic modulus and poisons ratio.

FIGURE 2.5: Transformation products of austenite [33]

The familiar mechanisms of plastic deformation are slip, mechanical twinning and creep. Phase transformation also can cause permanent deformation. In steels, the austenite can break up into large variety of microstructure that is distinguished by atomic mechanism as shown in Figure 2.5 of transformation. In a displacive transformation, the change in crystal structure is achieved by deformation of the parent structure. A reconstructive transformation is one in which the change in structure is achieved by a flow of matter, which occurs in such a way that strain is minimised.

FIGURE 2.6: Shape Changes accompanying unconstrained transformations [33]

All the transformations cause changes in shape (Figure 2.6) which for reconstructive transformations simply reflects the change of density. For displacive transformations, the shape change is an Invariant Plane Strain (IPS), i.e., a combination of shear on the invariant plane and a dilatation normal to that plane. The strain energy associated with constrained IPS is minimized when the product phase has thin plate shape. This is the reason why some steel grow in the form of plates. The permanent strain caused by any transformations is called transformation plasticity. A phase change in a stress free material is usually triggered by the heat treatment when the parent phase passes through an equilibrium transformation temperature.

Alternatively, the application of stress in isothermal conditions can trigger transformation in circumstances where it would not otherwise occur. Unusual effects can occur when stress and temperature work together. The transformation may occur at remarkably low stresses and at small deviations from equilibrium temperature. This is the main reason why a minute stress can cause development of microstructure and the same is true when it is vice versa. Also, transformation plasticity can be obtained at stresses much lesser or smaller than yield stress of parent phase. Residual stresses are introduced unintentionally during fabrication

process such as welding, machining, rolling, bending, torsion etc. And some illustrations have shown how these phase transformations can interact with the build up of the residual stresses. But there is little doubt that transformations play a major role in the development of the residual stress. For constructive transformations, it is the difference in density between parent and product phases that contribute to the transformation plasticity. The plasticity can be much greater for displacive transformations because of the large shear component of the shape deformation when these transformation products form. These are quite sophisticated effects which with few exceptions are not taken into account in most of the residual stress analysis.

All manufacturing processes introduce residual stresses into the mechanical parts which influence the fatigue behaviour, fracture strength, and even its corrosion resistance [34]. Currently there are very few metal working processes in the industry, which do not produce these residual stresses in the mechanical parts. The role of residual stresses is therefore of utmost importance while designing the mechanical component. Over the last few years much research has been carried out to understand the effect of these residual stresses on the mechanical performance of the part. The definition and origins of the residual stresses according to the production methods are mentioned in this section. This section also gives us outlook about the different types of techniques used to measure the residual stresses and overall necessity to combine the destructive (incremental hole-drilling method) and non destructive methods such as X-ray and neutron diffraction method in order to precisely evaluate and asses the distribution of residual stresses.

A residual stress by definition is a stress that remains in mechanical part even though it is not subjected to outside stresses or loads. Residual stress exists in practically all rigid parts, whether it is metallic or wood or polymer. It is the result of the metallurgical and mechanical history of each point and the part as whole during its manufacture.

There is an increasing interest to understand how the state of the residual stresses that govern the mechanical properties of material and its structure. The failure of

FIGURE 2.7: Different areas where residual stresses are considered [34]

a structure or mechanical component is not only due to the external loads but also due to residual stress. It is an important factor in this regard. The introduction of advanced materials has contributed to the development of knowledge in the field of residual stresses. In fact many new materials are composites of different materials for example metal-matrix composites, Chemical vapour deposition coatings which contain residual stresses. Figure 2.7 shows the different fields of research in which residual stresses are taken into account and its relevance in the industrial applications. Three main fields must be developed for a global approach of pre-stress engineering.

1. Measurement techniques for the quality control and processing analysis
2. Processing parameter optimization and processing modelling
3. Modern design tool for the life cycle simulation with residual stress consideration.

2.2.1 Origins of residual stresses

In general microscopic residual stresses can be induced due to:

- Nonhomogeneous plastic flow under the action of external treatment (shot peening, roller burnishing, hammer peening, shock laser treatment).
- Nonhomogeneous plastic deformation during non uniform heating or cooling (ordinary quenching, moulding).
- Structural deformation from metalworking.
- Heterogeneity of chemical or crystallographic order (nitriding or case hardening)
- Various surface treatments (coating, plating)
- Differences in expansion coefficients and mechanical incompatibility of the different components of composites (composites with metal and organic matrix)

Table 2.1 shows the different origins of residual stresses of metal working operations usually carried out in the industry. To manufacture a mechanical part one or more methods listed in the table are used [35]. To calculate the residual stresses existing in a part, the source of the stress must be identified first.

2.2.2 Modelling the process

The experimental techniques developed previously can contribute to the development of a residual stress prediction model. The results calculated by the model make it easier to take the residual stress into account during mechanical design of component. There are two kinds of models to be named; analytical model and numerical model. Analytical models were developed for shot peening and cold rolling while several finite element codes were used or developed for the welding, grinding,

PROCESS	*MECHANICAL*	*THERMAL*	*STRUCTURAL*
Casting	No	Temperature Gradient during cooling	Phase transformation
Grinding, Turning, Milling, Drilling, Boring	Plastic deformation due to the chip removal	Temperature gradient during machining	Phase transformation during machining
Welding	Shrinkage	Temperature Gradient	Change in Microstructure
PVD, CVD	Mechanical incompatibility	Mechanical incompatibility	Change in phase
Composites	Mechanical incompatibility	Mechanical incompatibility	No
Brazing	Mechanical incompatibility	Thermal incompatibility	New phase at interface
Electroplating	Mechanical incompatibility	Mechanical incompatibility	Composition of plating depending on the bath used
Quenching without a phase transformation	No	Temperature Gradient	No
Surface Quenching with phase change (Induction, EB, Laser, plasma, classical methods)	No	Temperature Gradient	Change of volume due to phase change
Bending, rolling, chasing, forging, extrusion, extrusion	Heterogeneous plastic deformation between the core and surface part	NO	Depends on material

TABLE 2.1: Origins of residual stresses resulting during different manufacturing process [35]

heat treatment (quenching), and thermal cutting. The results have shown good correlation between the predicted model and experimental results. But it can also be seen that three dimensional calculations are necessary to obtain good results in all the directions. If a two dimensional calculations are used, the residual stress evaluation correlates well in one direction only. So, in future, three-dimensional calculations will be of greater significance of real case modelling.

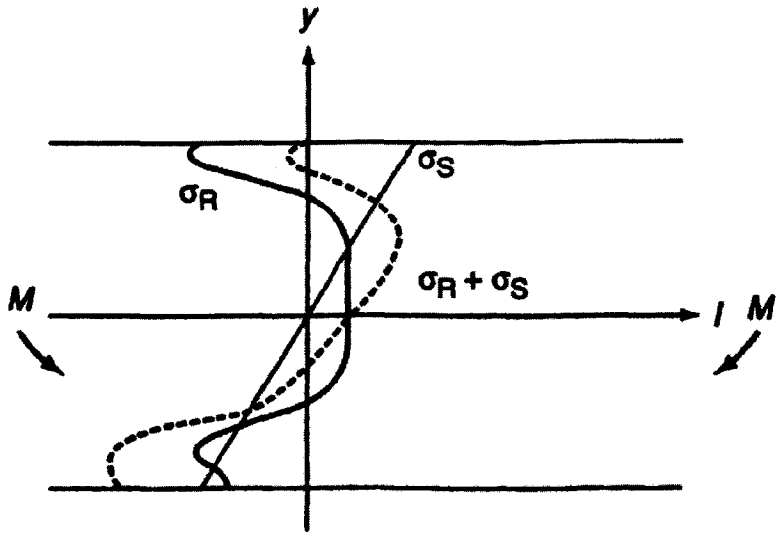

FIGURE 2.8: Superposing residual stresses on service loads

When a mechanical part is subjected to a field of elastic residual stresses characterized by a tensor σ_R, on which is supposed s field of service stresses defined by the tensor σ_S, the real stress to which the part is subjected is characterized by the tensor $\sigma_R + \sigma_S$ (Figure 2.8). If the residual stresses are added to the service stresses (residual tensile stress, for example), the part is overloaded due to the residual stress. If, on the contrary, an appropriate finishing operation (shot peening or roller burning) is used to introduce residual compressive stresses, the part is relieved of some of the load locally and the mechanical performance of the material is increased as a result. Figure 2.9 shows the properties of materials that are influenced by the residual stresses.

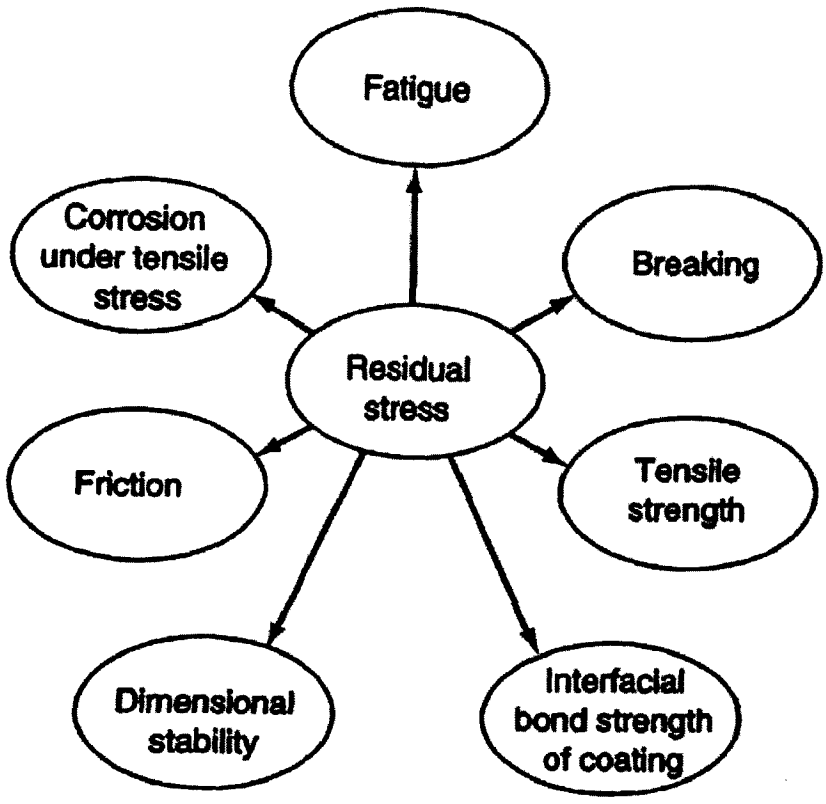

FIGURE 2.9: Effect of Residual stresses on performance of materials

2.2.3 Comparison between loading and residual stresses

Since the alteration of the micro residual stress caused by the manufacturing process changes the local hardness within a component and hence the local strength, it is convenient to compromise the corresponding influence on the fatigue behaviour of the component as a change of the local fatigue resistance of the steel used for the component [36].

On the other hand, stable macro residual stresses are the static stresses and may be regarded as locally varying mean stresses. However, it is important to realise that there are definite difference between loading mean stress and residual stresses.

Loading mean stresses exist as a consequence of acting external forces, moments, pressure and internal pressure and eventually temperature gradients. Residual

stresses exist as a consequence of inhomogeneous plastic deformation and/or as consequence of constraints between different constituents of component.

Distribution and sign of loading mean stresses depend on the external loading, the geometry of the component, the elastic-plastic deformation behaviour of the material (if maximum loading stresses exceed the yield strength of material or cyclic yield strength), and on thermo-physical materials properties (if temperature gradients exist).

Distribution and sign of residual stresses depend on the amount and extension of inhomogeneous plastic deformation in relation to the whole component volume, the interaction of mechanically and/or thermally driven deformation during manufacturing process, the strength of the material state, and the volume fraction, the elastic as well the thermo physical properties of the constituents of the components that impose contrarians of the each other.

- Loading mean stresses are in equilibrium with external forces and moment. Residual stresses are in equilibrium with themselves regarding balance of the forces and moments with relation to any sectional area and axis respectively. The latter is also true of the thermally induced loading stresses
- Loading mean stresses may be changed and finally disappear, if external loading and/or if existing temperature gradients are changed and finally removed. Residual stresses may be changed and eventually disappear by the thermally and/or mechanically induced relaxation.
- Loading mean stresses are influenced by the cyclic plastic deformation in stress-controlled loading, unless stress gradient become very high, for example in the root of the sharp notches, where mean stress redistribution may occur. Residual stresses always relax, if the cyclic loading exceeds certain threshold values.

2.3 Fatigue and Residual Stresses

Designers and materials engineers are today called upon to solve engineering problems of ever-increasing complexity. Yet there are weaknesses in our present-day communication systems which will have to be modified if we are to make substantial progress to keep our industries at the forefront of knowledge. For any country, it is an essential prerequisite to remain a leading export of manufactured goods, the basis on which the whole social system and relatively high standard of living depends [30].

Metal fatigue has been the subject of numerous research studies conducted by mechanical engineers, materials scientists, physicists, chemists, mathematicians, and structural engineers over more than 150 years. Although, valuable contributions to knowledge have been provided by all of these disciplines, an interdisciplinary understanding has been difficult to achieve because of two factors, namely, a limited appreciation of the boundary conditions of an individual approach when applied by a different discipline, and the disparate nature of the requirement of each separate discipline.

An engineer is mainly concerned with the effect on lifetime of external loading parameters (e.g., torque, bending moments, pressure) and the derivation of equivalent stresses and strains, safety factors, stress concentration factors, etc. that are used to provide a reliable design. This is usually attempted via a mono-loading fatigue endurance S-N curve (S denotes the stress and N denotes the number of cycles to failure).

In recent years significant advances have been made by mathematicians who determined the elastic and elastic-plastic stress field surrounding the tip of two and three dimensional singularities (cracks). They have also produced finite element programs to provide local and global stress-strain fields solutions pertaining to the complete three-dimensional geometries of engineering components and structures which could be subjected to complex three-dimensional loading systems.

Over the past few years significant advances have been made, particularly in the fields of cumulative damage, fatigue at notches, in phase and out of phase multi axial loading conditions, and mixed mode crack growth. This may well be welcome news, but the advances to be made will require materials scientists working on metal fatigue research to become involved in the mathematics of plasticity fracture mechanics and micro structural fracture mechanics. Conversely, it will be necessary for the design engineer to relate the external loading systems applied to a component to the critical crack growth planes which lead to failure. In short an interdisciplinary approach is now more desirable than ever.

Many factors controlling the fatigue resistance of a metal have been summarised. Fatigue resistances are proportional to crack propagation since the initiation phase is considered to be negligible in polycrystalline metals. The major factor in the resistance of a material to rack propagation is the effect of micro structural texture in regarding the development of a dominant crack which propagates to failure [37, 38].

Fatigue damage increases with applied load cycles in a cumulative manner. Cumulative fatigue damage analyses play a key role in life prediction of components and structure subjected to field load histories. Since the introduction of damage accumulation concept by Palmgren about 80 years ago and 'linear damage rule' by Miner about 60 years ago, the treatment of cumulative fatigue damage has received increasingly more attention. As a result many damage models have been developed. Even though early theories on cumulative fatigue damage have been reviewed by several researchers, no comprehensive report has appeared recently to review the considerable efforts made since the late 1970s.

Fatigue damage increases with the applied cycles in a cumulative manner which may lead to fracture; it is an old but not yet resolved problem. More than 80 years ago Palmgren [39] suggested the concept which is now known as the linear rule. In 1945 Miner [37] first expressed this concept in a mathematical form as $D = \sum \left(\frac{n_i}{N_{fi}}\right)$ where D denotes the damage, n_i and N_{fi} are applied cycles and total cycles to failure under the ith constant amplitude loading level respectively

since then, treatment of cumulative fatigue damage has received increasingly more attention. As a result, many related research papers are published every year and many different fatigue damage models have been developed.

2.3.1 Influence of Residual Stresses on the Cyclic Deformation Behaviour

The influence of macro and micro residual stresses on the cyclic deformation behaviour is studied very well after mechanical surface treatments, for example, by shot peening or deep rolling.

Characteristic cyclic deformation curves for stress-controlled push-pull loading of different heat treated smooth specimens of the steel AISI 4140 are compared in Figure 2.10 in un-peened and in shot peened conditions with compressive residual stresses at the surface [28]. In the normalized state (Figure 2.10(a)), the onset of cyclic deformation is different in both conditions, since the shot peened specimens with surface compressive residual stresses $\sigma^{r} = -400$ MPa show cyclic softening from the first cycle and higher plastic strain amplitudes during the first cycles for stress amplitudes σ_a between 250 and 350 MPa. After a certain number of cycles, the opposite tendency can be detected and the plastic strain amplitudes of the shot peened conditions are smaller than those of the un-peened material states. However, for the same σ_a values the plastic strain amplitudes of both conditions approach another at relatively high number of cycles. Corresponding results for quenched-and-tempered (730°C/2h) AISI 4140 steel are presented in Figure 2.10(b). In the unpeened condition, the characteristic cyclic deformation behaviour of quenched-and-tempered steels occurs with a quasi-elastic incubation period, which is followed by cyclic softening until crack initiation. After shot peening that generates surface compressive residual stresses $\sigma^{rs} = -410$ MPa, the onset of cyclic softening is shifted to smaller number of cycles. Furthermore, it is interesting to note that for identical stress amplitudes and comparable numbers of cycles, the higher plastic strain amplitudes are always measures for the shot peened specimens. Figure 2.10(c) shows a compilation of cyclic deformation curves

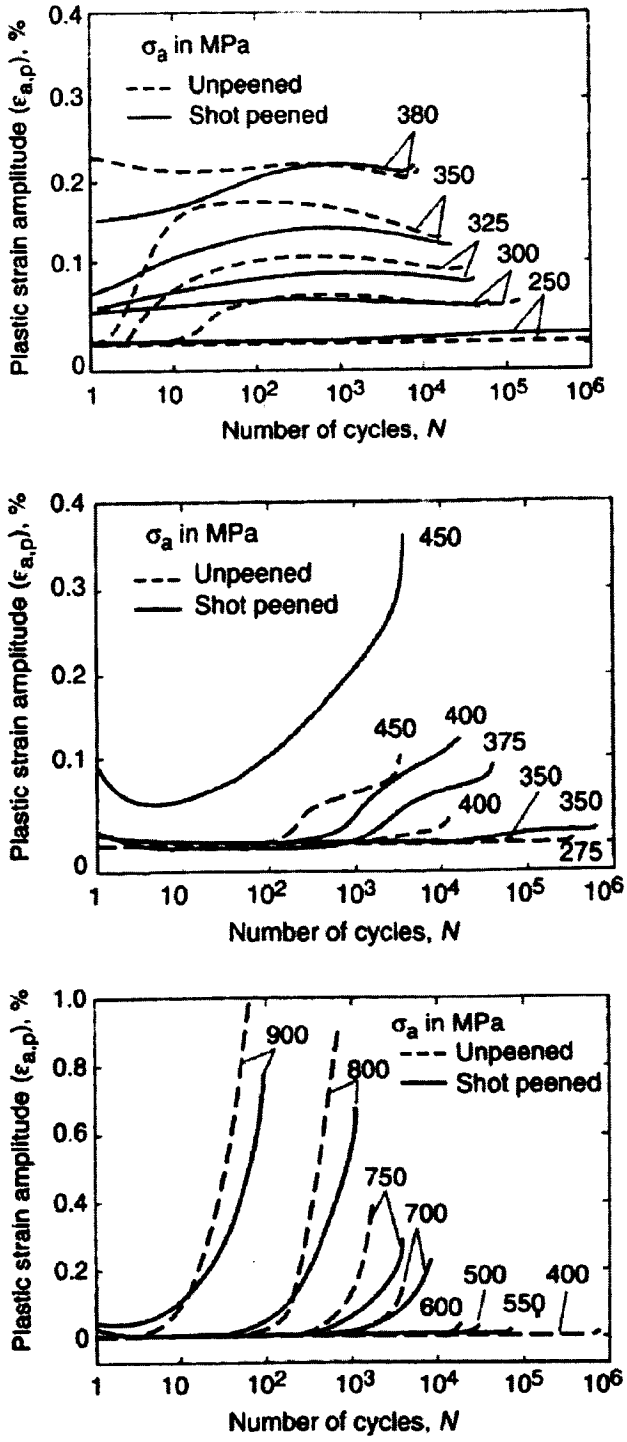

FIGURE 2.10: Cyclic deformation for stress controlled push-pull loading of smooth specimens of the steel AISI 4140 in un-peened and shot-peened conditions – (a) normalized, (b) quenched-and-tempered (700°C/2h), (c) quenched-and-tempered (570°C/2h) [40] (The material type used in flexible pipes has been detailed in Chapter 3.)

for another quenched and tempered (570°C/2h) AISI 4140 steel with a higher strength compared with the steel condition in Figure 13(b). In this case, the shot peened condition that has surface compressive residual stresses $\sigma^{rs} = -530$ MPa is characterized for all investigated σ_a values by small measurable plastic strain amplitudes during the first cycle that diminish or disappear first of a with an increasing number of cycles. After a subsequent regime of quasi-elastic behaviour, cyclic softening, which yields to lower plastic strain amplitudes and larger numbers of cycles to failure in comparison with the un-peened conditions is dominant.

The effect of deep rolling on the behaviour of the cyclic deformation curves is presented in Figure 2.11(a) for the normalized plain carbon steel SA1045 [40]. At comparable stress amplitudes essentially small plastic strain amplitudes are measured in the deep-rolled condition. In this materials state, the cyclic softening effects are extremely restricted but continue during the whole lifetime uncrack initiation. As a consequence of the small plastic strain amplitudes at identical stress amplitudes, higher numbers of cycles to failure are observed for the deep-rolled condition compared with the normalized ones. Figure 2.11(b) show the influence of deep rolling in the case of a nitro-carburized SAE 1045 steel. Due to the different microstructures in the near-surface areas of the specimens, the same stress amplitudes yield plastic strain amplitudes that are five time smaller than those of the normalized state.

The deep-rolling process modifies the cyclic deformation curves of the nitro-carburized specimens in a manner similar to the normalized specimens. However, the reduction of the plastic strain amplitudes is much less pronounced. Figure 2.12 shows plastic strain amplitudes as a function of the number of cycles plotted push-pull loading with the stress amplitudes indicated for normalized SAE 1045 steel [41]. Results for annealed as well as for shot peened or deep-rolling conditions are shown. One can clearly see that both mechanical surface treatments considerably diminish the plastic strain amplitudes. Due to the thicker affected surface layer in the case mentioned first, the effect for deep-rolled states is more pronounced than for shot peened states. Because fatigue damage is clearly correlated with plastic strain amplitude, the benefit of mechanical surface treatments becomes obvious.

FIGURE 2.11: Cyclic deformation curves for stress-controlled push-pull loading of specimens of (a) Normalised and (b) nitro-carburized of the SAE 1045 steel in un-peened and deep-rolled conditions [41]

The influence of mechanical surface treatments on cyclic plasticity can be summarized in cyclic stress-strain curves, which correlate stress amplitudes and plastic strain amplitudes; for example, half the number of cycles to failure. Figure 2.13, as an example, shows data for an austenitic AISI 304 steel in shot peened as well as deep-rolled conditions compared with untreated specimens [33, 34]. Effects of

FIGURE 2.12: Cyclic deformation curves of different mechanically push-pull loading in the push-pull loading in the low-cycle fatigue (LCF) regime of the plain carbon SAE 1045 steel. Stress amplitude $\sigma_a = 350$ MPa, Almen intensity $l = 0.120$ mm A, rolling pressure $p = 150$ bar; surface residual stresses: shot peening $\sigma^n \approx -500$ MPa deep rolling, approximately $-600/-350$ MPa. [34]

mechanical surface treatment are more distinct with a higher ratio between the area of affected surface layer and the cross section of the specimen. In the case presented here, hollow thin-walled specimens were prepared from compact specimens for analysis. As shown in Figure 2.13, cyclic yield strength considerably increases compared with compact specimens, if only the fatigue behaviour of the surface layers of mechanically surface treated components is investigated.

If residual stresses are present in the root of a notched specimen, marked changes always occur in the initial parts of the notch root cyclic deformation curves ($\epsilon_{a,p}/\log N$ curves) and in the notch root cyclic mean strain curves ($\epsilon_m/\log N$ curves) that depend on the sign and magnitude of the residual stresses. Characteristic examples are presented in Figure 2.14 for normalized specimens and Figure 2.15 for quenched-and-tempered specimens of SAE 1045 with a notch factor $K_t = -3.0$ that were investigated in push-pull tests [40, 41]. Figure 2.14(a) compares the cyclic deformation curves of material states with very low residual

FIGURE 2.13: Cyclic stress–strain curves of deep-rolled AISI 304 (rolling pressure 150 bar, surface residual stresses $\sigma_l^n \approx -350$ MPa) using compact as well as hollow specimens with different percentages of strain-hardened layers compared with an untreated state and a shot peened condition ($\sigma^n \approx -450$ MPa) [34]

stresses (produced by milling and subsequent annealing) with rather high residual stresses (produced by shot peening). In both conditions plastic deformation occurs in the first cycle at nominal stress amplitudes σ_n, above 150 MPa. The annealed state yields continuous cyclic softening for all investigated σ_n values. Contrarily, the initial plastic strain amplitudes of the shot peened condition that are much less dependent on the stress amplitude compared to the milled and annealed state are reduced during the first cycles. This is a result of residual stress relaxation that is the more pronounced the higher the nominal stress amplitude. The consequences are smaller effective stress amplitudes and smaller $\epsilon_{a,p}$ values in the following cycles. Hence, the observed cyclic work hardening is fictitious. However, at higher numbers of cycles, cyclic softening occurs with lower $\epsilon_{a,p}$ values than in the un-peened condition. On the other hand, as can be seen from Figure 2.14(b), the shot peening notch root residual stresses have an influence on the initial parts of the mean strain curves that were determined for different nominal stress amplitudes [40,41]. As a consequence of the cyclic deformation induced relaxation of the compressive residual stresses in the notch, the initial parts of the

FIGURE 2.14: True plastic strain amplitude (a) and plastic mean strain versus number of cycles (b) for stress-controlled push-pull loading of normalized notched specimens (notch factor $K_t = 3.0$) of the SAE 1045 steel in un-peened and shot peened conditions. [41]

$\epsilon_m / \log N$ curves show negative plastic means strains, where the magnitudes of ϵ_m increase with increasing nominal stress amplitude. The minima of ϵ_m are shifted to lower numbers of cycles with increasing $\sigma_{n,a}$ values. However, from the minima of ϵ_m at approximately 5% of the number of cycles to failure, the ϵ_m/N curves

FIGURE 2.15: True plastic strain amplitude (a) and plastic mean strain versus number of cycles (b) for stress-controlled push-pull loading of quenched-and-tempered (400°C/2h) notched specimens (notch factor $K_t = 3.0$) of the SAE 1045 steel in cut-milled and shot peened conditions with different surface residual stresses [40, 41]

show increasing mean strains for all nominal stress amplitudes. Simultaneously, a decrease of the tensile compliance in the hysteresis loops that intensifies with an increasing number of cycles is observed. By that, the compressive compliance is approximately constant.

This finding proves that this increase of the means strain with the number of cycles is caused by an increase of the number of microcracks and/or the growth of microcracks. These sections are indicated by dashed lines in the $\epsilon_m / \log N$ curves of Figure 2.14(b).

The true plastic strain amplitudes in the cyclic deformation curves of the quenched-and-tempered (400°C/2h) specimens in Figure 2.15(a) are influenced by the magnitude of the notch root residual stresses, but not by their sign [40,41]. All investigated conditions in Figure 2.15(a) show for the initial cycles fictitious cyclic-work-hardening effects due to the relaxation of residual stresses σ^n of the surface layers (σ^n = 460 MPa and −320 MPa produced by upcut milling as well as −710 MPa by shot peening). Up to $N = 20$ cycles, increasing magnitudes of the compressive residual stresses cause higher negative mean strains. However, positive milling residual stresses yield to positive mean strains. The increases in the plastic mean strains that appear for the numbers of cycles above the minimum of ϵ_m are caused also by microcracks as described previously.

Evaluation of Experimental Results:

In relatively soft material states, as for example in normalized as well as in quenched-and- tempered at high-temperature conditions, the consequences of mechanical surface treatments by shot peening or deep rolling on the cyclic deformation behaviour are mainly caused by near-surface micro residual stresses, that is, work hardening of the surface layers, because the macro residual stresses are relaxed very soon by cyclic plastic deformation. This relaxation of macro residual stresses is shown in Figure 2.16(a) for shot peening residual stresses in the notch root of a normalized SAE 1045 steel [34] under the loading conditions of Figure 2.14(a). The dislocation structures in the ferrite after the mechanical surface treatment are not stable and change during cyclic loading in energetically more favourable arrangements. The formation of typical fatigue-induced dislocation structures is combined with cyclic softening effects as presented in Figures 2.10(a), 2.11(a) and 2.14(a).

FIGURE 2.16: Residual stress relaxation during stress-controlled push-pull loading of notched specimens (notch factor $K_t = 3.0$) for (a) normalized SAE 1045 in shot peened conditions and (b) quenched-and-tempered (400°C/2h) SAE 1045 in cut-milled and shot peened conditions [40]

The small plastic strain amplitudes of the shot peened or deep-rolled conditions and the resulting increase in fatigue life are caused by the restricted mean free path of the mobile dislocations in the work-hardened surface layers.

In hardened as well as in quenched-and-tempered at low temperature conditions, the changes in the cyclic deformation behaviour result not only from surface hardening or softening effects, but also from the more stable residual stresses as can be seen in Figure 2.16(b) for notch root residual stresses of the quenched and tempered (400°C/2h) SAE 1045 steel under the loading conditions of Figure 2.15(a) [40, 41]. The consequences are a considerable influence of the residual stresses on the cyclic behaviour, especially with regard to the development of mean plastic strain of notched specimens (Figure 2.15(b)).

A study of the residual stress effects on the cyclic deformation behaviour seems to be possible by their simulation by applied mean stresses, which are homogeneously distributed over the cross section of the specimen. An example is presented in Figure 2.17 for smooth, normalized SAE 1045 steel specimens that were stress-controlled loaded in push-pull tests with a constant mean stress of $\sigma_m = -300$ MPa [41]. The cyclic deformation curves at stress amplitudes $\sigma_a = 125$ and 150 MPa in Figure 2.17(a) show first of all a quasi-elastic incubation interval, followed by considerable cyclic softening within some cycles. Subsequently, within some further cycles, cyclic work hardening occurs to such an extent that extremely low plastic strain amplitudes result. For $\sigma_a \geq 200$ Mpa, the compressive stress peak $|\sigma_m - \sigma_a|$, which is higher than the yield strength, induces plastic deformation in the first cycle. This procedure is followed by a rapid cyclic work hardening in such a manner that at cycles above 100 extremely low $\epsilon_{a,p}$ values are observed. As a consequence of the constant compressive mean stress, the specimens shorten for all investigated stress amplitudes, as proved by Figure 2.17(b).

For $\sigma_a \geq 200$ MPa, the mean strain increases considerably and continuously. However, for $\sigma_a < 200$ MPa the $\epsilon_{a,p}$ values saturate above 20 cycles.

Influence of Residual Stresses on S-N Curves

FIGURE 2.17: Plastic strain amplitude (a) and plastic mean strain versus number of cycles (b) for axial stress-controlled cyclic loading with mean stress $\sigma_m = 300$ MPa for specimens of the normalized SAE 1045 steel [41]

Low-Strength Steel: Figure 2.18 shows S-N curves for alternating bending of normalized SAE 1045 steel [42, 43]. The notched specimens had a stress-concentration factor $k_t = 2.5$. The stress gradient at the notch root related to the maximum

FIGURE 2.18: Alternating bending S-N curves of notched specimens of normalized plain carbon SAE 1045 steel after annealing, downcut milling and upcut milling [40]

stress $d\sigma/dz$ (normalized stress gradient η)

$$\eta = \frac{1}{\sigma}\frac{d\sigma}{dz}\bigg|_{z=0} \tag{2.1}$$

was 5 mm^{-1}. All data are nominal stress amplitudes and are valid for a failure probability of 50%. The bending fatigue strength was evaluated at an ultimate number of cycles $N_a = 10^7$. By downcut milling and upcut milling, surface residual stresses of 242 and -234 MPa, respectively, were generated.

The corresponding S-N curves are almost identical. A third batch of specimens was annealed 2 hours at 700°C after downcut milling. The annealing results in a reduction of bending fatigue life and bending fatigue strength [42, 43].

The alternating bending fatigue strengths of milled smooth and notched specimens with different geometries are plotted in Figure 2.19 as a function of the surface residual stresses [34]. Again, all data are given for a failure probability of 50%, and the bending fatigue strengths are nominal stress amplitudes at $N_a = 10^7$.

FIGURE 2.19: Alternating bending fatigue strength of milled smooth and notched specimens of normalised plain carbon steel SAE 1045 steel versus surface residual stress [41]

With increasing stress-concentration factor and decreasing stress gradient, the bending fatigue strength decreases. The influence of the stress-concentration factor is clearly visible from a comparison of the specimens with the same value $\eta = 2\ \mathrm{mm}^{-1}$, but different values $k_t = 1.7$ and 2.5, respectively. On the other hand, the increase of η from 2 to 5 mm^{-1} at specimens with $k_t = 2.5$ results in a significant increase of bending fatigue strength. It is also interesting to note that specimens with $k_t = 4.4$, $\eta = 15\mathrm{mm}^{-1}$ have a somewhat higher strength than specimens with $k_t = 2.5$, $\eta = 2\mathrm{mm}^{-1}$. However, with regard to the residual stress state, there is no significant influence on the bending fatigue strength, even though the range of residual stresses covered comes to more than 1000 MPa regarding specimens with $k_t = 4.4$, $\eta = 15\mathrm{mm}^{-1}$. Careful inspection of the hardness of the specimens tested shows that a positive slope of the lines in Figure 2.19 is not related to the changing (macro) residual stress state, but to different hardness of the specimen and hence, differences in the micro residual stress state produced by different machining procedures. After correction of the data points given in Figure 2.19 to the same hardness, it turns out that the bending fatigue strength is hardly changed

FIGURE 2.20: S-N curves of specimens made from normalized plain carbon SAE 1015 steel in the as-heat-treated state and after an addition deep rolling for (a) push-pull loading and (b) rotating bending. [34]

FIGURE 2.21: Alternating bending S-N curves of notched specimens made from quenched-and-tempered (60°C/2h) plain carbon SAE 1045 steel after different grinding processes [42, 43]

or slightly diminished at most, if the residual stresses change from compressive to tensile [44].

S-N curves for push-pull loading of smooth specimens made from normalized SAE 1015 steel in the as-heat-treated state and after an additional deep rolling are shown in Figure 2.10(a) [44]. Again, the fatigue behaviour in the range of finite fatigue life and the fatigue strength do not differ much. Figure 2.10(b) shows a plot of S-N curves for rotating bending of the same material states. Now, by deep rolling finite fatigue life is increased by one order of magnitude or more, and the bending fatigue strength is increased significantly.

Medium-Strength Steel

Figure 2.11 shows S-N curves that were determined in alternating bending on notched specimens of quenched-and-tempered (600°C/2h) SAE 1045 steel. All data are valid for a failure probability of 50% and $N_a = 10^7$. Three batches of specimens were manufactured by grinding. The grinding parameters (final feed, cutting speed) and the resulting depth distributions of residual stresses are given in

FIGURE 2.22: Depth distribution of the residual stress in notched specimens made from quenched-and-tempered (600°C/2h) plain carbon SAE1045 steel by different grinding processes with the indicated two steps of final feed and cutting speed [41]

Figure 2.22 [42, 43]. Specimens with small and with compressive surface residual stresses yield identical fatigue behaviour.

It should be noted that the surface layer bearing compressive residual stresses is rather small. Contrarily, the generation of tensile residual stresses causes a significant decrease of bending fatigue strength and a rather small decrease of finite fatigue life, which obviously vanishes at high stress amplitudes.

The alternating bending fatigue strength of ground smooth and notched specimen with different geometries made of the same material state is plotted in Figure 2.23 as a function of the surface residual stresses [34]. Similar to Figure 2.19, the influences of the stress-concentration factor and the normalized stress gradient are clearly discernible. However, contrary to the normalized steel there is distinct reduction of the bending fatigue strength with increasing tensile residual stress, this being more pronounced in the comparison of smooth specimens with notched specimens. In the range of compressive residual stresses covered, the influence of residual stress on bending fatigue strength is rather small.

FIGURE 2.23: Alternating bending fatigue strength of ground smooth and notched specimens made from quenched-and-tempered plain carbon SAE 1045 steel versus surface residual stress. [40]

The S-N curves of smooth specimens in the ground state and after an additional shot peening are compared in Figure 2.24(a) [42, 43]. There is a distinct increase of the bending fatigue strength by shot peening, but a rather small influence on finite fatigue life. Figure 2.24(b) compares S-N curves of notched specimens which were milled, ground, and shot peened after grinding.

Again, in the range of finite fatigue life, the influence of the different manufacturing processes is almost negligible. The relative increase of the bending fatigue strength by shot peening is more pronounced compared with smooth specimens. It is interesting to note that milled specimens have a higher bending fatigue strength than ground ones, even though they have lower compressive residual stresses (-159 MPa) at the surface than the latter ones (-221 MPa).

Figure 2.25 shows a plot of the alternating bending fatigue strength evaluated from Figure 2.24 as a function of the surface residual stresses. The arrows mark the shift in bending fatigue strengths and surface residual stresses produced by shot peening.

FIGURE 2.24: Alternating bending S-N curves of specimen made from quenched-and-tempered (600°C/2h) plain carbon SAE 1045 steel. (a) Smooth specimens after grinding and after additional shot peening. (b) Notched specimens after milling, grinding, and grinding with additional shot peening [41]

FIGURE 2.25: Alternating bending fatigue strength of quenched-and-tempered (600°C/2h) plain carbon SAE 1045 steel versus surface residual stress evaluated from Figures 2.23 and 2.24 [40]

Additionally, data points of ground specimens with negligible or tensile residual stresses shown in Figure 2.23 are included.

In the case of notched specimens, all data points lie on a common line with the slope -0.154 except for ground specimens with compressive residual stresses at the surface. Regarding smooth specimens, the influence of tensile residual stresses on the bending fatigue strength is much more pronounced than the influence of compressive residual stresses.

Figure 2.26 shows S-N curves for alternating bending of smooth specimens ($\eta = 1\ \mathrm{mm}^{-1}$) of blank-hardened AISI 5115 steel determined in the un-peened and various shot peened states including one with electrolytically removed surface layer [41]. The corresponding depth distributions of residual stresses are given in Figure 2.27. From the comparison of both figures, it becomes clear that the surface residual stress is not a suitable parameter for the assessment of the influence of the various treatments on the fatigue behaviour.

The influence of the deep-rolling force on the rotating bending fatigue strength

FIGURE 2.26: Alternating bending S-N curves of smooth specimens made from blank-hardened AISI 5115 steel in the as-blank-hardened and with different conditions shot peened states including one with a subsequently electropolished surface. 1. as-black-hardened; 2. shot velocity $v = 23$ m/s, coverage $c = 100\%$, mean diameter of the shot $d = 0.6$ mm; 3. $v = 53$ m/s, $c = 100\%$, $d = 0.3$ mm; 4. $v = 53$ m/s, $c = 100\%$, $d = 0.6$ mm; 5. $v = 81$ m/s, $c = 600\%$, $d = 0.6$ mm; 6. $v = 53$ m/s, $c = 100\%$, $d = 0.6$ mm, 100 μm surface layer electrolytically removed. [40]

of smooth and notched specimens made from quenched-and-tempered SAE 5135 steel is shown in Figure 2.28 In both cases, a maximum of the fatigue strength occurs at a certain force. However, the increase of the fatigue strength of notched specimens ($k_t = 2$) by deep rolling is much more pronounced than that of smooth specimens. In the end, the optimal bending fatigue strength of notched specimens which is nominal stress amplitude-is higher than the bending fatigue strength of smooth specimens.

High-Strength Steel

S-N curves for alternating bending of notched specimens of quenched SAE 1045 steel in differently ground conditions are compared in Figure 2.29. The grinding parameters (final feed, cutting speed) and the resulting depth distributions

FIGURE 2.27: Depth distribution of the residual stress in specimens made from blank-hardened AISI 5115 steel in the as-blank-hardened (1) and in different conditions of the shot peened state (3),(4), and (5) corresponding to Figure 2.26 [40]

FIGURE 2.28: Bending fatigue strength smooth and notched specimens made from quenched-and-tempered SAE 5135 steel versus deep-rolling force. [41]

FIGURE 2.29: Alternating bending S-N curves of notched specimens made from quenched plain carbon SAE 1045 steel after different grinding processes. [34]

FIGURE 2.30: Depth distribution of the residual stresses in notched specimens made from quenched plain carbon SAE 1045 steel and ground with the two steps of final feed and cutting speed indicated. [34]

FIGURE 2.31: Alternating bending fatigue strength of ground smooth and notched specimens of quenched plain carbon SAE 1045 steel versus surface residual stress. [34]

of residual stresses are given in Figure 2.30. Similar to ground quenched-and-tempered specimens, the fatigue behaviour of specimens with very small or compressive residual stresses (which have a very small penetration depth) hardly differ. Tensile residual stresses, however, not only cause a strong reduction of bending fatigue strength, but also of finite fatigue life. In Figure 2.31, the bending fatigue strength that was evaluated from Figure 2.29 and corresponding data from test on smooth specimens are plotted as a function of the surface residual stresses. The negative influence of tensile residual stresses on the bending fatigue strength of smooth specimens is even more pronounced compared to notched specimens. The influence of compressive residual stresses generated by grinding is much smaller than the influence of tensile stresses.

In Figure 2.32(a), the S-N curves of smooth specimens in the ground state and after additional shot peening are compared [34]. Similar to quenched-and-tempered specimens (see Figure 2.24), shot peening produces a significant increase of the bending fatigue strength. Contrary to the results of the medium-strength steel,

FIGURE 2.32: Alternating bending S-N curves of specimens made from quenched plain carbon SAE 1045 steel. (a) Smooth specimens after grinding and after additional shot peening.(b) Notched specimens after grinding, milling, and grinding with additional shot peening with shot of the indicated hardness [40]

however, there is also a very pronounced increased of finite fatigue life, which comes up to one and a half orders of magnitude at high stress amplitudes.

The S-N curve of notched specimens of the same steel state after grinding and after additional shot peening are shown in Figure 2.32(b). Compared to smooth specimens, shot peening produces a much stronger increase of the bending fatigue strength. Again, there is also a remarkable increase of finite fatigue life. Additionally, the S-N curve of milled specimen is included. Finite fatigue life and bending fatigue strength of these specimens are lower compared to shot-peened ones, even though they contain very high surface compressive residual stresses of -1200 MPa.

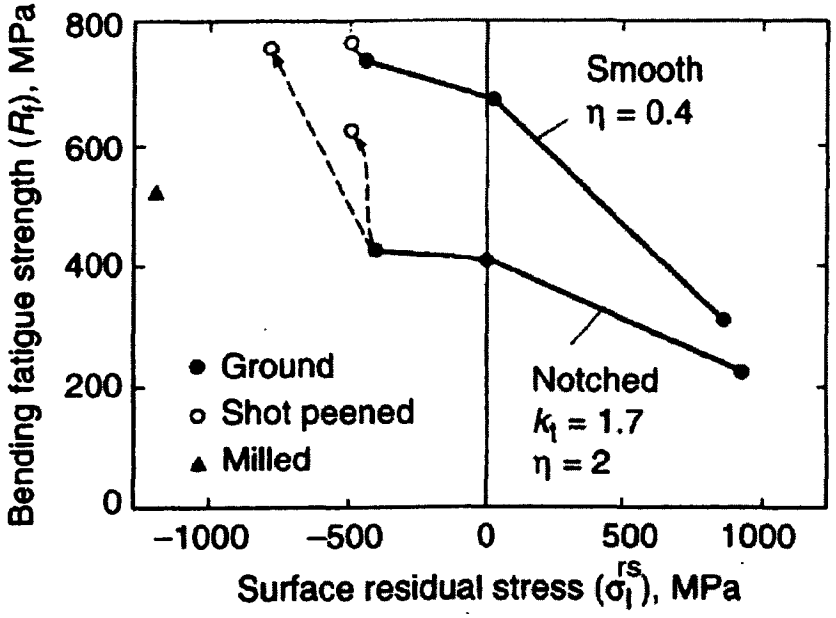

FIGURE 2.33: Alternating bending fatigue strength of smooth and notched specimens made from quenched plain carbon SAE 1045 steel with different surface conditions versus surface residual stress

In Figure 2.33, the bending fatigue strength data already plotted in Figure 2.31 are complemented by data evaluated from Figure 2.32. The arrows mark the shift in bending fatigue strengths and surface residual stresses produced by shot peening. Similar to the discussion of Figures 2.26 and 2.27, it becomes obvious that the magnitude of surface residual stress is not a suitable parameter for the assessment of the influence of shot-peening-induced residual stresses on the fatigue strength.

2.3.2 Influence on the fatigue strength (Crack Initiation stage)

Residual stress plays a crucial role with respect to the fatigue strength of materials. It can be considered to be mean of static stress superimposed on the cycle stress. As the mean stress σ_m increases the fatigue strength decreases. This has been demonstrated in the Heigh and Goodman's diagrams. Quenching treatment, after the induction heating, introduces very high residual compressive stresses into the hardened layer, which results from the increase in volume of the martensitic structure with respect to the ferrito-perlitic structure (this applied to the treatment of annealed steel, for example). In induction quenched cylindrical bars, the residual stress on the surface usually leads to a tangential residual stress equal to or slightly greater than the longitudinal stress. The thickness of material subjected to residual compressive stress is in the same order of magnitude as the layer transformed during treatment. Fatigue tests carried out by the French Technical Centre for the Mechanical Industry (CETEM) on the 36 mm diameter XC42 steel cylindrical bars, quenched after induction heating and subjected to repeated bending stress. The results obtained are presented in the table below.

2.3.3 Influence of residual stress on the tensile strength, friction and wear

The effect of residual stress on the tensile strength is obvious, particularly in structures made of composite materials or when the pre-stressed layer is very thick compared to the thickness of the part. In composites, residual stress is produced as result of the thermal and mechanical incompatibility of the reinforcement and matrix. This can influence the macroscopic properties of the composites under tensile or compressive stress.

Little research has been carried out on the effect of the residual stress on the friction and wear properties. Their role is often masked by the parameters. The increase of the hardness during treatment and changes in the toughness and adhesion of

Type and depth of the treatment at 45 mm HRC, mm	*Surface hardness, HRC*	*Fatigue limit after 5×10^6 Cycles, MPa*		*Residual stress stabilised at the fatigue limit, MPa*	
		σ_m	σ_a	Longitudinal stress	Transverse stress
Induction 2.7	55–56	596	584	−128 −243	−498 −571
Induction 4.2	55–56	623	610	−273 −347	−583 −676
Induction 4.7	54–59	670	660	−655	−603
Water Quenched after through heating without stress relieving annealing 3.5	60–69	780	750	−863 −777	−1132 −1156

TABLE 2.2: Effect of quenching conditions and residual stress on fatigue strength [45]

the anti wear coatings due to residual stress can considerably affect the resistance to friction. Up until now, the effect has been integrated into the global parameter of adhesion. In future, work should be carried in order to find the real effect of the residual stress.

2.3.4 Taking residual stress into account while calculating the fatigue life

In the previous section, the different effect of the residual stress on the mechanical strength of the structures and materials is mentioned. Although the ability to quantitatively estimate the fatigue life taking residual stress into account is just beginning, it is still too early to extend these predictions to other types of stress

that far more complex and involve physical and chemical phenomena. Statistics show that failure of purely mechanical original is mainly due to the fatigue. One obvious way to account for residual stresses on the fatigue behaviour is to treat them as local mean stresses.

2.3.5 Some aspects of fatigue in steels

The fatigue behaviour of metallic materials is characterized by the process. Generally it contains four successive stages A, B, C and D [46].

Stage A: Cyclic deformation with work-hardening or and work-softening effects in the total volume (homogeneous loading such as push-pull of smooth specimens) or in the highest loaded region (inhomogeneous loading such bending, torsion, or any loading of notched components) and developments of persistent slip bands at this surface.

Stage B: Micro crack initiation and propagation. Normal evolution of a macro crack in the surface region.

Stage C: Stable macro crack propagation connected with changes in the state of the materials in the crack tip plastic zone.

Stage D: Unstable crack propagation and failure.

An example of fatigue stages is shown with S-N Diagram (Wohler diagram Figure 2.34) for the plain carbon steel SAE 1020 which presents experimental results of the persistent slip band formation ($\sigma_a/\log N_S$ curve), micro crack initiation ($\sigma_a/\log N_i$ curve), failure ($\sigma_a/\log N_f$ curve).

Residual stresses are generated in the structural component during manufacturing processes such as forging, machining, heat treating, shot peening and many others [41]. These stresses are always a consequence of inhomogeneously distributed dimensional changes due to inhomogeneous plastic deformations, thermo-mechanical treatments and phase transformation. They can be either beneficial or detrimental

FIGURE 2.34: Wholer's Curve for slip band formation, micro-crack initiation and failure [40]

to component behaviour in service, depending on the materials state as well as the sign, magnitude, and stability of the residual stresses, mechanical loading and environmental conditions. Compressive macro residual stresses in the surface the region of materials with medium and high hardness increase the fatigue life and fatigue limit at the cyclic loading compared to materials states that are free of residual stresses. This improvement is caused by an increased resistance against crack initiation and to a certain extent, against crack propagation if the residual stresses are sufficiently stable in the areas of highest loading (in most cases the component surface areas). Moreover, compressive macro residual stresses can increase the resistance of certain materials against corrosion fatigue and stress corrosion cracking; they also improve the wear resistance. Therefore, in many cases compressive macro residual stresses are intentionally generated near surface regions by the controlled heat treatment or by the post treatments such as shot peening or deep rolling.

The stability or relaxation behaviour of the these residual stress at the purely thermal or mechanical loading as well as superimposed thermal and mechanical

loadings is thus of decisive importance for the service behaviour of components and hence of great interest from scientific as well as practical point of view. If residual stresses are relaxed by the annealing or mechanical treatment, they naturally have little if any influence on subsequent component failure.

Residual stresses can be reduced or completely relaxed by the application of mechanical and thermal energy. The elastic residual strain, ϵ_e, that is associated with residual stresses via Hooke's law can be converted into the micro-plastic strains, ϵ_p, by the suitable deformation processes. For example, this transformation can be achieved by the dislocation slip, dislocation creep, grain- boundary sliding and diffusion creep. If these processes occur to only a limited extent of not at all, relaxation of residual stresses is also conceivable by the crack formation and propagation. Relaxation of residual stresses in the real case occurs by the complex interaction of the large number of factors. It depends not only on the residual stress state itself but also on the material state, loading condition, geometry and environment of the component under consideration.

The best known and most important techniques for inducing the residual stress relaxation are annealing (tempering), uniaxial deformation and cyclic deformation. Relaxation can also be caused thermal cycling, quenching, and neutron bombardment, the effect of alternating magnetic field, vibration and partial damage.

2.3.6 Behaviour of micro residual stresses:

Micro residual stresses behave in a complex fashion during the relaxation of macro residual stresses by the uniaxial deformation. So far only isolated experimental data based on the X-ray profile analysis are available.

When a material is formed or machined both directed and inhomogeneous micro residual stresses are set up. Those of the first type are the result of back stresses due to the dislocation pileups at grain or phase boundaries and elastic strained second phases of heterogeneous materials. If these dislocations move in the reverse

directions during localized plastic deformation, the back stresses and hence the directed micro residual stresses are initially reduced. Further deformation causes renewed build up of back stresses in opposing directions associated with dislocation, multiplication and hardening, which must once again increase in the micro residual stresses.

Dislocation arrangements in random distribution or in tangles or cells give rise to inhomogeneous micro residual stresses. Micro plastic deformation can lead to the rearrangement of dislocations into arrangement of lower energy and thus bring about micro residual stress relaxation. If new dislocations are produced a renewed build up of micro residual stresses is superimposed on the relaxation process.

Reductions in the micro residual stresses in the hardened steel are observed on machining. Two superimposed effects can operate here. After hardening, very high density of dislocation is present either randomly distributed or in tangles. Micro plastic deformation brings about rearrangement of these dislocations into configurations with lower distortion energy and therefore a reduction in the micro residual stresses. On the other hand, solute carbon atoms may be induced to jump into the energetically more favourable octahedral sites in the martensite lattice under the influence of the stress field of the moving dislocation. This causes a reduction in the tetragonality and hence the lattice distortion due to the solute carbon atoms.

2.4 Elastic Plastic Bending

Bending of beams or simple bending theory is not that easily amenable to mathematical analysis and plastic bending is more complicated to understand. [47, 48, 49] In fact, the complete solution is as yet unknown and all existing theories make assumptions which lead to varying degrees of approximation to the correct result. These approximate theories are very useful, provided they are applied within the limitations of the basic assumptions and provided they have been checked experimentally for a particular application [50].

FIGURE 2.35: Bar of rectangular cross-section subjected to pure bending [36]

The difficulties involved in analysing plastic bending can be appreciated by considering the bending of a straight bar of rectangular cross-section in which the breadth and depth are of about the same magnitude. If such a bar is subjected to pure bending, shown in Figure 2.35 (i.e., a constant bending moment and therefore no shearing force); then provided the elastic limit is not reached at any point, transverse sections which are plane before bending remain plane after bending. If R is the radius of curvature of the neutral axis in the plane of bending, then the anticlastic curvature is $-v/R$ where v is Poisson's ratio. As bending continues, yielding at the outer fibres gradually spreads towards the centre of the bar but the strains are still largely controlled by the central elastic core. However the Poisson's ratio effect now varies over the cross-section, v being about 0.3 for elastic strains and 0.5 for plastic strains. To attain the necessary continuity of strain across the elastic-plastic boundary, some transverse stresses must be present. To overcome this difficulty, some writers assume that the material dealt with is incompressible, that is $v = 0.5$ in both elastic and the plastic strain. Whilst this facilitates a mathematically correct analysis, if it is applied to a real material, it is tantamount to neglecting the transverse stresses.

Again in elastic bending, the same compatibility conditions which hold for pure bending are assumed to hold laterally loaded beams, i.e., plane section remain

plane on bending, provided the shear stresses are small compared with the longitudinal bending stresses. This is so if the longitudinal dimensions are large compared with the dimensions of the cross-section. This same approximation is sometimes made in plastic bending and is additional to the neglect of the transverse stresses mentioned above.

2.4.1 Simple Theory of Plastic Bending (Straight Rectangular Section Beams)

The elastic stress distribution from bending theory over a bar of rectangular cross-section, Figure 2.35, subject to a pure bending moment M is linear, as shown in Figure 2.36(b). The maximum stresses occur at distances from the neutral axis of $h/2$ and are given by:

$$\sigma_{\max} = \frac{M}{I} \cdot \frac{h}{2} \tag{2.2}$$

Where I is the second moment of area of the section about the neutral axis NN. Suppose the beam is made of a material whose stress-strain curve is the same in pure tension and compression and is as shown in Figure 2.37. As M increases, the stress distribution remains linear until $\sigma_{\max} = Y$ the yield stress, Figure 2.36(c). With further increase in M, the linear distribution ceases. The strain at a distance y from the neutral axis, provided the strains be small is y/R, where R is the radius of curvature of the neutral fibre of the bent beam. For a given M, R is constant (being very large) across the section and hence the strain is directly proportional to y, provided section originally plane remain plane. If the strain in the outermost fibres, i.e., at $y = \pm h/2$ is ϵ_A the corresponding stress, σ_A may be obtained directly from the stress-strain diagram. In fact the stress distribution at each point on the cross-section is obtained simply by re-drawing on the base or zero stress line, the stress-strain diagram, see Figure 2.36(d), one portion being positive (tensile stresses), the other negative (compressive stresses), the origin of the σ/ϵ curve being placed on the neutral axis. Equality of these positive and negative areas ensures zero total force on a section as long as the section is symmetrical about

NN. The external moment is given by

$$M = \int_{-h/2}^{+h/2} \sigma by \, dy \tag{2.3}$$

expression for M, using a Non-linear Stress–Strain Law. Assuming that the stress-strain relation is

$$\sigma = Ee + Fe^n \tag{2.4}$$

FIGURE 2.36: Stress distribution over a bar of rectangular cross-section [50]

And since $e = y/R$, then, with a notation which is clear from Figure 2.38

$$\begin{aligned} M &= \int_{-h/2}^{+h/2} \left(\frac{Eby^2}{R} + \frac{Fby^{n+1}}{R^n} \right) dy \\ &= \frac{E}{R} I_1 + \frac{F}{R^n} I_n \end{aligned} \tag{2.5}$$

Where $I_1 = \int_{-h/2}^{+h/2} by^2 \, dy$ and $I_n = \int_{-h/2}^{+h/2} by^{n+1} \, dy$. I_1 is the expression for the second moment of area commonly used in strength of Materials. I_n is the integral arising from the non-linear behaviour of the material.

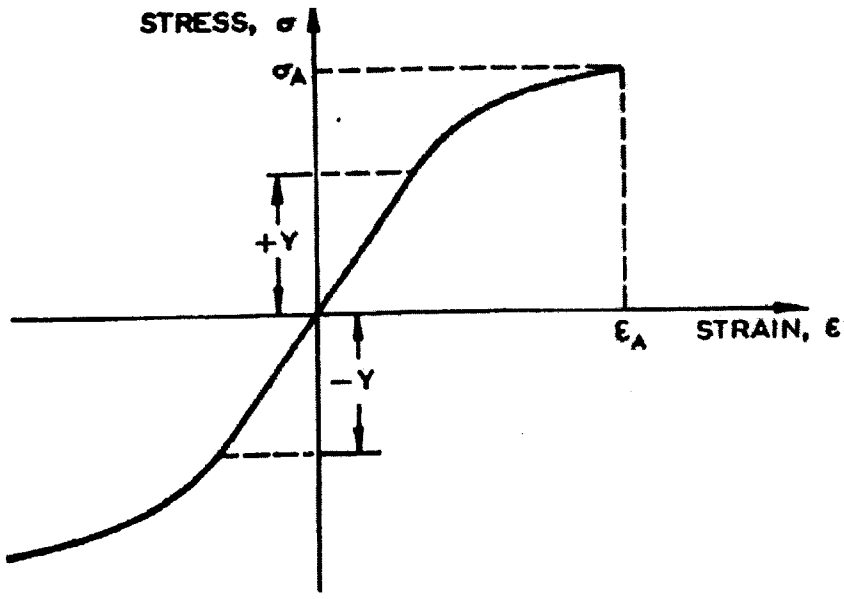

FIGURE 2.37: Stress–strain curve

FIGURE 2.38: Bar of rectangular cross-section subjected to pure bending [50]

Substituting $E = 0$ in the stress-strain relation (2.1)

$$\frac{M}{I_n} = \frac{F}{R_n} = \frac{\sigma}{y^n} \tag{2.6}$$

Follows, being a little more general than the conventional trinity of equation used by engineers in the elastic case, i.e., when $n = 1$. The value of I_n is then, if b is constant,

$$I_n = \frac{bh^{n+2}}{2^{n+1}(n+2)}$$

Expression for Deflection

From the elementary non-linear bending theory for straight beams, when the material of the beam has different stress-strain properties in tension and compression was given by St. Venant and account of this is given in [31] Timoshenko.

Since R is large, then as in elementary beam theory dy/dx is small and negligible in the expression for curvature.

$$\frac{1}{R} = \frac{d^2y/dx^2}{\{1+(dy/dx)^2\}^{3/2}} \tag{2.7}$$

Thus the expression for the deflection of a point in a beam can be calculated by substituting for $1/R$, d^2y/dx^2 and using equation (2.6) Thus

$$\frac{d^2y}{dx^2} = \left(\frac{M}{FI_n}\right)^{1/n} \tag{2.8}$$

Applied to the simple cantilever of length L carrying an end load W, from Figure 2.39, $M = W(L-x)$ and

$$\frac{dy}{dx} = -\frac{C(L-x)^{1/n+1}}{(1+1/n)} + B \tag{2.9}$$

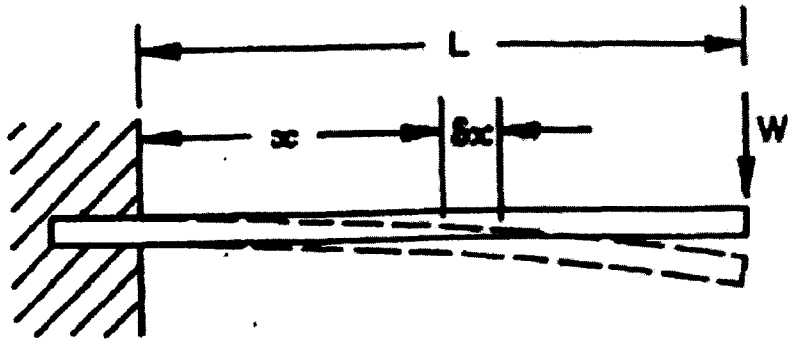

FIGURE 2.39: Cantilever beam with end load W.

$dy/dx = 0$ at $x = 0$, and thus integration constant $B = CL^{1/n+1}/(1/n+1)$, where $C = (W/FI_n)^{1/n}$. Integrating again,

$$y = \frac{C(L-x)^{1/n+2}}{(1/n+1)(1/n+2)} + Bx + D \tag{2.10}$$

When $x = 0$, $y = 0$ and $D = -CL^{1/n+2}/(1/n+1)(1/n+2)$.

Thus,

$$y = \frac{CL^{1/n+2}}{(1/n+1)(1/n+2)}\left[\left(1-\frac{x}{L}\right)^{1/n+2} + \frac{x}{L}\left(\frac{1}{n}+2\right) - 1\right] \tag{2.11}$$

The deflection under the load is δ_w and

$$\delta_w = \frac{CL^{1/n+2}}{(1/n+1)(1/n+2)}(1/n+1) = W^{1/n}f \tag{2.12}$$

In the elastic case, $n = 1$ and

$$\delta_w = \frac{WL^3}{3FI} \tag{2.13}$$

This example illustrates the obviousness of approach for this and similar types of problem. Many results for y, dy/dx, I_n and δ for complicated cases are given in Phillips [51].

When a load W_1 other than W is applied to the end of the cantilever then

$$\delta_{W_1} = W_1^{1/n}f$$

The deflection due to the simultaneous action of W and W_1 is

$$\delta = (W + W_1)^{1/n}f \tag{2.14}$$

Note that

$$\delta \neq \delta_{W_1} + \delta_{W_2} \quad \text{i.e., } (W+W_1)^{1/n} \neq W_1^{1/n} + W_2^{1/n}$$

unless $n = 1$, and hence the principle of superposition is not permissible except when $n = 1$.

Shear Stress Distribution

A very simple application of the use of this particular stress–strain law is to find the shear stress distribution in a rectangular beam subject to simple bending. Referring to Figure 2.42, which shows a portion of the beam in Figure 2.39, the shear

stress, on plane $ABCD$ is, following the usual elementary methods of strength of materials,

$$\tau b\,\delta x = \int_y^{h/2} b\,\frac{\partial \sigma}{\partial x}\,\delta x\,dy \tag{2.15}$$

Now from equation (2.6), $M = \sigma I_n / y^n$ and thus

$$\frac{\partial M}{\partial x} = \frac{I_n}{y^n}\frac{d\sigma}{dx} \quad \text{but} \quad \frac{\partial M}{\partial x} = -W \quad \text{and so} \quad \frac{\partial \sigma}{\partial x} = -\frac{W y^n}{I_n}$$

Hence,

$$\tau = \int_y^{h/2} -\frac{W}{I_n} y^n\,dx = -\frac{W}{I_n}\frac{\lfloor (h/2)^{n+1} - y^{n+1} \rfloor}{(n+1)} \tag{2.16}$$

The ratio of the maximum shear stress on the neutral axis for this material to that for a linear elastic material is $2(n+2)/3(n+1)$.

Idealized Materials in Bending

The moment M_E required to bring the outermost fibres of a rectangular section beam of perfectly plastic-elastic material, to its yield stress is

$$M_E = bh^2 Y/6 \tag{2.17}$$

When the applied moment $M > M_E$, the stress distribution across the section is as in Figure 2.36(e). As the radius of curvature of the beam decreases the thickness of the layer of yielded material increases and the elastic-plastic boundaries approach the neutral axis; when this boundary is distant y from the neutral axis, the moment is given by,

$$M = Yb(3h^2 - 4y^2)/12 \tag{2.18}$$

In mild steel the yielding does not proceed in this fashion; the yield in beams wide relative to their thickness-approaching a plane strain situation is discontinuous and dark bands of plastically deformed material at $\pm 45°$ to the surfaces are visible. In between the bands, light-coloured elastic material is visible; the apices of the bands suggest an advancing plastic-elastic interface. As the bending moment increases, this latter interface advances towards the neutral axis, the quantity of unyielded material nearer the neutral surface being progressively reduced, from

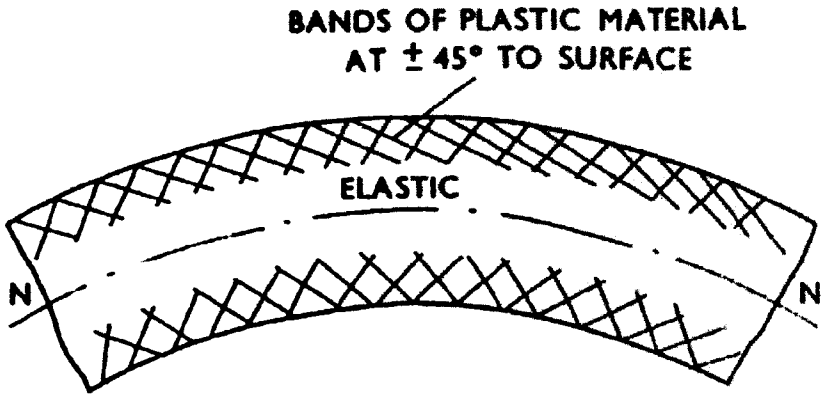

FIGURE 2.40: Plastic yielding of mild steel plate due to a couple

Figure 2.40(a) and (b). Clearly, there always remains a residual layer of elastic material, no matter what the size of M.

But through it there may be a very large gradient of stress. The thinner this elastic core, the less it will be in error to assume that the material is finally plastic across the whole section though the radius of curvature progressively decreases; two plastic stress blocks thus represent this limiting case from Figure 2.36(f). The more closely this case is a approached, the smaller does the radius of curvature of the beam become and the more in error the initial assumptions of the analysis. This ultimate case also displays a stress discontinuity, i.e., sudden jump from $+Y$ to $-Y$, across the neutral axis. However, M_p, the moment required to make the section fully plastic is found from equation (2.18) by substituting $y = 0$, which gives,

$$M_p = bh^2Y/4 \tag{2.19}$$

The result in equation (2.19) is also obtained if the beam is considered to be made of rigid-perfectly plastic material. Whilst this idealized type of material is less realistic than the former, it enables a self-consistent argument to be maintained. Since elastic strains in a rigid-plastic material are zero, there can be no deformation or deflection of a rigid-plastic beam until the moment is so large than the whole of the material of the section has become plastic. The existence of a residual elastic core at any time implies complete rigidity; when once the whole section is

plastic, the beam will 'collapse' or bend without hardening. This collapse load, M_p, is thus half as large again as M_E. It demonstrates that in elastically designed members (buckling excepted) there is a considerable reserve of strength due to the possibility of utilizing their plasticity. It also leads to a new method of designing certain structures which frequently entails much less effort than does an elastic analysis.

Shape Factor

For the case of the rectangular section beam of ideal elastic-perfectly plastic material above, the ratio $M_p/M_E = 1.5$; this ratio of the bending moment required to make a section fully plastic, to that carried by the same section elastically, with the extreme fibre stress just attaining the yield stress, is known as the shape factor.

For a circular section beam, of radius a, it is easily shown that,

$$M_p = \frac{4}{3}a^3Y \quad \text{and} \quad M_E = \frac{\pi}{4}a^3Y \tag{2.20}$$

Thus its shape factor is $16/3\pi \approx 17$. Evidently then, the full load carrying capacity of a circular section bar (based on the completely plastic section) is underestimated by about 41%, by the elastic moment with the yield stress reached in the outermost fibres.

For beam sections which are not symmetrical about any plane perpendicular to the plane of bending, the neutral plane must first be found; for purely linear elastic bending the neutral plane passes through the centroid of the section, but when the section is partly plastic the neutral plane no longer coincides with the elastic neutral plane. Indeed the neutral plane shifts as the depth of the plastic layer in the beam increases. The position of the neutral plane in a section of a beam which is wholly plastic is, however, easily found from the same force equilibrium considerations as prevail for the elastic case. For a beam subject only to a bending moment, the next tensile forces on one side of the neutral plane must equal the net compressive forces on the other. Since the normal bending stress on the section

is every where constant and equal to Y, the equilibrium condition simply requires the neutral plane to be planed in such position that the area of the section above it equals the area of the section below it. An example is that of a beam section which is an isosceles triangle of height h and base length B, any neutral plane in bending being parallel to the base, from Figures 2.41(a) and (b).

(i) For purely elastic bending the neutral axis is distant $H/3$ above the base and it is easily shown that when the bending stress just reaches the yield stress at the apex of triangle,

$$M_E = \frac{YBH^2}{24}$$

FIGURE 2.41: Bending of beam having non-symmetrical cross-sections [50]

(ii) For full plastic bending the neutral axis is distant $H/\sqrt{2}$ below the apex; the net tensile force on the section may be assumed to act through the centroid of the triangular portion of the section which is above the neutral plane i.e., at G_1 and the net compressive through G_2 the centroid of the trapezium below the neutral

plane. It may be shown that,

$$M_p = \left(2 - \sqrt{2}\right) \frac{YBH^2}{6} \tag{2.21}$$

The shape factor of this section is $4\left(2 - \sqrt{2}\right) \approx 2.34$.

Certain section of beam which possess only one axis of symmetry, like the triangular one just discussed, may possess a boundary which can only be treated numerically, e.g., the bulb section of Figure 2.41(c).

For most practical purposes the fully plastic bending moment can be obtained by simple experiment. A thin metal sheet or cardboard lamina cut-out of the section shape is taken and with the help of a planimeter, its area is found. The position of the neutral plane for plastic bending NN can be found; the area above NN must equal that below it. The lamina is then cut along NN and by balancing each of the two portions in turn on a knife edge, the centroid of each is found, i.e., G_1 and G_2. Immediately we have $M_P/Y = 1/2$ area of lamina times the distance G_1G_2.

Plastic Asymmetrical Bending

Asymmetrical bending occurs whenever the plane of an applied bending moment is not parallel or perpendicular to an axis of symmetry of the cross section.

Figure 2.41(d) shows a general cross-section of a beam of cross-sectional area A with an arbitrarily chosen neutral plane. If the section is fully plastic then for force equilibrium due to bending stresses normal to the section, the area of the section in tension on one side of the neutral axis, A_T, must equal the area of the section in compression on the other side of the neutral axis, A_C. We must have,

$$YA_T - YA_C = 0 \tag{2.22}$$

Also then, $A_T = A_C = A/2$. The position of the neutral axis for each given direction is thus provided from the family of area bisectors of the section.

The net tensile force $A_T \cdot Y$ acts through the centroid G_T of A_T and the net compressive force $A_C \cdot Y$ through G_C the centroid of A_C. Hence the full plastic

moment of the section is M_P and

$$M_P = r \cdot AY \tag{2.23}$$

the direction of the axis of M_P being perpendicular to $G_T G_C \cdot 2r$ is the distance $G_T G_C$ and the midpoint of $G_T G_C$ is obviously the centroid of the whole section G.

The locus of G_T and G_C is called the centroidal locus, as shown in Figure 2.41; when this is known, M_P about any axis is easily found, r being the distance from G to the locus in a direction perpendicular to the moment axis. Further, the tangent to the centroidal locus at the point giving r, provides the direction of the neutral axis. This follows from the fact that a given diameter of the centroidal locus is perpendicular to the moment axis; in the limit an 'adjacent' diameter is also perpendicular to the same moment axis and thus the lines joining the points at the ends of the two diameters -tangents- must also be parallel to the two moment axes and hence the neutral plane.

Plastic Bending Followed by Elastic Unloading: Residual Stress Distribution

The beam of non-hardening material, of rectangular cross-section, Figure 2.35, is loaded so that the whole of the section becomes elastic-plastic, Figure 2.36(e). The moment required to bring this about is $bh^2Y/4$. If this bending moment is removed, it is equivalent to adding a negative bending moment of amount $bh^2Y/4$. The beam springs back or recovers elastically; it is supposed that the recovery in each layer of the beam is elastic. This being so, the elastic strain of recovery varies linearly with the distance from the neutral axis; the elastic recovery stresses being greater in the farer layer from the neutral axis. The elastic recovery near the axis will be comparatively small. This recovery is represented in Figure 2.42(a) by CC'. The moment of the area of the triangle OAC about NN must be the same as that of $OABD$. The value of σ_{REC} is easily shown to be $3Y/2$ and the actual residual stress distribution is shown shaded in Figure 2.42(a). From the Figure 2.42(a) it is apparent that there will thus be compressive residual stresses in the fibres of the beam between F and B and F' and D', and tensile residual

FIGURE 2.42: Residual stress distribution and spring back in beams of elastic-perfectly plastic material [50]

stresses between F and D, and F' and B'; $BF/FD = 1/2$ or BF and $B'F'$ are the outer 1/6 of the whole beam thickness.

Springback Calculations

(i) PLANE STRESS

The determination of the residual stresses in a beam of ideal elastic perfectly plastic material when $M_E < M < M_P$ is in principle identical with that just discussed for the case when $M = M_P$. In Figure 2.42(b), $ABDOD'B'A'A$ represents the elastic-plastic stress block due to M; $ACOC'A'A$ represents the elastic recovery

stresses and its moment is also M. Thus, the net residual stress distribution is as shown in Figure 2.42(c).

If the radius of curvature of the neutral axis for the beam in this elastic-plastic condition is R,

$$\frac{y}{R} = \frac{Y}{E} \tag{2.24}$$

Hence, substituting for y in equation (2.18),

$$M = b\left[3h^2Y - 4Y^3R^2/E^2\right]/12 \tag{2.25}$$

Now the change in the radius of curvature due to spring back is R_E and

$$M = EI/R = Ebh^2/12R_E \tag{2.26}$$

Figure 2.41(c) shows a beam which has undergone a deflection due to M of Δ; when unloading occurs the elastic spring back is Δ_E so that the final deflection is Δ_F. We have,

$$\Delta_F = \Delta - \Delta_E$$

And because $\Delta \cdot 2R \simeq L^2$,

$$\frac{1}{R_F} = \frac{1}{R} - \frac{1}{R_E} \quad \text{or} \quad \frac{R}{R_F} = 1 - \frac{R}{R_E} \tag{2.27}$$

R_F is the final radius of curvature. Equating (2.5d) and (2.5e) and substituting in (2.5f), we find

$$\frac{R}{R_F} = 1 - 3\left(\frac{YR}{Eh}\right) + 4\left(\frac{YR}{hE}\right)^3 \tag{2.28}$$

$$= \left(\frac{YR}{Eh} + 1\right)\left(2 \cdot \frac{YR}{Eh} - 1\right)^2 \tag{2.29}$$

When $R/R_F = 0$, there is complete spring back, i.e., the bending is wholly elastic; if, at the other extreme, $R/R_F = 1$, there is no spring back at all.

Figure 2.41(d) shows how R/R_F varies with YR/Eh.

PLANE STRAIN

In the section immediately above, the bending discussed is plane stress bending; dimensions b and h were about equal and thus there was no significant stress in the plane perpendicular to the bending plane. If b is very much greater than h, anticlastic curvature is suppressed apart from small regions near the two sides of the beam; the greater portion of the beam, from Figure 2.41(e), is flat and thus strain in the direction of b, or z, is zero. For purely elastic strains,

$$e_z = 0 = (\sigma_z - v\sigma_x)/E; \tag{2.30}$$

σ_y is assumed everywhere to be zero and v is Poisson's ratio. Also, $e_x = (\sigma_x - v\sigma_z)/E = y/R$, and hence,

$$e_x = Ey/R + v \cdot \sigma_z \tag{2.31}$$

Substituting in (2.5k) from (2.5j) for σ_z and simplifying,

$$\sigma_z = \frac{Ey}{(1-v^2)R}$$

Hence,

$$M_E = \int_{-h/2}^{h/2} \sigma_x y \, dy = Eh^3/12R(1-v^2) = Eh^3/12R \tag{2.32}$$

From (2.5p) it is seen that when plane strain bending occurs we must use $E/(1-v^2)$ or E' rather than just E as in plane stress bending. Thus the expression equivalent to (2.5j) for plane strain bending is

$$\frac{R}{R_F} = 1 - 3\left(\frac{YR}{Eh}\right)(1-v^2) + 4\left(\frac{YR}{Eh}(1-v^2)\right)^3 \tag{2.33}$$

This last expression is plotted in Figure 2.42(d).

It may be observed, however, that the direct yield stress in plane strain bending for a Mises material is $(2/\sqrt{3})\cdot Y$ but for a Tresca material is just Y; from experimental results the latter is most appropriate for mild steel in simple bending.

Residual stresses in beams of real materials may be estimated, in principle, in the same way, using the real stress-strain curve of the material though the computation is tedious (Figure 2.42(g)) Such a procedure is valid, provided the residual stresses are everywhere less than the yield stress of the material in reversed loading. This means not merely the primary yield stress, but something less than it; this is to say that the Bauschinger effect must be kept in mind. In principle, also, it is no more difficult to deal with non-rectangular section.

2.5 Residual stress measurement techniques

In the last few years, various quantitative and qualitative methods of measuring residual stresses have been developed. These techniques are used for the processing optimization, and quality control of the material. In general, a distinction must be made between destructive and non destructive methods. The first series of methods is based on destroying the state of equilibrium in the mechanical component. The residual stress is then evaluated from its relaxation. However, it is only possible to measure the consequences of stress relaxation and not the relaxation itself. For example, displacement, strain, fractures. In most cases, the change in strain is selected as parameter to be studied. Then the following procedure is used:

- Creation of new stress state by machining or layer removal.
- Detection of the local change in the stress by measuring the strain or displacement.
- Calculation of the residual stress as a function of the strain measured using the elastic theory (analytical approach or numerical calculation s such as FEM).

During the recent years, the incremental hole-drilling method is extensively used. It is sensitive to the first of residual stress. The principle of this technique is simple.

It involves monitoring the change in strain when a hole is drilled in a component with residual stress. These strain measurements can be related to the original residual stress distribution in the analyzed sample at the hole location. The relation between the strain and residual stress can be calculated using calibration coefficients.

The X-ray and neutron diffraction methods are based on the measurement of lattice strains by studying variations in the lattice spacing of polycrystalline materials. The first method measures the residual strain on the surface of the materials and second measures the residual strain within the material sample.

The residual stresses can be taken in account during design of mechanical components. Although this leads to a better knowledge of the fatigue life of parts and reduces the safety coefficients at design stage, it also poses a host of new problems on quality assurance level. All the statistical controls are only applied today to few critical components in aerospace and nuclear industry; this practice has the potential to become widespread. There-fore there is an immediate need to develop rapid ways of checking residual stresses. The methods used in the industries today (X-ray diffraction and the incremental hole method) will not be sufficient in the near future. Other Non Destructive Testing (NDT) techniques (ultrasound, magnetic methods, and acoustic emission) are presently being developed.

2.5.1 Measurement of residual stresses

Out of many methods and techniques proposed for the measurement of residual stresses, only a few may be applied in practice on components ranging from small to very large such as bridges and aircraft. These few include X-ray diffraction, and blind hole drilling with electrical resistance strain gauges. For some of the methods described, the component in which residual stresses are to be measured must be brought to the measure instrument, but for others the measurement devices are portable and may be brought to the component. However in some cases it may be feasible to remove the section from component and brought to the residual

stress measurement instrument. Great caution must be observed in this sectioning because it will change the stress field by relieving and inducing stresses.

Any manufacturing process that changes the shape of solid or where severe temperature gradient exist during the process, causes residual stress. By their very nature, processes that change the shape of a solid cause non-uniform plastic deformation in the solid which lead to the residual stress. These processes include forging, rolling, drawing, machining etc. Also processes that produce high thermal gradients in solid often lead to residual stress. These processes include quenching, casting, welding. Further, the processes that include localized phase changes produce residual stress. These processes include martensitic hardening.

The residual stresses caused by the manufacturing processes usually show very steep residual stress to distance gradients as shown in Figure 2.43.

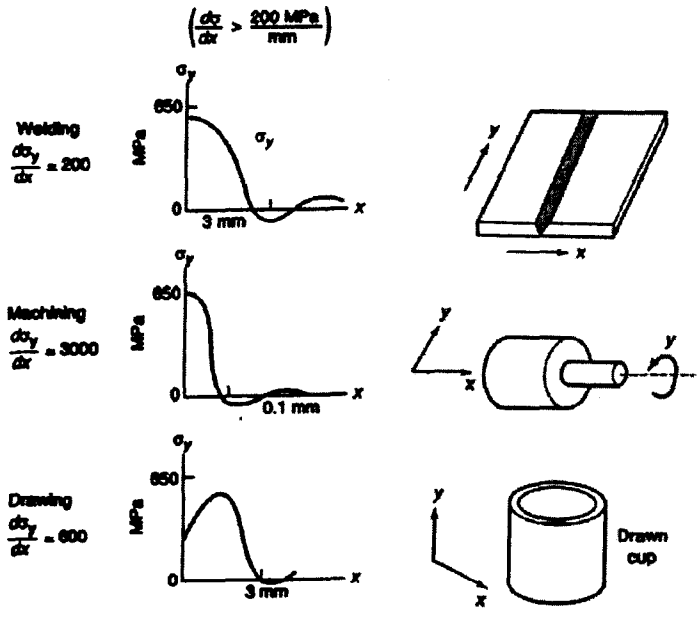

FIGURE 2.43: Residual stress magnitudes typical of 650 MPa yield strength steel

The steep gradient s typical of residual stresses induced by the manufacturing processes has resulted in the disagreement between residual stresses measurement made by the mechanical stress relaxation type methods. The disagreement is

nearly always because the volume of the component of which the stress is measured is not the same in the two methods (Destructive method & XRD method) and thus a different portion of stress is measured by each showed that the hole-drilling method resulted in measured stresses approaching that of the stresses measured at the surface by XRD when the hole drilling results were extrapolated to the surface. Furthermore, because of the steep gradient, unless the stress field caused by the process is well understood stress measurement must be performed at many locations in the manufactured solid in order to establish the magnitude and distribution of stress field of interest. Many researchers in residual stress technique have focused on the enhancing the accuracy of the residual stress measurement and have ignored fact that from a practical stand point, hundreds of stress measurements are needed to define the stress field of interest. Thus many of the residual-stress measurement technique require too much time to perform and are thus impractical. This also includes some the techniques used in XRD, strain gauge and other methods.

2.5.2 Need for residual stress measurements

There must be a valid reason and understanding for measuring residual stress in any component. The major concerns for residual stress measurement are:

- Failures that are suspected as being caused by fatigue, corrosion fatigue, stress corrosion, and hydrogen embitterment.
- Assessment for continued serviceability of a component, for example, life assessment; that is usually focussed on a concern for the in service failure.
- Distortion occurring during processing of a component.
- Distortion of components during storage or in service.

It is very important to understand the mechanism for the inducement of residual stress field of concern. When manufacturing processes or sometimes repair works

judged the most likely source of residual stress, it is often possible to predict the magnitude and distribution of the residual stresses. A preconceived model of the residual stress field will aid in the investigation of the residual stresses and location and number of measurement that need to be made.

A number of procedures and methods have been applied to determine the residual stresses extant in a metallic component, usually as a result of manufacturing processing. However stress is never the quantity measured because stress is quantity that is applied to metal and can only be measured in the process of the application [36]. What is invariably measured to determine residual stress is elastic strain-either the elastic strain resulting directly from the existing residual stress in the metal or the elastic strain change resulting from relief of some portion or all, of the existing residual stress. The stress that is causing, or has caused the strain is then calculated using the applicable elastic constants for the metal.

Mainly there are two types of measurement techniques which are in practice today.

1. Non destructive procedures: – In which we measure the strain response of the metal in response to the residual stresses.

2. Destructive procedures: – In this type of procedures we measure the strain change caused in relieving some or all of the residual stress in the metal.

2.5.3 Destructive measurement procedures

The first concern in selecting destructive residual measurement procedure is whether it is reasonable to destroy one or more components or sample in order to determine the residual stresses.[36] Usually this implies that one or a few of the component are a small portion of the total number produces. Also coupled to this decision is whether the one or more components in which the residual stresses are to be measured are representatives of all the others. In other words, how great is the expected variation of the residual-stress field from part to part.

Destructive methods of residual stress measurements are fundamentally stress-relaxation procedure; that, the information is obtained by relaxing the residual stress in some finite-volume element of the component and measuring the resulting strain change. The strain change is then used, along with applicable assumptions about the nature of the stress field to reconstruct the original stress field. Assumption about the nature of the stress field is whether it is sufficient to assume that the gradients are one or two or three dimensional. Once the decision is made to measure the residual stresses by destructive methods the following procedure has to be followed in typical stress relief method.

2.5.4 Stress-field condition

The engineering problem for which residual stress information is needed must be analyzed. This need is often a result of failure of the component during its service life. Distortion of the product in storage or during manufacturing can also be a concern. The shape of the component, cylindrical, disk, plate etc. or may be some irregular shape much considered. Also along with this, the process by which these residual are generated must be analyzed. The justification for the assumption about the stress field condition such as axial symmetry for the cylinder in which the dominant residual stress field is caused by the quenching during the heat treat processing of about stress uniformity in the surface place of plate where stress gradient with dept is the major concern.

These assumptions and considerations have lead to the methodology where we can construct computational models of stress field from measured strains.

2.5.5 Stress field condition assumptions:

Many engineers and researchers have come up with an approach to measure residual stress using destructive methods with the aid of assumptions about the stress field conditions. These include certain uniaxial, biaxial, tri-axial stress field assumptions as listed in table 2.3.

TABLE 2.3: The destructive residual stress measurement procedures [51]

2.5.6 Strain measurement technique

The method of strain measurement technique and consequently the number and spatial frequency of measurements can be determined. The strain measurement technique selected will greatly affect the resolution of the stress measurement because of the spatial precision inherent in the technique.

There are a number of techniques that been used to measure the strain induced by the relief of stresses due to sectioning or material removal in destructive residual stress measurement. These include mechanical gauges (dial gauges), employed with specially made jigs and fixtures, reflected light schemes, photo elastic, coasting, and electrical resistance, strain gauges and electro resistance strain gauges. However, since the 1960s, the use of the latter has become more important. Due to the variety availability and precision of these gauges, they are available as uniaxial, bi-axial, and rosette gauges of many sizes. Also from 1970s XRD has been used to get the rapid and numerous stress measurements on the sectioned components to gain information regarding the internal stress field. With the strain measurement technique, first the measurement location must be established and element prepared for the measurement by for example attaching strain gauges. Then it is followed by isolation of gauges element and post stress relaxation measurement.

2.5.7 Strain measurement methods

As discussed earlier several methods are also applied for the measurement of strain. Namely,

- Mechanical gauges
- Electrical-resistance gauges
- Optical gauges
- Birefringent method
- Diffraction methods (X-ray and neutron)

- Ultrasonic methods
- Magnetic methods

2.5.8 Non-destructive Procedures

The methods described in this section all measure the change in dimension or strain of the component produced by the removal of the finite volume of stressed metal from the component. Thus they involve measurement of strain by removing the materials so as to perturb the residual-stress field. On the other hand, non-destructive procedures measure a dimension in the crystal lattice of the metal or some physical parameter affected by the crystal lattice dimension. Whenever a mechanical force, resulting in stress that is less than the yield strength is placed on a solid metal component, that component distorts and strains elastically. The elastic strain results in a change in the atomic lattice dimension, and this dimension or change is measured by the non-destructive stress measurement procedures. For example the diffraction methods X-ray and Neutron diffraction methods measure the crystal dimension and this dimension can be related to the magnitude and direction of the stress that the metal is subjected to whether that stress is residual or applied. Subsequently X.-ray diffraction technique exploit the fact that when a metal is under the stress, applied or residual, the resulting elastic strains cause the atomic planes in the metallic crystal structure to change their spacing. X-ray diffraction can directly measure this inter-planar atomic spacing from this quantity, the total stress on the metal can then be obtained. Since the metals are composed of the atoms arranged in regular 3D array to form a crystal, most metal components of practical concern consist of many tiny grains randomly oriented with respect to the their crystalline arrangement and fused together to make a bulk solid.

When such a polycrystalline metal is placed under stress, elastic strains are produced in the crystal lattice of the individual crystallites. i.e., when an applied stress or residual stress is within the material, is below the yield strength of the

FIGURE 2.44: Typical X-Ray Diffraction methods [36]

material, is taken up by inter-atomic strain. X-ray diffraction techniques can actually measure the inter-atomic spacing that are indicative of the elastic strain in the specimen. Stress values are obtained from these elastic strains in the crystals by knowing the elastic constants of the material and assuming that stress is proportional to strain in a reasonable assumption for most metals and alloys of concern.

Neutron diffraction method The neutron diffraction method is capable of measuring the elastic strains induced by the residual stresses though the volume of relatively thick steel components with spatial resolution as small as one cubic millimetre.

Such capabilities provide for residual stress measurement inside the components without sectioning or removing the metal layer from the component. Principal neutron methods as with XRD measure the spacing between crystallographic planes in

FIGURE 2.46: Drawing showing mini XRD with major dimensions [51]

a component, and this spacing is affected by the residual stress and applied stress. The spacing between a selected set of crystallographic planes is related to the angle of incidence and diffraction of the neutron radiation which are equal and the wavelength of the monochromatic radiation by Bragg's law. The elastic strain induced by the residual stress is perpendicular the diffracting crystallographic plane then is related to d by:

$$\epsilon = (d - do)/do \tag{2.34}$$

Where, do is the distance between the unstressed crystal planes.

If the principal stress directions are unknown, strains in at least six directions must be measured to determine residual stresses acting on the volume of the material in which strains are being measured.

Residual stress in the forming of materials

Except casting components, all the metal products are subjected to more than one metal working process. Such operations can be very diverse, but all have the same primary objective: to produce a desired shape change. Metal forming can be divided into hot forming and cold forming. Cold forming is defined as forming processes or plastic deformation operation carried out at temperature below the recrystallization temperature of work piece materials, but more often it is simply referred to as forming process at room or ambient temperature.

In a nutshell, residual stress plays very important role with respect to the different properties of materials. The gain obtained from the presence of the residual stress can enormous. Here it has been shown that it is now possible to predict the fatigue life of materials, taking residual stress into consideration. The results also show that it is possible to predict residual stress relaxation and fatigue life, with consideration of the influence of the residual stress by the FEM. It has been found that calculated results of fatigue life at surface agrees very well with experimental results.

With the development of the different experimental, numerical techniques and numerical methods, it is now possible to introduce residual stress into the design office for the integrated design of mechanical components.

This offers a new concurrent engineering approach applied to the design of mechanical parts taking residual and applied stress into account. Figure 2.47 shows the different connections between residual stress-integrated design and other sectors that use the concurrent engineering approach. A mechanical component design can simulate dynamic characteristics, material processing, and product life.

Consideration of residual stress is becoming increasingly important for mainly two reasons; the introduction of multi-materials that induce residual stress and

FIGURE 2.47: Connections between residual stress integrated design and other sectors [52]

need for the design to reduce the weight of the components in order to remain competitive in terms of cost and quality of product. Basic research has brought a better understanding of phenomena relating to the residual stress. For industrial application future developments in the following areas is necessary.

Measurement techniques

- Improvements in the ultrasonic and magnetic measurement methods.
- Integration of portable optical method for strain measurement in destructive techniques.

Processing of materials

- Development for the industrialization of new pre-stress processes, ultrasonic shot peening, laser shock, surface nano-crystallisation and so on.
- Optimization of the residual stress in advanced materials, functional gradient coating system, CV, DLX, coating, metal matrix composites, electronic packaging

Modelling

- Development of the advanced tools for the prediction of initial residual stress in the various process; forging, casting, machining, welding, coating, composite processing, electronic packaging manufacturing, mechanical surface treatment.
- Integration of the residual stress modelling method into the global life design and creation of optimization codes for the design mechanical components using the concurrent engineering approach.

2.6 Summary

Unbonded flexible pipes are designed and analysed in accordance with the relevant API standards. The design of pressure armour wire is covered in the API Specification 17J [65] which define the design guidelines and technical requirements for safe, dimensionally and functionally interchangeable unbonded flexible pipes. The same API specification also defines the minimum system requirements; design loading cases for analyses; minimum material requirements and finished product acceptance criteria. The accountability of residual stress in the material is covered in the API specification 17B [66]. It is generally believed that safe pipe design is guaranteed by complying with API specifications 17J and 17B.

For the design of pressure armour, the API Specification proposes the use of stress "utilisation" which is the ratio of average hoop stress in the layer and the structural capacity of the material. The structural capacity shall be either the yield strength or 90% of the ultimate tensile strength (UTS) of the wire material, whereby the average stress is to be calculated based on distributing the total layer load uniformly over all wire in the layer.

According to API 17J, the utilisation of the pressure armour wire is limited by the operation and service conditions. However for the case of Normal recurrent operation, the utilisation can be up to 0.55, whilst for the case of Normal extreme

operation, the utilisation can be up to 0.85. For the Factory Acceptance Test (FAT) condition, a maximum utilisation of 0.91 is given. The API Specification does not define or recommend any specific analytical or numerical tools for evaluation of the "utilisation" factor, nor does it give any recommendation for stress analysis or strain calculations. Effects like local stress concentrations and residual stress from manufacturing which are important for service life are not considered in design calculations.

During pipe manufacture, the pressure armour wire experiences severe plastic deformation coupled with a rather complicated stress-strain history as it undergoes a sequence of bending and twisting events. Due to practical difficulties no post-deformation stress relief operation can be conducted after the wire has been wrapped to the pipe. Stress analysis of pressure armour is usually performed considering only the applied load conditions; the plastic deformation introduced during the wire forming process is rarely considered. It is believed that the prestress introduced in the pressure armour wire during the manufacture of the pipe would significantly influence the stress distribution and the magnitude of the local stress in the wire. The local stress distribution in the pressure armour layer is usually obtained from FE analysis. Axisymmetric wire models are commonly used since they permit the modelling of the interaction of neighbouring wires while conforming to the pipe structure, however, an accurate assessment of the effect of aforementioned residual stress is not feasible with such models. The literature review reveals that there is no previous work has been carried out on detailed 3D analysis of residual stress in flexible pipes either by analytical or numerical methods. Further study of the effects of residual stress on service loads on pipes has not been done and the current work is an attempt to fill the gap in knowledge base.

In the present research work a new method of stress analysis is presented for the pressure armour and tensile armour layers. The method uses an FE 3D wire model and allows the local stress distribution in the wire to be evaluated considering the residual stress induced in the wire during the pipe manufacturing. The method is demonstrated for both pressure armour wire and tensile armour wires. The results

from the 3D model are compared with those from the 2D axisymmetric analysis. The effects of residual stresses due to manufacturing process have been considered for service loads.

Chapter 3

The Finite Element Strategy

3.1 Introduction

Over the last thirty years, the finite element method has gained wide acceptance as a general purpose tool for structural modelling and simulation. The finite-element method is used to solve a mathematical model, which is the result of an idealization of the actual physical problem considered. The mathematical model is based on assumptions made regarding the geometry, material conditions, loading, and displacement boundary conditions. The governing equations of the mathematical model are in general partial differential equations subjected to boundary conditions. These equations cannot be solved in closed analytical form. Therefore, numerical methods have to be used to obtain a solution. One such numerical method is the Finite Element method. Finite-element methods are in abundant use in today's engineering practice through various general-purpose commercial computer programs and many special-purpose programs written for specific applications. These techniques are, to an increasing extent, being used to help identify good new designs and improve designs with respect to performance and cost. Typical finite element programs consist of several hundred thousand lines of procedural code, usually written in FORTRAN which stands for formula translation. The codes contain many complex data structures which are accessed throughout the

program. For the sake of efficiency, the various components of the program often take advantage of this accessibility. For example, elements, nodes, and constraints may directly access the matrices and vectors involved in the analysis to obtain and transmit their state information.

The overall FE modelling strategy for flexible pipe is shown schematically in Figure 3.1. The strategy involves satisfying equilibrium and compatibility conditions for the pressure and tensile armours to find common interface pressure and contact loading. Service loads are applied for total stress analysis. The analysis starts with 3D FE modelling of both wires to simulate residual stresses as shown by the two extreme end blocks in the diagram of the Figure 3.1. A similar second 3D FE model is generated for both wires for pressure analysis as shown by middle blocks in the diagram of the Figure 3.1. The FE results are compared with XRD measurements of est samples. The stresses from the residual stress analysis are fed into the pressure analysis models and applied with internal and external pressures. The radial expansion and contraction of wires are plotted to determine common interface pressure satisfying equilibrium and compatibility conditions. Factory acceptance test is carried out to check the residual stress relaxation.

Pressure armour layer and tensile armour layer have been considered mainly for the analysis with residual stresses and contact behaviour. Since two layers are designed to carry different loads when the pipe is in service, each component is separately analyzed for their corresponding loads. The geometry and structural configuration of both layers are different. This makes it extremely difficult to apply boundary conditions to consider them in one single model. Also the transfer of residual stresses from pre-analysis is impossible to satisfy equilibrium and compatibility conditions. Residual stresses affect both in different ways for local plastic deformation. Contact in Pressure armour coils gives rise to friction and fretting damage and there is no contact between pressure armour layer an tensile armour layer.

Some manufacturing processes can result in residual stresses and strains in a finished component, which remain in the component throughout the service life.

Many manufacturing processes can be simulated with a high degree of confidence as in case of any FE based stress analysis. The transfer of the residual condition to initialise the in-service loading analysis is not performed routinely. This present work investigates the effects of residual stresses developed during manufacturing on pipe's structural performance. A method for simulating and transferring the effects of the manufacturing process to a structural behaviour of a flexible pipe is discussed.

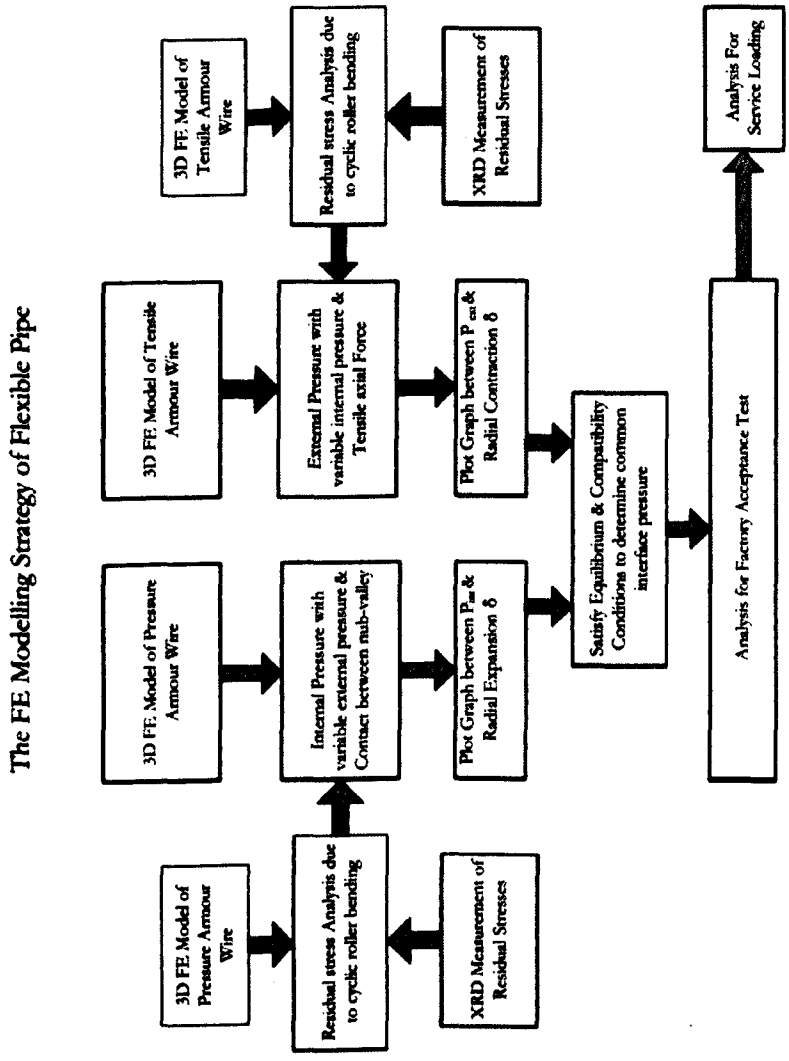

FIGURE 3.1: FE Strategy for Flexible Pipe to analyse Residual Stress and Service Loads

X-Ray measurement of residual stresses have been carried out and good agreement between numerical and experiment is demonstrated.

Internal fluid pressure unwinds the coils applying side wall to wall contact pressure. Due to this pressure and radial expansion of coils, a grinding action occurs which damages (fatigue) the mating sections of wire. Owing to the manufacturing processes involved, these two components suffer from the effects of residual stress before they are actually put into service. The residual stresses are high enough to cause plastic deformation under service loads such as bending and torsion. Hence both pressure armour and tensile armour have to be modelled for pre-stresses before analyzing for fluid pressures, axial and torsional loads. A residual stress analysis is carried out to simulate the manufacturing process (cold working), obtaining fairly accurate values of residual stress distribution. Further, the models pre-stressed with residual stresses are analyzed for service loads. The pressure armour is subjected to internal fluid pressure and variable external pressure with contact between adjacent layers. Tensile armour is subjected to external pressure and variable internal pressure with axial force as shown in Figure 3.2.

Graphs are plotted to satisfy equilibrium and compatibility condition to find common interface pressure, radial displacement and contact pressure. FAT condition is simulated to see the level of residual stress relief. Service loads are then applied for total stress analysis. Experimental results of residual stress measurement by XRD are compared to FE values and are in close agreement. Further variable pressures are applied on tensile and pressure armour wires to determine interface pressure and overall structural response. This is achieved by considering the 1/8th diameter of the pressure and tensile armours in contact and applying corresponding boundary conditions. The method takes full advantage of helical symmetry of both pressure armour and tensile armour layers. The results of this simplified analysis will be used to compare the full 3D FE analysis.

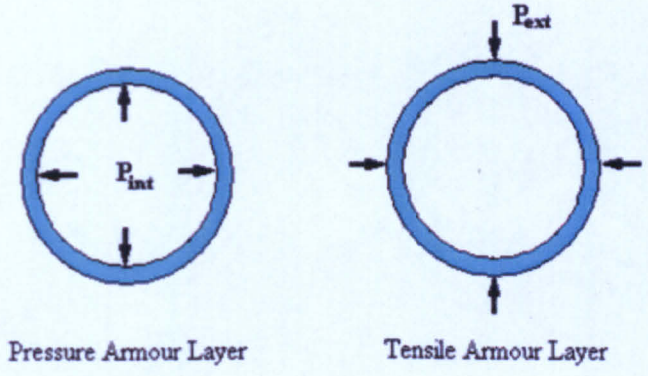

FIGURE 3.2: PA and TA loads for FE Analysis

3.2 FE Model of Pressure and Tensile Armour wires

Mainly two load bearing layers are considered for finite element analysis; first pressure armour layer which is designed to provide hoop strength against pressure as shown in Figure 3.3, secondly, tensile armour layer to provide longitudinal strength to withstand tensile load due self-weight as shown in Figure 3.4.

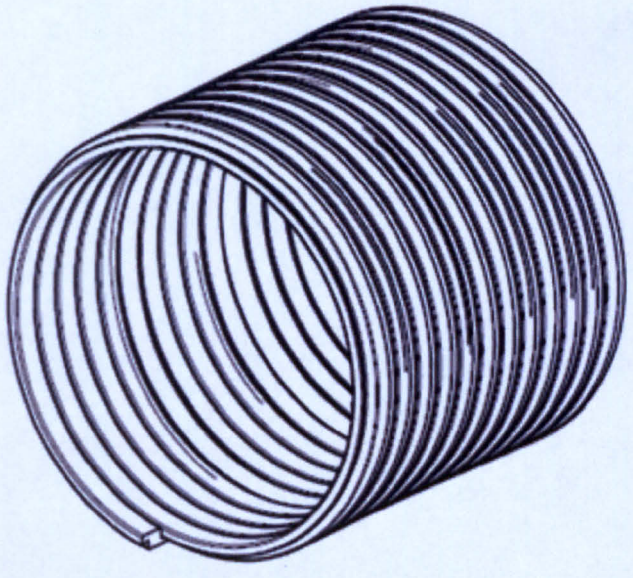

FIGURE 3.3: Pressure Armour Layer

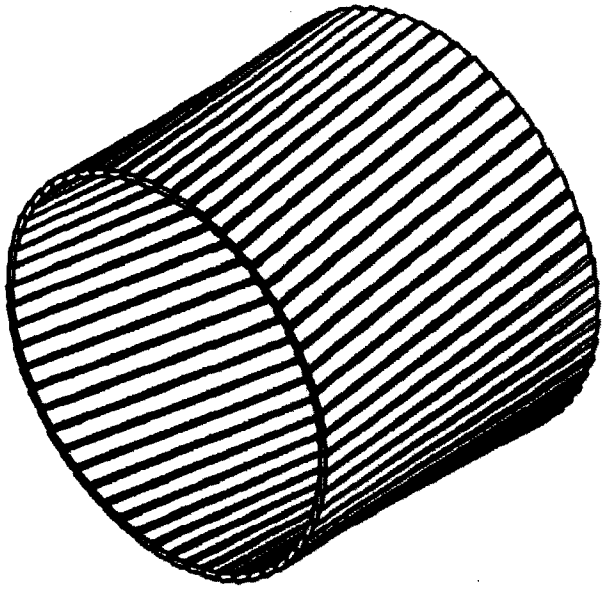

FIGURE 3.4: Tensile Armour Layer

The layers are unbonded in the sense; there is a relative motion between layers and wires under the action of external loads. The pressure armour and tensile armour wires are separated by non-metallic layer of material in order to avoid abrasion during service or installation. The helical pitch of tensile wire is large compared to pressure wires resulting in right angled contact between wires. The two wires are modelled separately with individual boundary conditions but form a segment of a section of flexible pipe. The interlocking arrangement of pressure armour wires and the pipe manufacturing process is shown in Figure 3.5.

The clearance between nub and valley and clearance between adjacent wires are to provide axial and circumferential flexibility. When the pipe is transported to sea, it is wound on large bobbins and carried on barges, then it is unwounded to install, the flexibility plays a crucial role to avoid damage. The tensile armour wires support the weight of pipe when it hung vertically into sea at depths ranging from 100 m to 2500 m. As the deep water exploration becomes inevitable, the pressure and tensile armour wires are subjected to large strain both during installation and operation. The tensile armour wires are under tension and they get compressed due to their helical arrangement, imparting lateral strength to pressure armour wires.

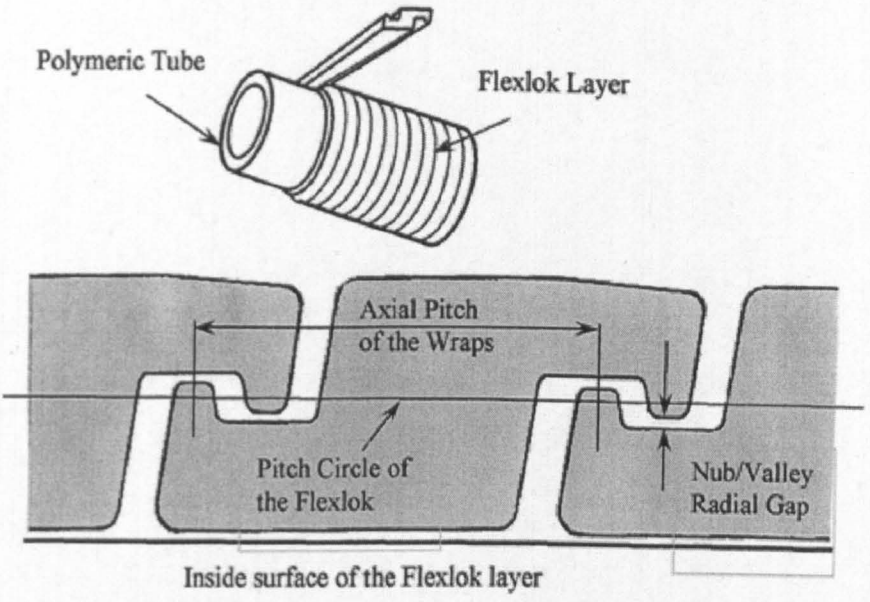

FIGURE 3.5: Pressure armour wire winding and interlocking mechanism

The finite element model of pressure armour wire consists of two adjacent wires incorporating nub-valley contact so as to simulate bending and pressure loadings. Since pressure armour wire has unique profile to accommodate interlocking, there are regions where contact occurs. In order to minimise the FE calculations half sections of adjacent wires is considered as shown in Figure 3.6. The sectioned faces of two wires represent the continuity of the pipe's length.

To model this behaviour, these two faces have been tied. That is, the nodes on face 'A' are tied or coupled with corresponding nodes on face 'B'. The displacement of nodes in all the three directions on face B reflect the displacement of nodes in all the three directions on face A. If a node on face A moves a unit length in X direction so does the corresponding node on face B and is similar in the Y and Z directions.

The finite element mesh is created as shown in Figure 3.7 which is extruded 3D model of 2D elements. The commercial code ANSYS is employed for the present work. The 2D mesh is created using MESH200 elements and new generation SOLID186 elements are used for 3D extrusion. The SOLID186 has 3 degrees of

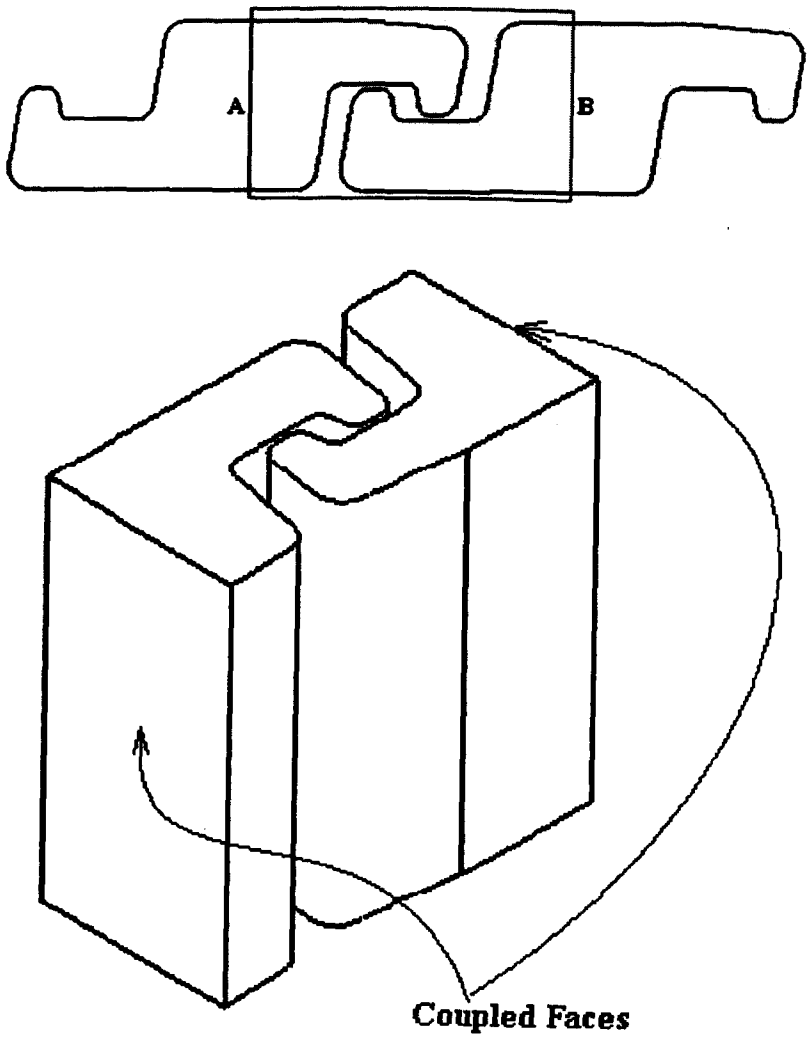

FIGURE 3.6: Pressure armour wire and FE model

freedom; translations in the nodal x, y, and z directions. The element has plasticity, hyperelasticity, stress stiffening, creep, large deflection, and large strain capabilities [52]. It also has mixed formulation capability for simulating deformations of nearly incompressible elastoplastic materials, and fully incompressible hyperelastic materials.

Elastic material properties are defined by specifying Young's modulus and Poisson's ratio. Since the present case is elastic-plastic bending, the tangential modulus has to be defined. Most common engineering materials exhibit a linear stress-strain relationship up to a stress level known as the *proportional limit.* Beyond this limit,

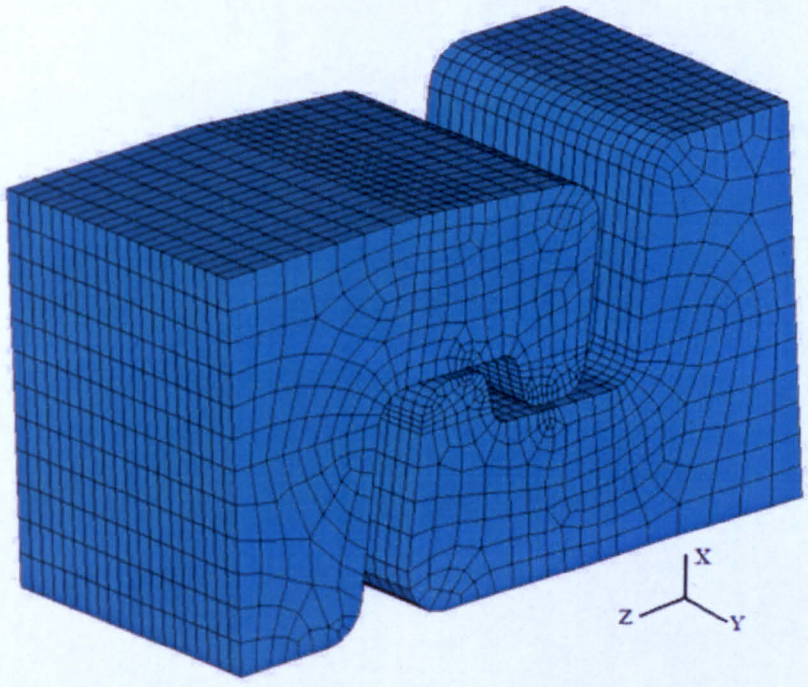

FIGURE 3.7: FE mesh of Pressure Armour wire

the stress-strain relationship will become nonlinear, but will not necessarily become inelastic. Plastic behaviour, characterized by non-recoverable strain, begins when stresses exceed the material's *yield point.* Because there is usually little difference between the yield point and the proportional limit, the software assumes that these two points are coincident in plasticity analyses. An example of engineering stress-strain curve is shown in Figure 3.8 with various terms highlighted. Plasticity is a non-conservative, path-dependent phenomenon. In other words, the sequence in which loads are applied and in which plastic responses occur affects the final solution results.

In elastic-plastic bending, loads should be applied gradually as a series of small incremental load steps or time steps, so that the model will follow the load-response path as closely as possible. The automatic time stepping (AUTOTS) [26] feature in software will respond to plasticity *after* the fact, by reducing the load step size after a load step in which a large number of equilibrium iterations was performed or in which a plastic strain increment greater than 15% was encountered. If too large a step was taken, the program will bisect and resolve using a smaller step

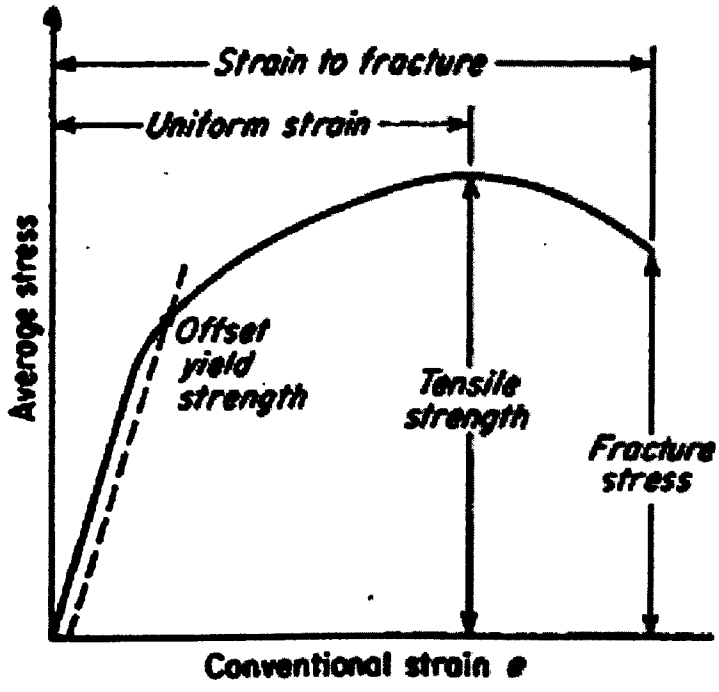

FIGURE 3.8: Engineering Stress–Strain curve

size.

There are two options, namely, TB, KINH, and TB, MKIN, available to model metal plasticity behaviour under cyclic loading. These two options use the Besseling model also called the sub layer or overlay model. The material response is represented by multiple layers of perfectly plastic material; the total response is obtained by weighted average behaviour of all the layers. Individual weights are derived from the uniaxial stress-strain curve. The uniaxial behaviour is described by a piece-wise linear "total stress-total strain curve", starting at the origin, with positive stress and strain values. The slope of the first segment of the curve must correspond to the elastic modulus of the material and no segment slope should be larger. In the following, the option TB, KINH is described first, followed by that of TB, MKIN.

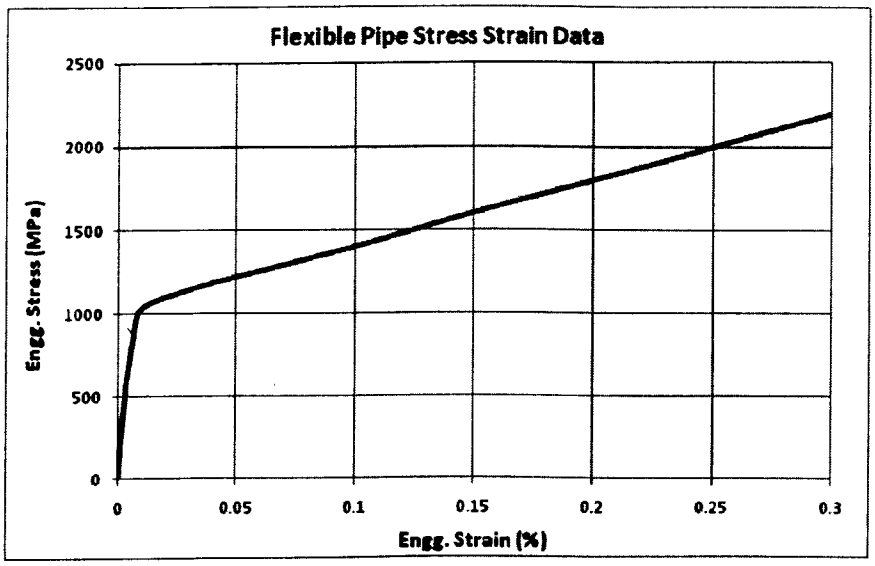

FIGURE 3.9: Material property used in program

The KINH option is recommended because layers are scaled (Rice's model), providing better representations. The KINH option allows defining up to 40 temperature-dependent stress-strain curves [52]. To define more than one stress-strain curve for temperature-dependent properties, each curve should contain the same number of points (up to a maximum of 20 points in each curve). The assumption is that the corresponding points on the different stress-strain curves represent the temperature dependent yield behaviour of a particular sub layer. Multilinear kinematic hardening material model is used for the present analysis. The stress-strain points used in software is plotted and same points are defined in the program as shown in Figure 3.9. The material properties of the flexible pipe is summarised as below:

- Material Type: High Strength Carbon Steel
- Modulus of elasticity: 205 GPa
- Poisson's Ratio: 0.3
- Yield Strength: 1093 MPa (Tensile)
- Density: 7850 Kg/m3

3.3 Contact Modelling

Contact problems are highly nonlinear and require significant computer resources to solve. Due to the nonlinear nature of the contact mechanics, such problem in the past was often approximated by special assumptions within the design process. Due to the rapid improvement of modern computer technology one can today apply the tools of computational mechanics to simulate applications which include contact mechanisms numerically. This can be to an accuracy which is sufficient for design process. However, even now most of the standard finite element software is not fully capable of solving contact problems, including friction, with robust algorithms. Hence there is still a challenge for the finite element society to design efficient and robust methods for computational contact mechanics.

Due to this verity, contact problems are today combined with large elastic or inelastic deformations, including time dependent responses. Hence a modern formulation within computational mechanics has to account for all these effects, leaving the linear theory as a special case. For most industrial applications numerical methods have to be applied since the contacting bodies have complex geometry or undergo large deformations. Today one can distinguish several branches in computational mechanics which are applied to solve different classes of contact problems. Finite element methods, applied to problems undergoing small and large deformations, as well as in elastic range or inelastic range. Discrete element methods, used to compute problems in which up to 10^8 particles coming into contact. Multi-body systems are based on a description of bodies as rigid ones. These systems generally small, and can be applied to model the dynamic behaviour of engineering structures in which contact is also allowed.

Generally, in the case of contact, two different states of structural systems are possible. One is related to open gap, the other to the closed gap. Both cases were solved using a different equation system which means that the topology of the structure changes due to the contact. This points out one of the difficulties when solving contact problems: the system matrix changes its size (or non-zero form) with active or inactive constraint equations. This can also include a change

of topology when one finite element node moves during the deformation process from one element to another. Further more, there is a choice between different methods for the treatment of contact problems, including the Lagrange multiplier or penalty formulations. The former introduces additions variable in the systems but does fulfil the constraint equations correctly, the later leads to non physical penetration but has no additional variables. So both methods have advantages and disadvantages which are beyond scope of present work.

Contact problems fall into two general classes: rigid-to-flexible and flexible-to-flexible. In rigid-to-flexible contact problems, one or more of the contacting surfaces are treated as rigid (i.e., it has a much higher stiffness relative to the deformable body it contacts). In general, any time a soft material comes in contact with a hard material, the problem may be assumed to be rigid-to-flexible. Many metal forming problems fall into this category. The other class, flexible-to-flexible, is the more common type. In this case, both (or all) contacting bodies are deformable (i.e., have similar stiffness). An example of a flexible-to-flexible contact is bolted flanges.

To model a contact problem, the parts must be identified to be analyzed for their possible interaction. If one of the interactions is at a point, the corresponding component of the model is a node. If one of the interactions is at a surface, the corresponding component of the model is an element: a beam, shell, or solid element. The finite element model recognizes possible contact pairs by the presence of specific contact elements. These contact elements are overlaid on the parts of the model that are being analyzed for interaction. The contact region is between adjacent wires of pressure armour layers shown in Figure 3.10.

Contact elements are generated at the interface by CONTA 173 & TARGE 170. Element faces are determined from the selected node set and the load faces for that element type. The operation is similar to that used for generating element loads from selected set of nodes, except that elements, instead of loads, are generated. All nodes on the face are selected for the face to be used. If nodes are shared by adjacent selected element faces, the faces are not free and no element will be

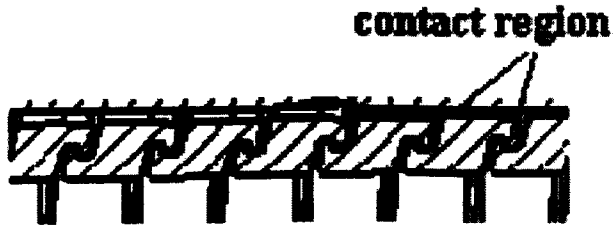

FIGURE 3.10: Pressure Armour interlocking & contact region

generated. Elements created by ESURF will be oriented such that their surface load directions are consistent with those of the underlying elements. Generated elements, as well as their orientation, should be checked carefully. Generated elements use the existing nodes and the active MAT, TYPE, REAL, and ESYS attributes, except when Tlab = REVERSE. The reversed target and contact elements will have the same attributes as the original elements. If the underlying elements are solid elements, Tlab = TOP or BOTTOM has no effect. By default, when the command generates a target element the shape will be the same as that of the underlying element. While not recommended, you can issue ESURF,,,TRI to generate several facet triangle elements.

The Procedure of solution for non-linear contact analysis

This can be classified under three categories as below:

- Identification of the convergence problem.
- Solve for convergence.
- Get accurate solution.

The following flow chart summarizes the problem as shown in Figure 3.11 and Figure 3.12

1. Identification of convergence problem.

- Draw the Free body diagram (FBD) of the problem, this helps in identifying the contact element angle and the load path.

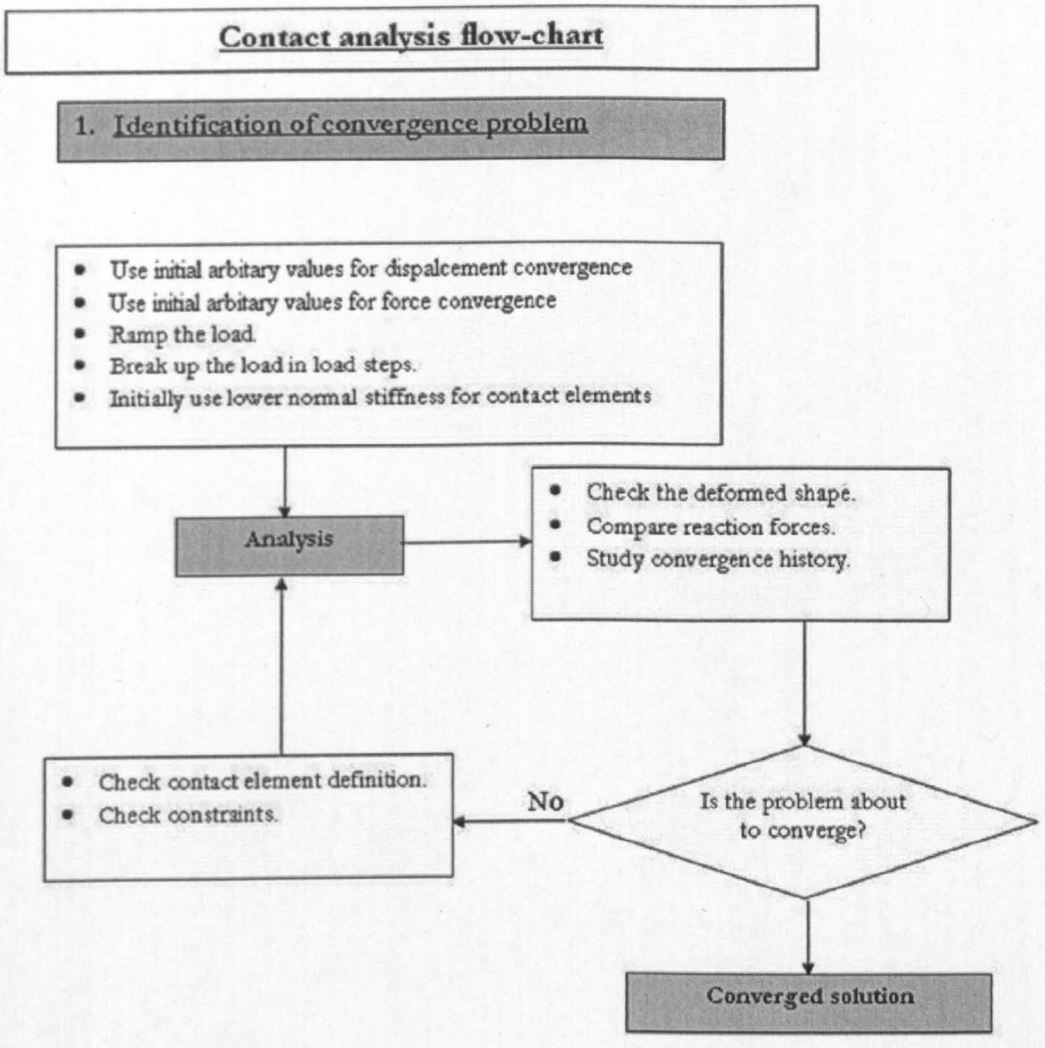

FIGURE 3.11: Contact analyses procedure for convergence

- Compare the deformed shape with expected sketches.
- Compare the reaction forces with hand calculations.
- Study the convergence history.

From the convergence histories find out if the problem is,

- Bouncing
- Bisecting

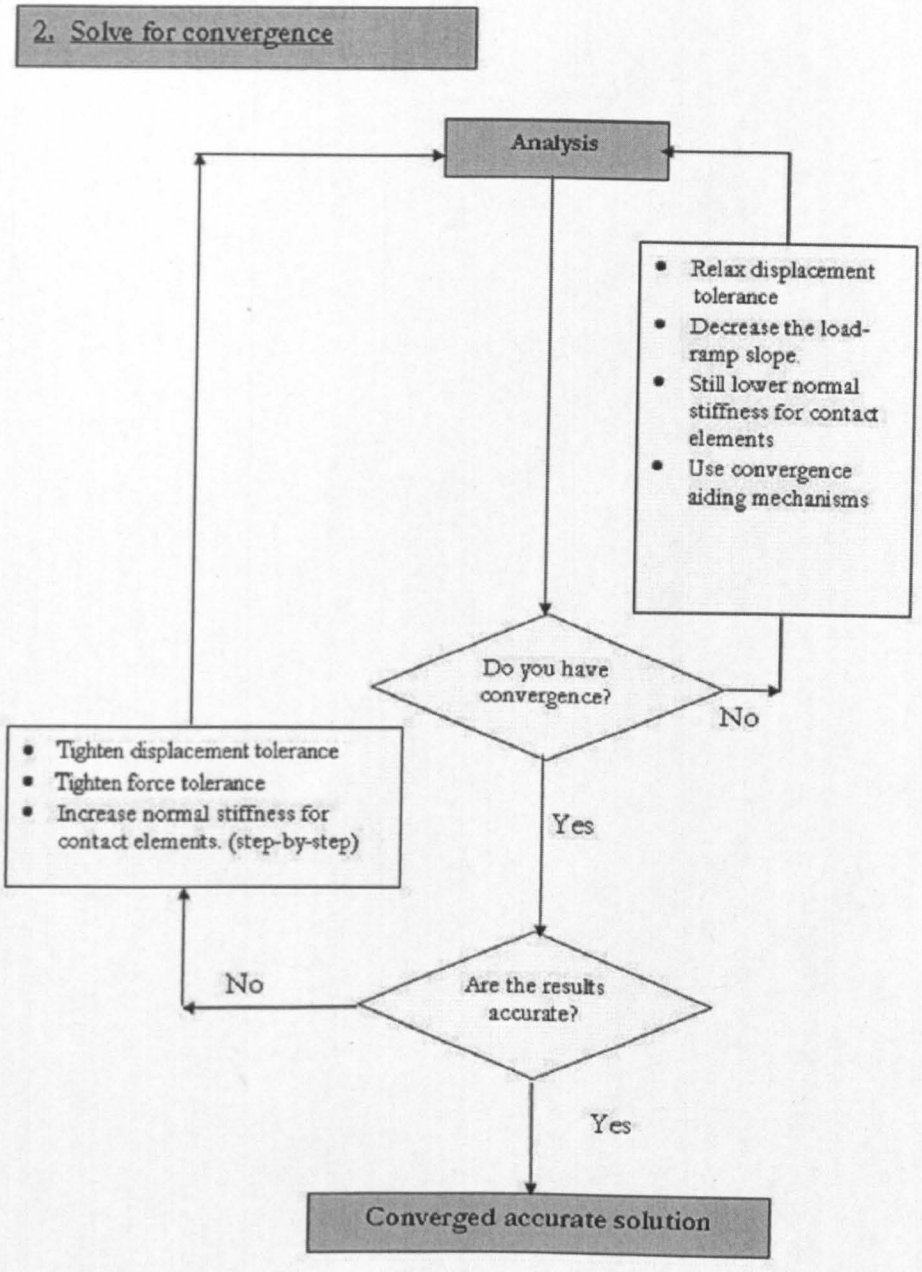

FIGURE 3.12: Contact analysis convergences

- Diverging

If the analysis is not doing any of the above and the problem is not solving then the reason could be because of,

- Improperly defined Constraints or

- Improperly defined Contact elements (like contact element angle)

2. Solve for Convergence

Use loose displacement convergence criterion:

As an aid to get convergence, use relaxed displacement criterion. Displacement-based criterion is a relative measure of convergence, hence much easier to satisfy. For example, during structural analysis of rotor assembly an initial displacement convergence value could be 0.01.

Use loose force convergence criterion:

To obtain convergence, use very loose force convergence tolerance. For example, during structural analysis of rotor assembly initial force convergence tolerance value could be 5000 N.

Ramp the load:

Applying the load or ramping the load gradually, within a load step can lead to convergence. This can be done by specifying sub steps.

Break up the load in load steps:

Applying the loads in load steps also helps in ramping the load.

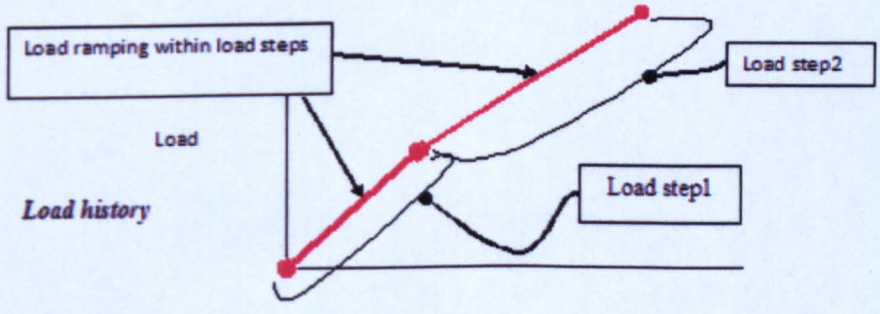

FIGURE 3.13: Ramp Loading

Use lower normal stiffness for the contact elements:

To help obtain convergence, use a low value for the normal stiffness for the contact elements initially. A general method for estimating the normal stiffness value:

Assume the contact region displacement (d) = 1 mm

Number of elements / mm^2 (near the contact region) = N / mm^2

Normal contact element stiffness to be used = kN / mm

Therefore, force / area = 1 (mm) × N (elements / mm^2) × kN (Newtons / mm) = N × kN (newtons / mm^2)

Compare the above number with Young's Modulus. The final value for (force / area) number should be about 100 times larger than E, for displacement controlled problem. In the case of force controlled problem, this number could be lower than E. If convergence is still a problem, then try any one or combination of the points mentioned below will help.

Relax displacement criterion:

Widen the displacement criterion boundary (if 0.01″ was used try using 0.1″)

Decrease the load-ramp slope:

Apply the load more gradually. Increasing the number of sub-steps using the "NSUBS" command could do this.

Still lower normal stiffness for contact elements:

Decrease the normal stiffness for the contact elements (if 30E4 N/mm was used try 30E3 N/mm)

Use soft Link elements:

There are three different methods by which Link elements can be used for convergence. To avoid rigid body motion, tie the parts, which are in contact with the soft link elements as shown in Figure 3.13.

- Solve the model, as an individual part along with contact elements and find out which part is unstable. Tie that part, which is unstable by using link elements with the node outside the model, which is constrained in all

directions. The corresponding nodes with the part are chosen in such a way that to arrest all movement of that part as shown in Figure 3.4.

- Insert Link elements across the contact surfaces. It is not very robust, which requires that you should know in advance which surfaces could be in contact. Especially with a transient, this can change and could be tough to accomplish. Hence, this method cannot be used in analyses, which includes Transient Structural phenomenon.

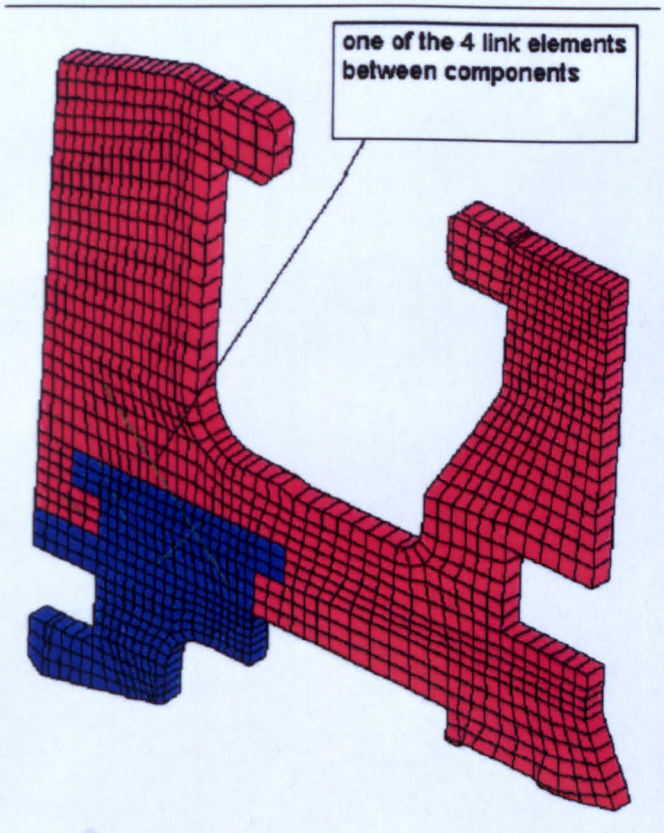

FIGURE 3.14: Link elements tying various parts

In the Link elements, one can play with Stiffness and Area to get convergence. If link elements are too stiff then they will transfer more force than contact elements. To ensure accurate solution, the link elements used to aid convergence should not transmit large forces. A force about 0.1% of the total force transmitted by the contacts is considered safe.

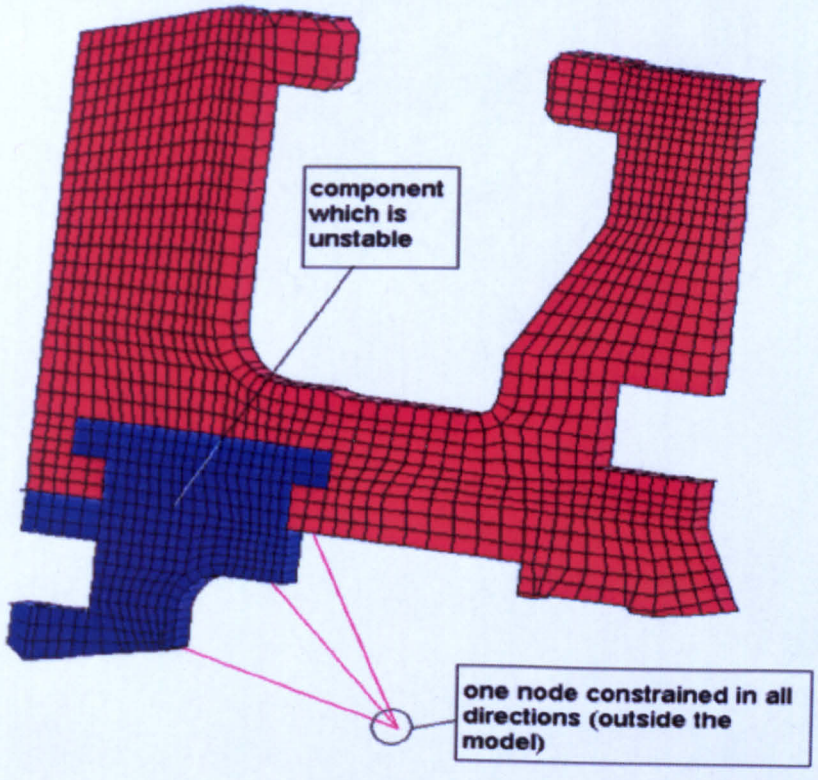

FIGURE 3.15: Link elements constraints

To arrive at an appropriate stiffness value for Link elements, first find the load transferred by link elements with very high stiffness value and then do reverse calculation to find the stiffness value for a force corresponding to 0.1% of total load transferred by contact elements. Find the Stiffness using formula,

$$(AE/L)$$

where, A is the area of link elements, E is the Young's modulus applied and L is length of link elements.

Find the deflection using this stiffness and the force transmitted by each link element from analysis, by delL= Force from analysis/Stiffness.

For the above delL, find the stiffness corresponding to the allowable force that can be transmitted by Link elements. Find the E value in a reverse manner and apply over the model.

To keep the Link force low, one needs to keep the deflection and stiffness low. Too low stiffness could make the stiffness matrix an ill-conditioned one and also it is not allowed to develop tension. Hence, it has to be optimized.

Apply Initial Interference

The whole idea behind this method is explained as follows.

If the model looks like Figure 3.16(A) and to make it stable, it would be changed to Figure 3.16(B).

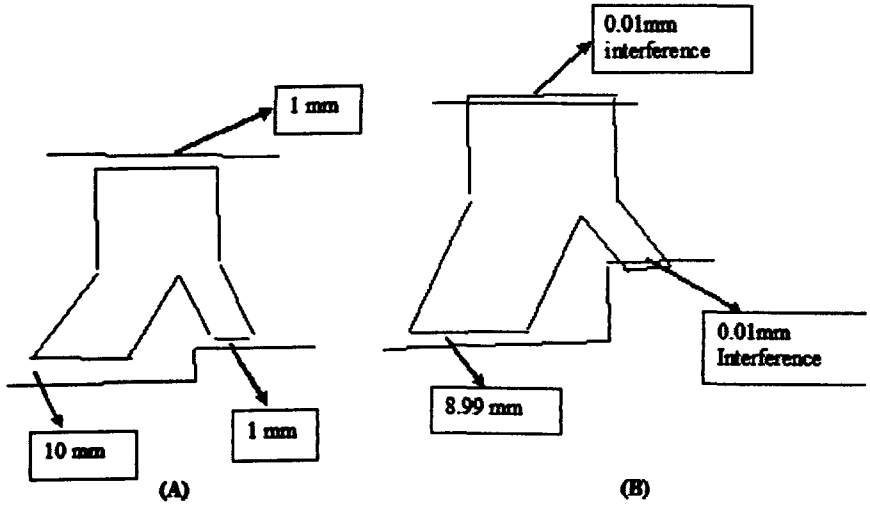

FIGURE 3.16: Contact interface

Obviously, A and B are not identical, idea is B will act similar to the way A behaves.

This is the best solution to insure stability and maintain a robust design. It works when the problem is not displacement controlled. Therefore it can get away with a small contact stiffness, x N/mm. A very small initial interference I mm, together with a low contact stiffness, x N/mm result in $x \times I$ N of load transmitted across the gap per contact set. This is a "pre-load".

Start with a higher interference value, run without loads (i.e., only with interference), examine the stress distribution, these stresses are not at all correct. They are due to interference that doesn't exist in the real part. If they are small enough

(is purely an engineering judgement), then it is fine. If not, reduce the interference some more. Small initial interferences result in more iteration. If it is too small the model is unstable. In general, engineering judgement says an unreal (fake) stress of 5 MPa or less in non-critical regions (not highly stressed in real part), and 1 MPa in critical regions probably is right.

This method will remain stable, but may require adjustment of the initial interference, depending on the following:

- The pre-stress is equal to the pre-load times the number of contacts per square mm, which acts like a pressure load. If the pre-stress is more than 5% of the real stress in the regions of interest, adjustment probably needs to be made. This is not a hard and fast rule, but just an engineering judgement situation. If the pre-stress occurs in an area that is not life-limiting then it can be ignored.
- Thermal growth can cause an increase in "pre-load" across a gap, unnecessarily increasing the pre-stress.
- If more than $x \times I$ newtons of load is reacted for each node on one face, the opposite face will have no load, and the model will be unstable again.

Note: The above point can be explained with the help of following example:

Imagine a bar from one wall to another. The bar is heated, causing a compressive load of 100 N (for example). So each end reacts out 100 N, net force on the bar is zero. Which is why, it is not in motion. Assuming some real world friction at each end (m=0.5, for example), this bar is not going anywhere. Now, slowly grab the bar in the middle and pull in the direction of the bar's axis (long way). If it is pulled by 10 N, the reaction load at one end of bar is 90 N, other 110 N. Still stable, pull 75 N, loads are 25 N and 175 N. Still stable, pull 101 N and reaction load is 101 N on one end, zero on other. This time it is not stable. Solution diverges, an infinitesimal transverse force puts the system out of balance, and the bar is in motion.

If each side of an initial interference is carrying close to 3 N, the initial interference can be reduced to reduce the pre-stress. In other words, each opposing interference pair can be adjusted independently to maintain stability by minimize pre-load.

Apply Pre-Displacement:

Apply prescribed displacements between the parts, which are in contact in the first load step. Then delete the displacements in the subsequent load-steps. The idea is to actuate the contact elements. Again, this is also not very robust, which requires that you should know in advance which surfaces would be in contact. Especially with a transient, this can change and could be tough to accomplish. Hence, this method cannot used in analyses, which includes Transient Structural phenomenon.

Use Couplings:

Define couplings between the mating parts. Couplings should be deleted in sub-sequent load steps. It is advised to delete the couplings one-by-one, as by doing so the load is applied gradually.

All the methods discussed above are effective, only when the behaviour of the model is known in advance. This can be done for structural analysis by calculating the net force balance in the model and finding the way the model behaves.

One important thing is debugging on a partial model instead of full model. Hence computer time is not an issue. Select only the portion of the model, in such a way to simulate the entire model (for example, for cylindrical model, selects few elements from symmetry face). Use this model for getting the converged solution. Once, the solution converges, get back to full model.

Tighten displacement criterion:

Once convergence is achieved with a loosened displacement tolerance value, this value should be tightened. Tighten the displacement convergence tolerance value step-by-step.

If the tolerance is within the range of $0.1''$ tighten to $0.05''$ to $0.001''$ to $0.1E-3''$. Restarting from the converged solution can solve the problem.

Tighten force criterion:

Force based convergence criterion provides an absolute measure. Displacement based convergence criterion provides a relative measure. Therefore, to get accurate converged solution force based convergence criterion (some time's moment-based criterion depending on the problem) should be used. Displacement-based criterion could be used in addition to the force-based convergence criterion. Restarting from the converged solution could do this.

Increase normal stiffness for contact element (step-by-step):

The normal stiffness for the contact elements has to be made stiffer. Increasing the stiffness step-by-step can do this. If the tolerance is within $30E4$, increase to $60E4$ then to $30E5$ then to $30E6$. Restarting from the converged solution is a good practice.

Reduce the stiffness of Link elements:

The stiffness for the Link elements has to be made softer. Reducing the stiffness step-by-step can do this. Check the amount of load transferred by link elements and compare with total load acting in model or total force transmitted by contact elements. Restarting from the converged solution can solve this problem.

Identify whether the problem is displacement controlled or force controlled. If displacement controlled then check carefully for very accurate displacements, so a pass-through check needs to be performed. If force controlled, check whether the forces at the contact elements agree to hand calculations.

Check the displacement change between any two consecutive runs; if the change is less than 1% then stop, it must have reached the target.

No spurious stresses should be noticed at the contact region.

Restarting an analysis involving contact elements

To restart an analysis due to non-convergence, the following needs to be done:

The following files should be available;

- `Jobname.db`
- `Jobname.emat`
- `Jobname.esav` or `jobname.osav`. For restarting an unconverged analysis rename `jobname.osav` as `jobname.esav`.

In ANSYS it is possible to change the normal stiffness (KN) for the contact elements by a restart procedure. But it is not permissible to change any other real constants for the contact elements. Therefore, if KN is changed, the sticking stiffness (KS) value cannot be allowed to set by default value (default value for KS is KN), because ANSYS tries to define KS when KN is changed. To take care of this problem KS should be defined explicitly whenever KN changes. The value for KS should be consistent in all the load steps.

Sample macro:

```
ET,10,12,                    ! Defining contact12
Theta=90                    ! For example
Kn=30E4                    ! Normal stiffness
Int=0.01                     ! For example

R,10, theta,Kn,int,

! sticking stiffness (KS)  = (KN)

/solu
antype,static,restart
rmodif,10,2,60e4
rmodif,10,5,30.e4
```

```
! explicitly defining KS

nsubst,5
lswrite,2
save
lssolve,2,2
allsel
save
fini
```

To abort a analysis cleanly follow these steps:

- Create a file called `jobname.abt` in the running directory
- Write "nonlinear" in the first column of the file
- Analysis stops at the end of current sub step.

When there is friction present in the problem, it is a good idea to first solve the problem ignoring friction. Friction is path dependent, so one needs to apply the loads in the same order in which the part experiences them. For a run with friction, applying spin loads and then applying pressures in the next load step will give different results than when pressures are applied initially and then spin loads in the next load step.

The value of sticking stiffness KS needs to be high (about 20% of KN) for easy convergence and not zero.

CONTAC52s can be used instead of 49s whenever possible. Generally these elements do not lead to convergence difficulties. With 52s, there is no need to ramp the load and doing so just leads to extra iterations. Non-convergence in case of 52s can be handled by changing the Normal stiffness KN.

Either couplings/displacements can be used to aid convergence or links can be used with ramped loads. It may not necessary to use both at the same time. Each is a strategy to prevent pass-through, either approach alone should be sufficient.

One way to debug an un-converged solution is to look at the solution, especially the deformed shape. Even when the model doesn't converge, it normally puts out displacements but not stresses (sub step 99999). One can use the NSEL command to select all the nodes that have moved more than 5 inches (say). That normally turns out to be some distinct portion of the model you thought was restrained but was not.

It is better to make sketches of the model and thinking about stability than any adjustment of parameters like KN.

A requirement could be that before trying to solve the problem even once, the engineer has to make a free body diagram of each part and show the forces on the part and how they are expected to be reacted. It has been found that the results do not vary by much for changing value of TOLN. A good rule of thumb is to have the TOLN value fixed at 2% of the element length.

3.4 2D and 3D model Comparison

Though flexible pipe is cylindrical in its structure, the normal thick cylinder theory cannot be applied as it is not continuous as the normal pipe, otherwise 2D axisymmetric analysis would suffice the structural behaviour subjected to lateral pressure. The three load bearing layers of pipe made of wires wound in helical fashion makes it complicated to be considered for axisymmetric modelling. On top of that residual stresses are non-uniform along the length of wire, to be able to analyse true deformation, 3D model is necessary. A cylindrical segment of pipe is considered to be a part of wound wire which behaves axisymmetrically in 3D space.

With exact boundary conditions and a cylindrical co-ordinate system a solid model is used to deform like a segment of pipe. The comparison of 2D axisymmetric and 3D model with radial stress SX and contact is shown in Figure 3.18 and Figure 3.19 respectively. A cylindrical co-ordinate system is generated to apply

boundary conditions to 3D model, where X, Y and Z axes changes to radial, hoop and axial respectively with respect Cartesian global co-ordinate system. Internal pressure of 60 MPa and external pressure of 30 MPa is applied on both 2D and 3D cases to compare the results. The pressure values are chosen are arbitrary and for demonstration purpose only. However the actual design pressure is 41MPa and factory acceptance test (FAT) pressure is 62 MPa. The maximum pressure at which the pipe bursts is 83.37 MPa. Maximum and minimum radial stresses of about -102.74 MPa and 44.18 MPa is observed in 3D case as shown in Figure 3.19, while -84.41 MPa and 42.72 MPa in case of 2D axisymmetric as shown in Figure 3.18. The contact behaviour is also studied between nub-valley areas and is depicted clearly in both figures. Figure 3.20 shows the variation of stresses across the pressure armour wire.

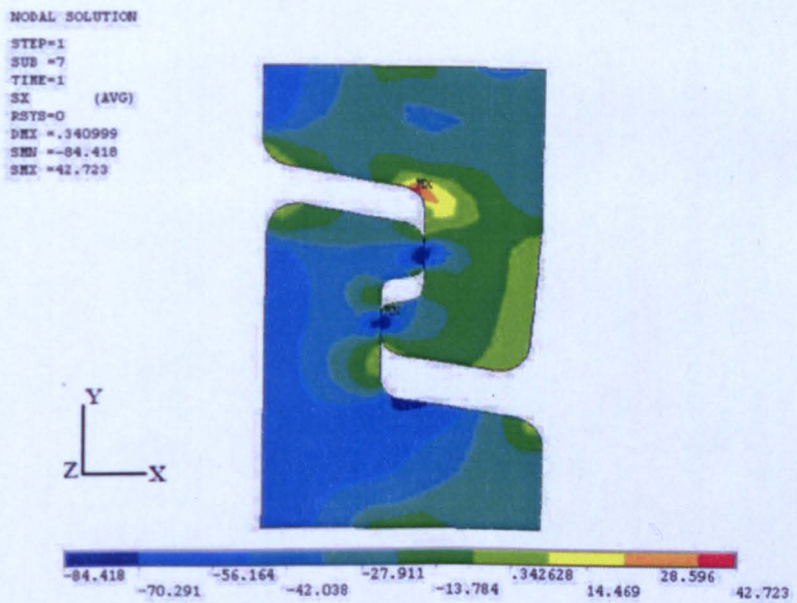

FIGURE 3.17: 2D Axisymmetric Analysis subjected radial internal and external pressure

The graph shows the stress variation across the wire thickness of pressure armour layer. The sudden drop in stresses is the gap between two adjacent wires. Apart from this sudden change at the gap, the stress values are in good agreement with theoretical values. This indicates the 2D and 3D models give fairly accurate results. But the structure of the pipe and wire orientations is such that 2D approximation

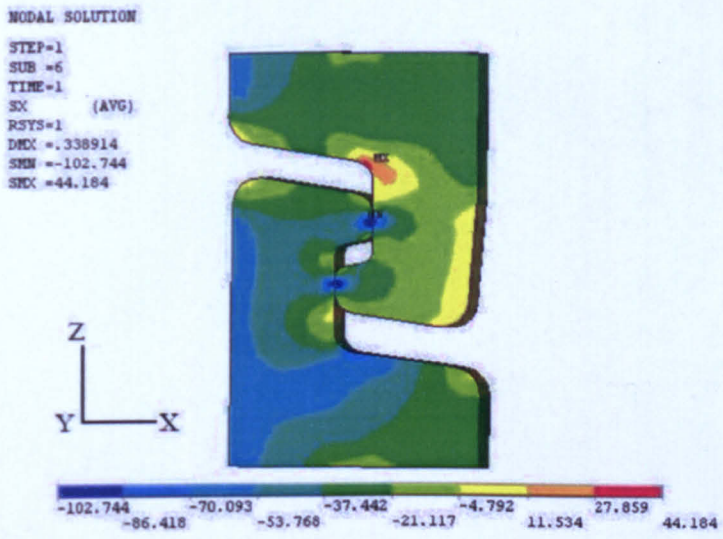

FIGURE 3.18: 3D Axisymmetric Analysis subjected radial internal and external pressure

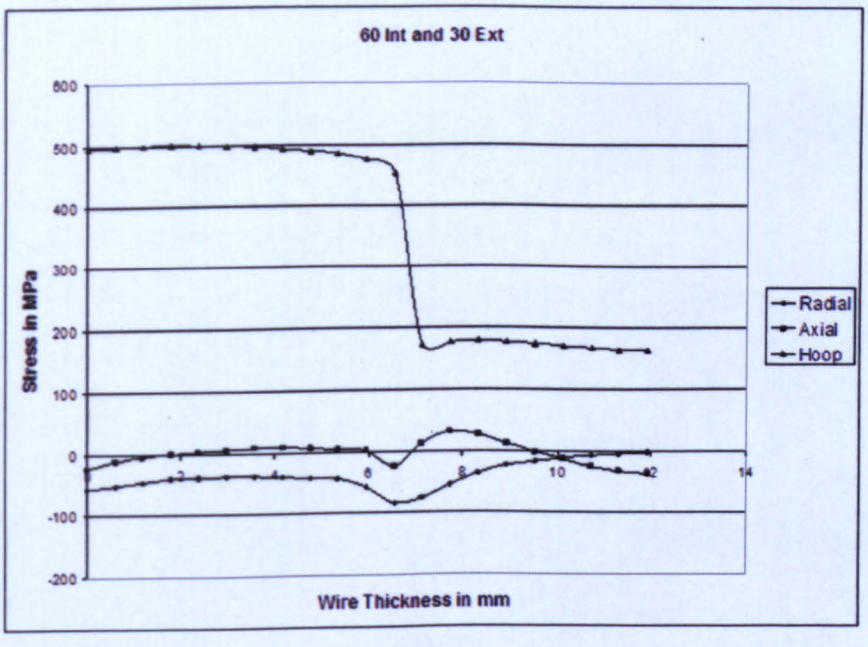

FIGURE 3.19: Radial, axial and hoop stress variation in pressure armour wire subjected to internal and external pressure

cannot be used as the residual stresses vary across the length of the wire. This limitation has to be avoided by using a 3D model which will behave similar to axisymmetric model. So the new technique to analyse 3D axisymmetric behaviour is achieved by using a cylindrical co-ordinate system. The comparison proves that

the 3D axisymmetric boundary conditions yield similar results to 2D axisymmetric values.

Chapter 4

The Bending & Pressure Analysis

4.1 Bending Analysis

There are two stages in fabrication of pipe where plastic deformation takes place, which induces residual stresses in wire material: first, at the rolling stage, where compressive stresses are imparted, secondly during pipe forming, both tensile and compressive stresses are induced. The rolling process is schematically illustrated in Figure 4.1.

Due to different radius of curvature of bending, non-linear behaviour of material and different direction, accurate calculation of residual stress is difficult [32]. Consequently the magnitude of residual stresses aid local plastic deformation under service loads. Previous studies have shown that residual stresses can be as high as half the yield stress of the material [19]. As shown in some of the failure cases in rail industry, residual stresses alone can be the cause of crack initiation and propagation [27].

The wires used to make the pipe are transported to plant in coils, where these are straightened by passing through rollers before bent on to pipe as shown in Figure 4.2 and Figure 4.3. Material undergoes plastic deformation during the process and residual stresses are set up in the newly manufactured pipe. The

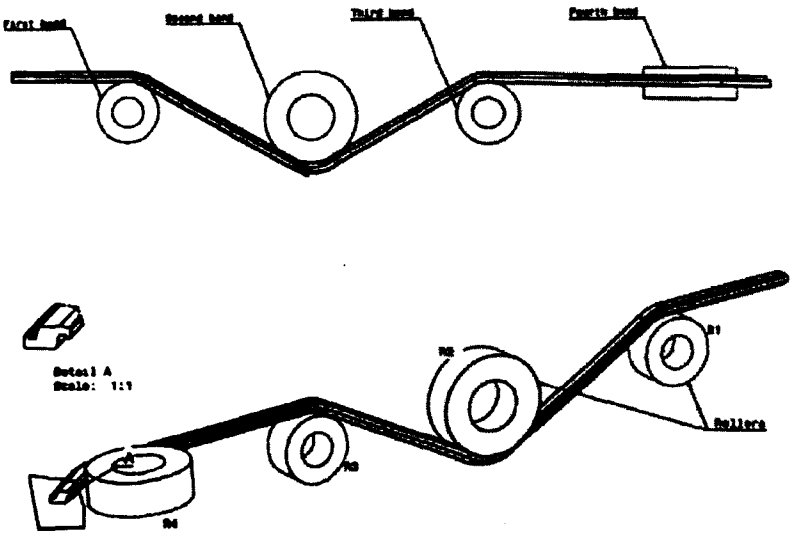

FIGURE 4.1: Rolling plastic deformation of pressure armour wire

current work focuses on stresses induced due bending via rollers. FE analysis is carried out to accurately assess the stresses caused due to each bending stage.

4.2 The Manufacturing Process of the Pipe

The collapse resistant layer or carcass layer (Figure 1.3) manufacturing process is designed to maximise production output. The machine design incorporates the use of dual raw material supply drums, allowing continuous operation with material loading and carcass manufacture occurring simultaneously. The flat stainless steel strip passes through a series of specially designed forming and closing rollers. The formed strip is helically wound around a mandrel that interlocks each wrap and provides a continuous length of carcass with a specific internal and external diameter. The interlocking feature of the carcass allows flexibility and longitudinal expansion of the finished pipe. The layer is immersed in the bore fluid.

The fluid barrier thermoplastic layer is extruded over the collapse resistant layer to form the fluid-conveying conduit. The fluid barriers along with the flex-liner and flex-shield layers are applied by means of an extrusion process. Although

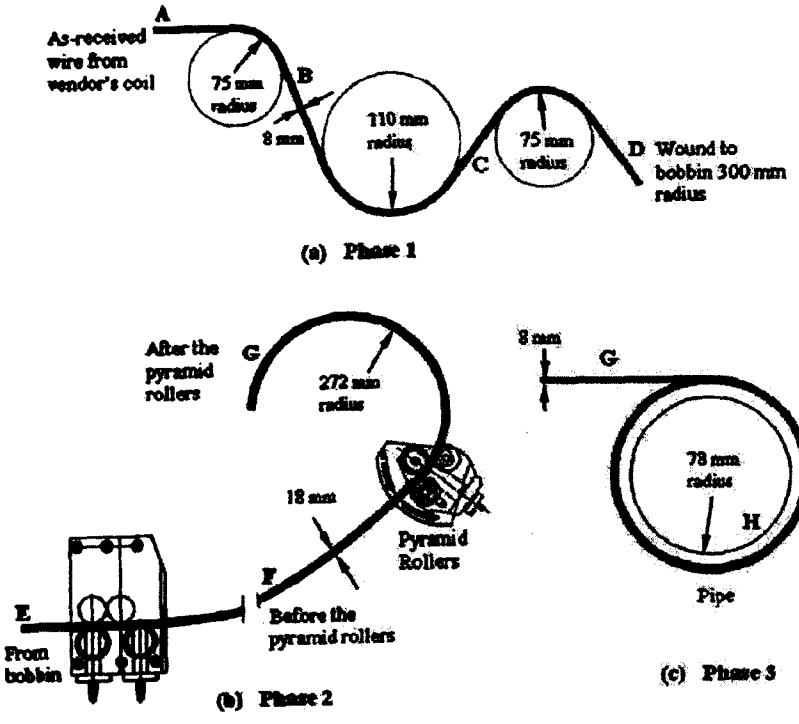

FIGURE 4.2: Different phases of pipe fabrication process

the polymer layers may serve different functions in the pipe design, they are all applied to the pipe in a similar process. The molten polymer is applied as the pipe passes through the extrusion cross-head. The pipe then passes through a series of cooling/curing steps. Control of the polymer output and line speed, coupled with the use of specially designed tools, ensures that the thickness of the extruded polymer around the previous layer meets the specifications laid down by the pipe design requirements, material type and/or layer function. In smoothbore applications, a flex-liner polymer fluid layer replaces the metallic carcass. The flex-liner layer is processed the same as the other extruded polymer layers with the exception of the vacuum sizer unit being used for the first cooling/curing step. The vacuum sizer unit is utilised to set the outer diameter of the flex-liner layer.

The hoop strength layer or flexlok layer (Figure 1.3) is a circumferentially wound pair of profiled wires applied to the pipe, to resist internal and external pressure in the hoop direction. The manufacturing process is designed to pre-form the wire as it is helically wrapped around the pipe. The pre-forming and wire application

FIGURE 4.3: Top: Phase 1 unwinding from bobbin stock; Middle: Phase 2 The wire is bent in the lateral plane through a set of pyramid rollers to form the helix angle required in the pipe; Bottom: Phase 3 Finally, formed wire wrapped on to pipe

process is accomplished via specially designed tools, and the process controls, product diameter and wire pitch. All flexlok and flex-press layer wire welds are made using a computer controlled heat pressure welding process. A anti-wear layer or flex-wear taped layer can be applied as required by the product design during the manufacturing process of these layers to reduce friction between adjacent steel layers. The wire profile allows the wires to interlock as they are wound around the pipe providing a smooth, flexible, continuous layer to support the barrier layer. The flex-press layer has a rectangular profile wire which is applied to the pipe in very high pressure applications where additional hoop strength is required above that which the flexlok layer alone can provide. The wire is circumferentially wound over the flexlok layer in the reverse direction.

The tensile strength layers or flex-tensile layers consist of contra-wound layers of rectangular profile flat wires helically applied to the pipe. The layer is primarily responsible for providing the pipe with axial tension strength, but also increases burst strength. During the design process, the size and/or number of wires and the lay angle are adjusted to optimise material usage while meeting the strength requirements of the pipe. The manufacturing process pre-forms the wire as it is spirally wrapped around the pipe. The pre-forming and wire application process is accomplished via specially designed tools, and the process controls the product diameter and wire pitch. All armour wire welds are made using a computer controlled, heat pressure welding process.

Taped flex-wear layers are applied between adjacent metallic layers as a manufacturing aid to reduce friction between metallic armour wires and to support the tensile armour wires against bird caging during spooling operations and in deepwater applications. The manufacturing process is designed to helically wrap either single or multiple layers of insulation tape onto the pipe. The insulation tape wrapping is followed immediately by the tandem application of a flex-tape layer. The flex-tape layer provides 100% coverage of the insulation layer prior to applying the flex-shield layer.

The boundary conditions for circular bending are summarized below. Referring to Figure 4.4, the displacements are applied in Cartesian co-ordinate system on three faces of the model.

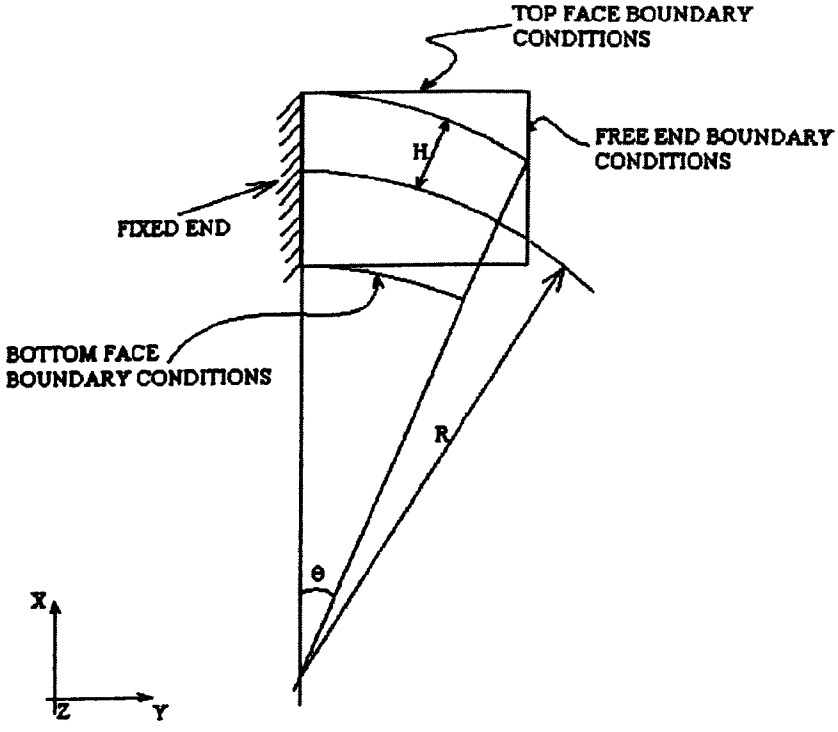

FIGURE 4.4: Boundary conditions of bending deformation

Displacement along hoop direction (Length wise) $= UY$

Displacement along radial direction (Height wise) $= UX$

Top face

$$UY = (R+H)(\sin Z/R) - 1$$
$$UX = (R+H)(\cos Z/R - 1) \tag{4.1}$$

Bottom face

$$UY = (R - H)(\sin Z/R) - 1$$
$$UX = (R - H)(\cos Z/R - 1) \tag{4.2}$$

Rolling of pressure armour wire is analysed by considering the 3D model as cantilever beam. One end is fixed and other sides are subjected to displacement boundary conditions. These displacements are applied on each node by calculating the precise value so that the deformed wire conforms to roller radius, i.e., bend in circular arc. The wire is passed between series of rollers of varying radii in opposite directions. The analysis is carried out as separate load steps for different direction and radii. There are total seven bending simulations with last load step being wound to pipe radius. Since the stresses in the wire are path dependent, the stresses generated in each load step is carried over to subsequent load step. A hysteresis plot of bending stress at a node in the model is produced to see the variation of stresses due to change in radius and direction as shown in Figure 4.5.

This stress data is carried up to last load step to see the effect of pressure loadings. Initially all bending operations are carried out in Cartesian co-ordinate system and at the end of seventh load step; a cylindrical co-ordinate system is used to apply pressure loadings. The cylindrical co-ordinate system is essential in order to simulate 3D axisymmetric behaviour. The nodes in the model are constrained in the hoop direction so that it acts like a pipe segment. This will be treated as the eighth load step. The wire bending procedure is carried out by considering the model as a cantilever beam. The free end and the other two surfaces are applied with accurate boundary conditions (BC) to wrap conform) the wire on to roller.

The roller radius and the bending direction is changed as the wire passes through different roller and finally to pipe making process. The procedure is explained by following steps.

1. The displacement BC are applied to conform the wire to first roller radius

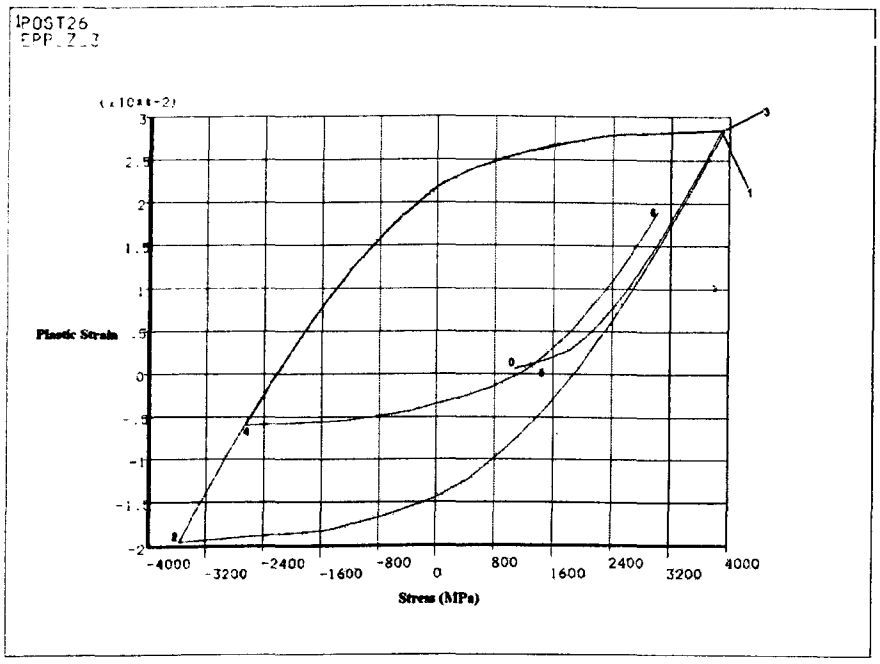

FIGURE 4.5: Hysteresis loop of bending load-steps from 1 to 6 extracted from single node on one side

2. The displacement BC are applied to conform the wire to second roller radius
3. The displacement BC are applied to conform the wire to third roller radius
4. The displacement BC are applied to conform the wire to fourth roller radius
5. The displacement BC are removed and the wire is sprung back with residual stress
6. The displacement BC are applied to conform the wire to fifth roller radius (off plane)
7. The displacement BC are applied to conform the wire to final wrapping on to a pipe.
8. The residual stresses at this stage are written to a file with element and node data.
9. The stored data is read into a similar other FE model with similar mesh.
10. This model is analysed with internal and external pressure with 3D axisymmetric boundary conditions.

The procedure is written as a set of input instructions to the FE solver and is flexible to conduct a parametric study.

4.3 Pressure Analysis

For bending analysis, the boundary conditions and geometry are created in the Cartesian co-ordinate system. To create a model to analyze pressure loads which, is a pipe or to be precise a segment of a pipe, a cylindrical co-ordinate system is used. A 3D model of the pipe segment is created with active cylindrical co-ordinate system (local system) for pressure analysis. The default co-ordinate system of the software is global Cartesian. A global coordinate system can be thought of as an absolute reference frame. The program provides three predefined global systems: Cartesian, cylindrical, and spherical. All three of these systems are right-handed and, by definition, share the same origin. They are identified by their coordinate system (C.S.) numbers: 0 for Cartesian, 1 for cylindrical and 2 for spherical as shown in Figure 4.6.

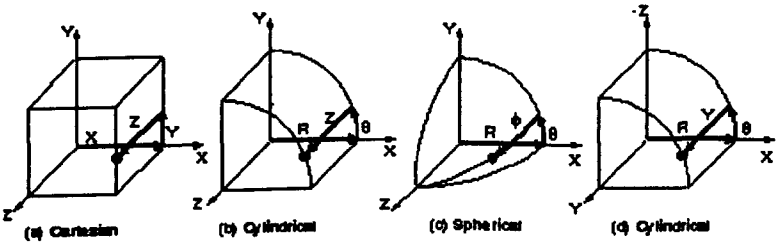

FIGURE 4.6: Different Co-ordinate Systems

A 3D axisymmetric model with two half sections of the wire has been modelled subjected to internal pressure. The mesh and the orientation of the two wire segments are as shown in Figure 4.7. The angle of the segment is a 30° arc with 20 elements in hoop direction. 2D element MESH200 is used to mesh the area and SOLID 185 element is used to extrude 2D elements. SOLID 185 elements have 8 nodes with three degrees of freedom at each node. The model consists of 12785 elements and 15762 nodes. A local cylindrical co-ordinate system is used

to define the FE model with X being radial direction, Y circumferential and Z axial direction. The two axial face nodes have been coupled to one another in all three directions to simulate the continuity of the wire. Pressure of 60 MPa is applied on the inner surface of the wire and all nodes have been constrained in the circumferential direction. These boundary conditions simulate 3D axisymmetric behaviour. The internal pressure is applied in steps to record radial displacements to be used to plot against tensile armour analysis.

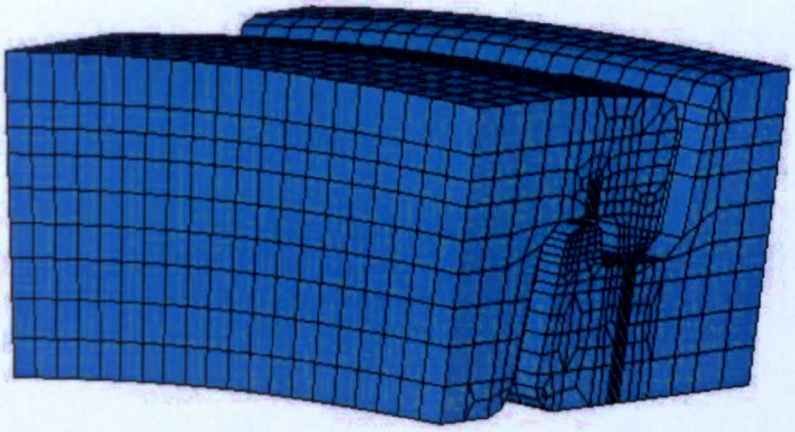

FIGURE 4.7: 3D Axisymmetric model of pressure armour wire

Tensile armour analysis is similar to pressure armour analysis with less intricacy. A segment of tensile armour wire is considered for analysis as shown in Figure 4.8. Rectangular area is meshed with 2D elements and these are extruded into 3D solid elements along the helical path. The model consists of 25000 elements and 33066 nodes. Each node has 3 degrees of freedom. The FE model of tensile armour is as shown in Figure 4.9. External pressure of 30 MPa is applied on the outer surface and one end of the wire is constrained in the axial direction only. Similar to pressure armour wire, all nodes are constrained in the circumferential direction to simulate 3D axisymmetric behaviour. Pressures are varied in steps to assess radial compression to plot against pressure armour displacement.

Residual stresses from both pressure armour and tensile armour models are transferred to their corresponding 3D axisymmetric models and the analysis is continued

for pressure loads. The results from the cyclic bending process are stored in a file in ASCII format with extension IST, meaning initial stresses. Each node's stress data is saved in tabular format as shown in Figure 4.10. The node data available in this form is from the element integration points. Since the 3D axisymmetric model consists of similar mesh, this stress data can be read into it as initial stress. Thereby the effects of residual stresses on pressure loadings can be studied.

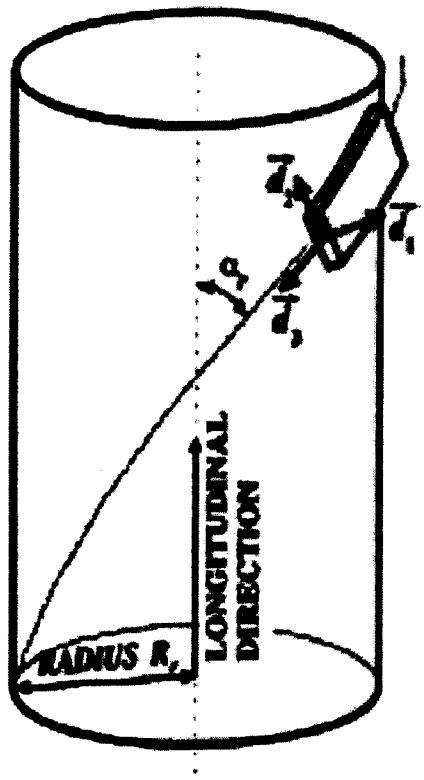

FIGURE 4.8: Tensile Armour wire model

Initial stress as a loading can be specified, when doing a structural analysis. Initial stress loading is only allowed in a static or full transient analysis (the analysis can be linear or nonlinear). Initial stresses can be applied only in the first load step of an analysis. Initial stresses are treated as if they are applied on elastic materials. Constant stresses can be specified using the ISTRESS command. ISFILE command is used to read initial stresses from an input file, and to list and delete initial stresses. Command arguments allow the initial stresses to be limited to certain material types. This first line for each element is followed by subsequent

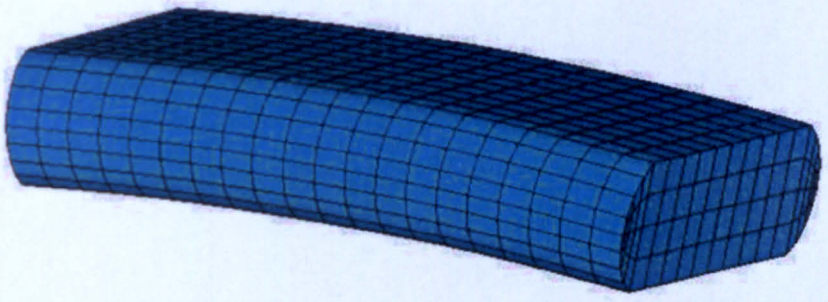

FIGURE 4.9: Tensile Armour FE model

fileseven.ist - Notepad

File Edit Format View Help

```
!
! ******* INITIAL STRESS FILE  file.ist
!
!
!INITIAL STRESS RECORD FOR ELEMENT     2981
!      SX            SY            SZ            SXY           SYZ           SXZ
eis,     2981,1
  -329.061      -1359.24      -103.594      -18.3442      -4.06001      -49.0438
  -352.338      -1377.76      -104.280      -17.1588       2.22833      -53.6337
  -347.081      -1433.03      -170.837      -15.5808      -11.4614      -52.6582
  -325.914      -1413.71      -168.828      -20.0185      -5.22059      -48.6581
  -334.890      -1359.54      -101.493      -19.9259      -5.94109      -46.6449
  -361.182      -1377.95      -99.2863      -15.4733      0.153542      -42.3954
  -363.668      -1432.87      -158.454      -13.8974      -9.49856      -43.2359
  -339.732      -1413.46      -159.295      -21.4100      -3.36054      -47.4861
!
!INITIAL STRESS RECORD FOR ELEMENT     2821
!      SX            SY            SZ            SXY           SYZ           SXZ
eis,     2821,1
  -336.899      -1245.02       16.5654      -16.8309      -1.28776      -94.2458
  -331.918      -1300.80      -30.9225      -17.9966      -1.60616      -94.8434
  -265.690      -1268.45      -29.1034      -17.5973      -1.06520      -94.6512
  -261.997      -1216.69       13.7248      -18.6943      -1.92365      -93.5305
  -336.250      -1245.30       14.6125      -15.7710      -2.44647      -93.2965
  -332.685      -1300.94      -31.6049      -16.9948      -0.608544     -92.3060
  -267.845      -1268.25      -28.7394      -18.5934      -0.111953     -92.9724
  -263.016      -1216.47       12.9371      -19.7508      -2.85526      -93.5463
```

FIGURE 4.10: Initial stress file with stress data for each element

lines that specify the element stress records for each stress point in the element. When $LOC = 0$, only one stress record at the centroid of each element is specified. When $LOC = 1$, the number of stress records for each element is equal to the number of element integration points for the element. The program logic expects six stress tensor components in each stress record. Based on the element type, the program will read only the relevant stress tensor components from each stress record. When $LOC = 3$, the stress record for the first element in the initial stress file will be used to specify the uniform initial stresses for all elements. The initial stresses are specified in the element local coordinate system. The initial stress file written by the ISWRITE command has the same format as described for the input file.

Chapter 5

The Experimental Work

5.1 Measurement of Residual Stresses

The experiments are being carried out to investigate the residual stresses developed during wire wrapping in order to simulate the actual manufacturing process. The standard universal testing machine is used to bend the wire and X-Ray diffraction method is adopted to measure the residual stresses. The figures 5.1 and 5.2 show the test setup with the pressure armour wire and strain gauges. The wire is supported on a disc of certain diameter and load is applied so as to wrap the wire conforming to the disc diameter.

After bending the wire in UTM, the test piece is placed in X-Ray diffraction machine for measurement. There are four locations where the stresses are measures viz; both surface sides, nub and valley regions. Each reading takes about 14 hours of machine time. The XRD machine is connected to a computer where the data is transferred. Results are shown in Figure 5.4.

The test piece is bent successively in different direction with corresponding radii and it is restrained to avoid spring back with bolt connection. It is mounted on the work table of XRD machine with suitable fixtures to secure the test piece. The results are summarised in Figure 5.5 with bending stress values.

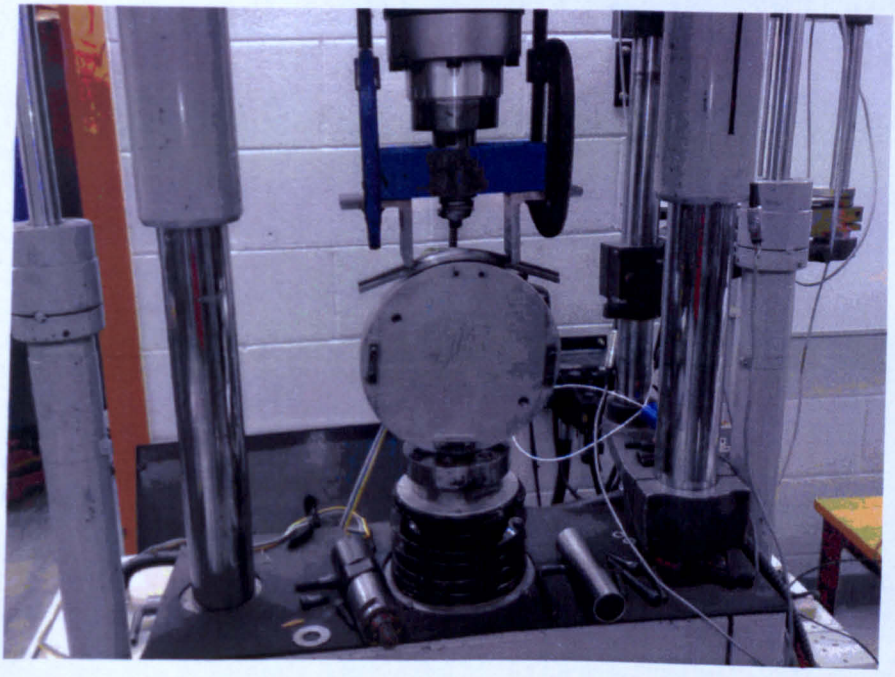

FIGURE 5.1: Experimental setup of wire bending

Bends	Stresses in MPa			
	Top	Bottom	Nub	Valley
1st 80mm CW	1445.33	−1153.45	810.76	−755.03
2nd 115mm CCW	−1132.62	1209.81	−654.36	762.44
3rd 80mm CW	1367.01	−1014.89	796.52	−723.77
4th 305mm CCW	−1078.27	1177.79	−610.1	701.18
Straightening	90.45	−278.33	−435.87	134.91
Side 305mm	−1204.55	458.28	−1182.32	1071.66
7th 115mm CW	1327.89	1445.34	876.19	−899.44

X-rays are electromagnetic radiation similar to light, but with a much shorter wavelength. They are produced when electrically charged particles of sufficient energy are decelerated. In an X-ray tube, the high voltage maintained across the electrodes draws electrons toward a metal target (the anode). X-rays are produced at the point of impact, and radiate in all directions. Tubes with copper targets, which produce their strongest characteristic radiation ($K\alpha 1$) at a wavelength of about 1.5 angstroms, are commonly used for geological applications.

If an incident X-ray beam encounters a crystal lattice, general scattering occurs.

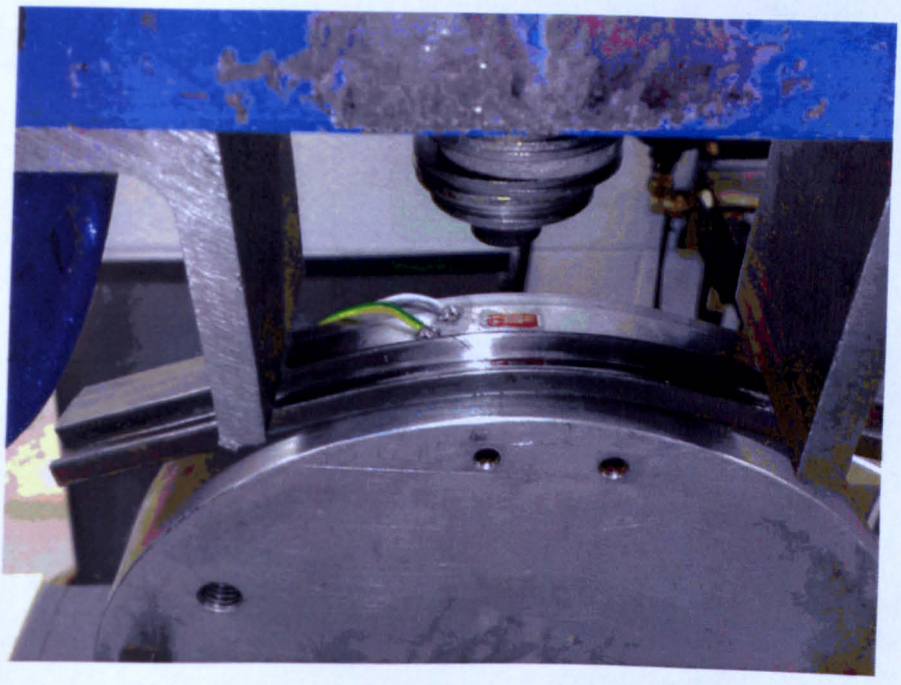

FIGURE 5.2: Bending of pressure armour wire with strain gauge

Although most scattering interferes with itself and is eliminated (destructive interference), diffraction occurs when scattering in a certain direction is in phase with scattered rays from other atomic planes. Under this condition the reflections combine to form new enhanced wave fronts that mutually reinforce each other (constructive interference). The relation by which diffraction occurs is known as the Bragg law or equation. Because each crystalline material has a characteristic atomic structure, it will diffract X-rays in a unique characteristic pattern.

The basic geometry of an X-ray diffractometer involves a source of monochromatic radiation and an X-ray detector situated on the circumference of a graduated circle centred on the powder specimen. Divergent slits, located between the X-ray source and the specimen, and divergent slits, located between the specimen and the detector, limit scattered (non-diffracted) radiation, reduce background noise, and collimate the radiation. The detector and specimen holder are mechanically coupled with a goniometer so that a rotation of the detector through $2x$ degrees occurs in conjunction with the rotation of the specimen through x degrees, a fixed 2:1 ratio.

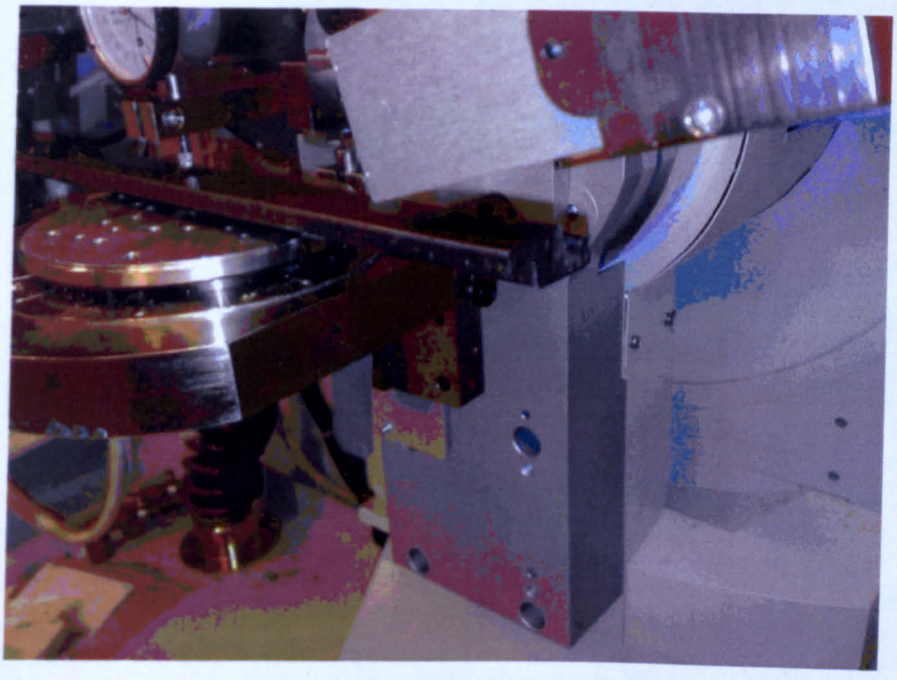

FIGURE 5.3: X-Ray Diffraction measurement of test piece

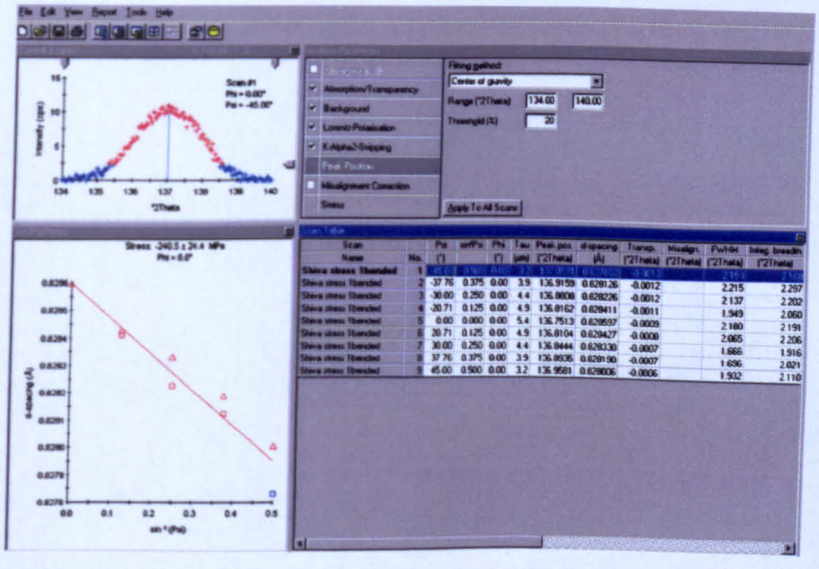

FIGURE 5.4: XRD Reading with X-pert software

A curved-crystal monochromator containing a graphite crystal is normally used to ensure that the detected radiation is monochromatic. When positioned properly just in front of the detector, only the $K\alpha$ radiation is directed into the detector, and the $K\beta$ radiation, because it is diffracted at a slightly different angle, is directed away. The signals from the detector are filtered by pulse-height analysis,

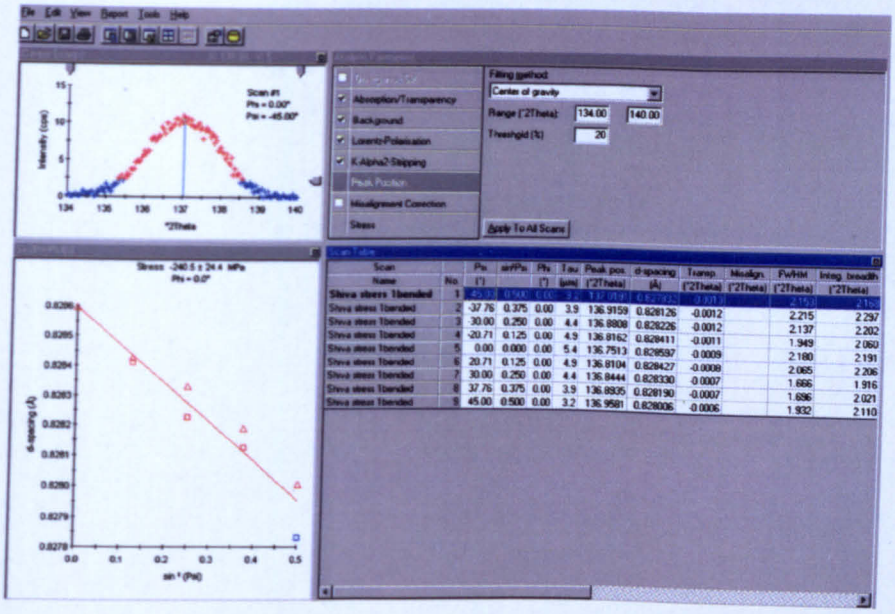

FIGURE 5.5: XRD stress values of bends at different locations of pressure armour wire

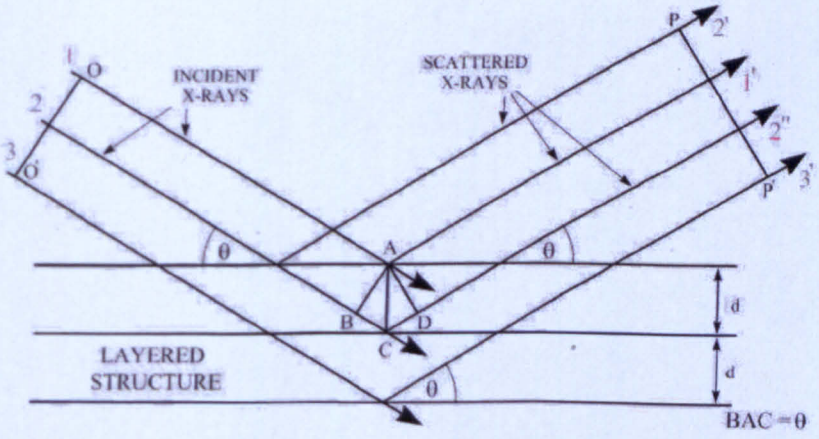

FIGURE 5.6: X-Ray Diffraction method

scaled to measurable proportions, and sent to a linear ratemeter for conversion into a continuous current. Common output devices include strip-chart recorders, printers, and computer monitors.

As known from the literature [53], the planes (3 1 0) are the most commonly used to measure the residual stress due to its higher Bragg's angle. In this particular case due to the poor signal, the plane (1 1 0) was chosen. The result of these

measurements verified by the change of the angle 2θ (44.456°), determined the interplanar variation due to the applied strain.

Chapter 6

Results and Discussion

A new procedure is developed to analyse local plastic deformation in unbonded flexible pipes used in offshore oil and gas industry. The pipe consists of several layers of metallic and non metallic materials; three of these metallic layers carry bulk of structural loads namely, a pressure armour and two tensile armour layers. These layers consist of wires wound in a helical fashion to make co-axial flexible conduit. During the pipe manufacturing (a cold forming process), the armour wire is, however, subjected to a sequence of cyclic bending and twisting deformations which take it beyond its material elastic limit. An attempt has been made to model the amount of residual stress evolved during manufacturing stage and its effects on overall pipe's performance while in service.

The response of two different layers of a flexible pipe is analysed. Elastic-plastic bending is simulated in succession of six bends of different radii and different direction. Multilinear kinematic hardening has been used. Geometric nonlinearity has also been taken into account. The parameters and variable loads are listed in the program input listing. The new developed procedure is parametric in the sense that different values of roller radius, wire thickness, pipe diameter, internal pressure, external pressure can be tested to perform parametric studies. The contact between the nub and valley within pressure armour wire is also considered which can perform stick, slip and sliding mechanism with varied load cases. Several test cases are run and axial strain in the wire when bent on the rollers is found

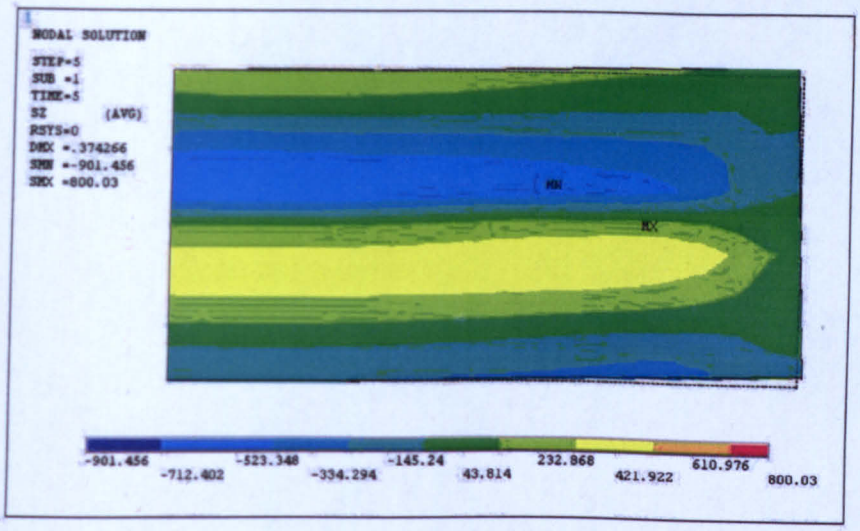

FIGURE 6.1: Residual stresses after release of displacements

to be 0.0064 to 0.0081 and the axial stresses are 1400 MPa to 1700 MPa (Nodal averaged).

When the wire is released, the axial stresses decrease to 800 to 850 MPa which is close to yield. It is interesting to note that even though the stresses developed during roller bending are high, obviously they are at much lower values before the final bend takes place to fabricate a pipe. Depending on the region of pipe length, the residual stresses can be critically high or can be close to yield point due to different loads on pipe while transporting, installation, hydro test, operational conditions. The peak stress values are observed on the outer and inner surfaces of the wire decreasing towards mid section as shown in the Appendix A. As would be expected, the ratio of peak stresses to average bulk stresses decreases after yielding.

By simulating the loading and unloading, this model can predict the amount of residual stress set up at each cycle. Plots of residual stresses of six sequential bending are shown in Appendix A. A Similar procedure is carried out on tensile armour wire and corresponding stress contour values are depicted in the Appendix B. To determine the effects of internal pressure and external pressure, the analysis is

carried out in two stages. First store stress data with corresponding nodes and elements of cyclic bending analysis. Secondly apply these stresses as initial stresses in a 3D axisymmetric model to test the pressure effects. Residual stress distribution after five consecutive bending operation and release is plotted as shown in Figure 6.1.

The 3D axisymmetric model of Pressure armour layer, when subjected to different external pressure and constant internal pressure with residual stresses is plotted in the graph as shown in Figure 6.2

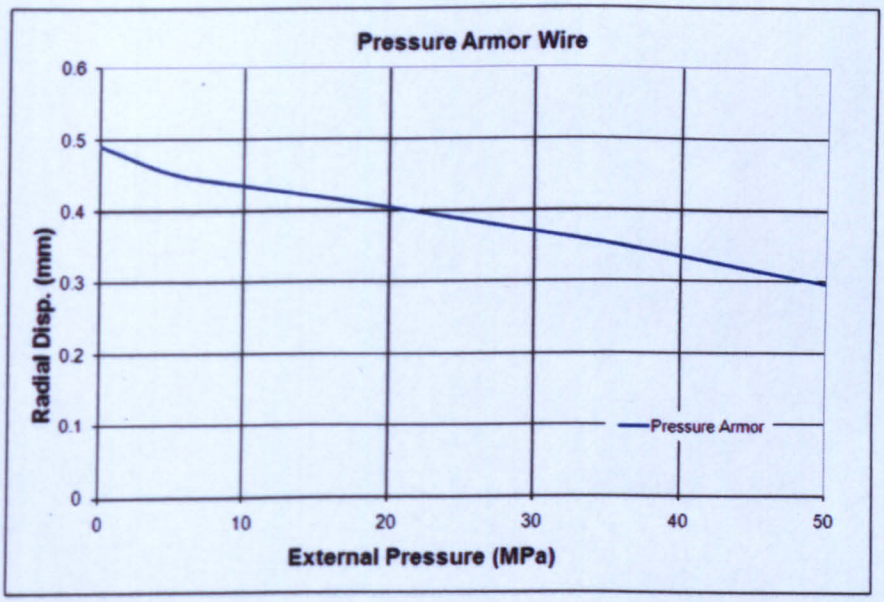

FIGURE 6.2: Pressure armour under pressure with residual stresses

The 3D axisymmetric model of Tensile armour layer, when subjected to different internal pressure and constant external pressure with residual stresses is plotted in the graph as shown in Figure 6.3. The graphs are superimposed to find an accurate interface pressure between two layers which is shown in Figure 6.4.

The axisymmetric analysis of the section has shown that the average hoop stresses were about 644 MPa and Von Mises around 700 MPa without considering initial plastic deformation and corresponding residual stresses. The pipe is pressurised to 60 MPa which rises Von Mises stress to 1200 MPa which is above the yield strength (1100 MPa) found in the 3D model. This high pressure yields the material and

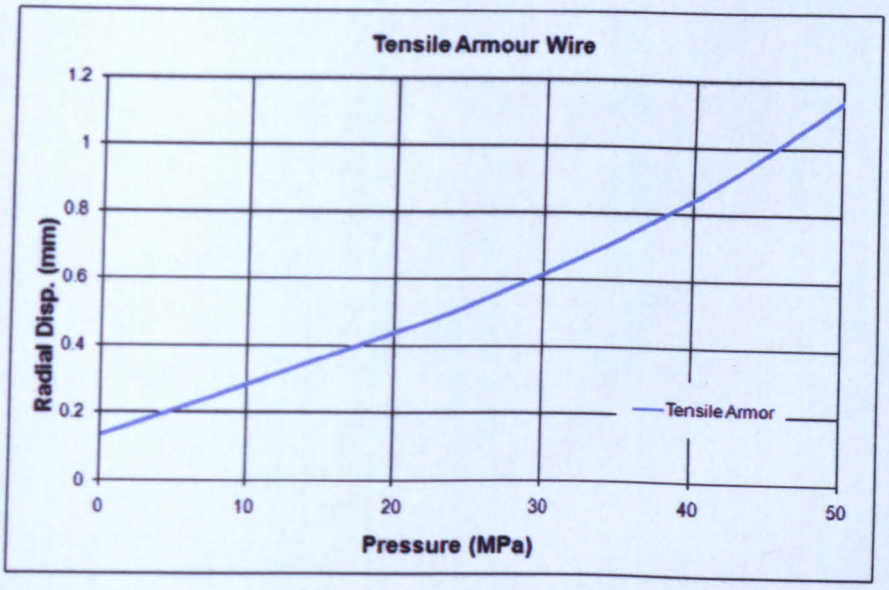

FIGURE 6.3: Tensile armour under pressure with residual stresses

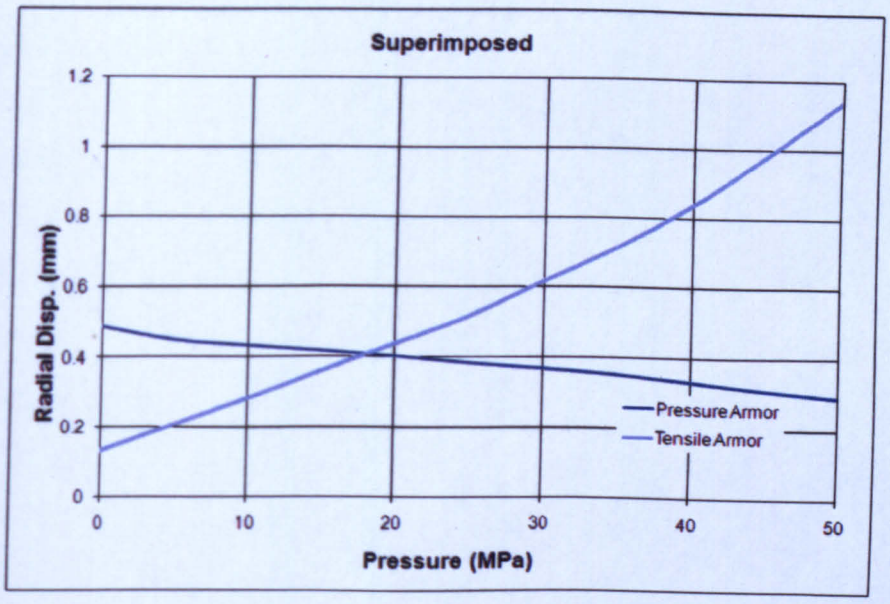

FIGURE 6.4: Superposition of graphs to find interface pressure

adds residual stresses to those already present in the material due to forming. Also results indicated that compressive hoop stress does not exceed the maximum hoop stress before FAT pressurisation. The design pressure which is 41.2 MPa deforms the material quite uniformly after FAT depressurisation. Although spring back behaviour relieves the residual stresses to some extent, the difference in stress values show an indication of the need for a better numerical model. To have fairly

precise understanding of local stress distribution, considering all variables the pipe is subjected to, 3D finite element nonlinear analysis is required.

Figure 6.5 shows the hoop stress distributions in the pressure armour wire layer after it had been wrapped to the pipe. At this stage, the hoop stress distribution shows a rather symmetrical pattern about its principal bending axis across the width of the wire. The outer section of the wire is dominated by the tensile hoop stress while the inner section by the compressive hoop stress. Figure 6.6 shows the corresponding stress distribution under pressurisation of 50 MPa. It is seen that the section, dominated by the tensile hoop stress, increases noticeably as the pressure load stretches the wire tangential to the pipe hoop direction. It is also noted that stress concentration around the corners is not significant since the dominating stress is in the outer extreme fibre of wire.

During the loading steps 1 to 6, as shown in Figure 4.5, the extreme fibres in the pressure armour wire undergo cyclic plastic deformation and when the wire has been wrapped to the pipe (step 6) it exhibits some residual stress. The application of a first high internal pressure to the pipe i.e. FAT condition would increase the tensile plastic strain in the material, while the maximum Von Mises stress remains approximately at the same level during the forming process.

This state of stress-strain would give the most severe loading case and the highest hoop stress in the wire material. The removal of internal pressure after FAT would unload the wire material elastically. Depending on the location analysed in the wire different stress-strain path will occur. For example, the material at the inner extreme fibre of wire will go through a similar stress-strain path, but with compressive stresses instead of tensile stresses.

The stress–strain behaviour of the wire material between pressurization and de-pressurisation load steps was considered to be very important in the analysis of the pipe integrity. During depressurisation of the pipe after FAT, the stress re-laxing occurs and the material settles back into the elastic state. In this case, re-pressurisation of the pipe, usually the service loading, which is much less than FAT pressurisation, would increase the stress in the wire elastically. Since the

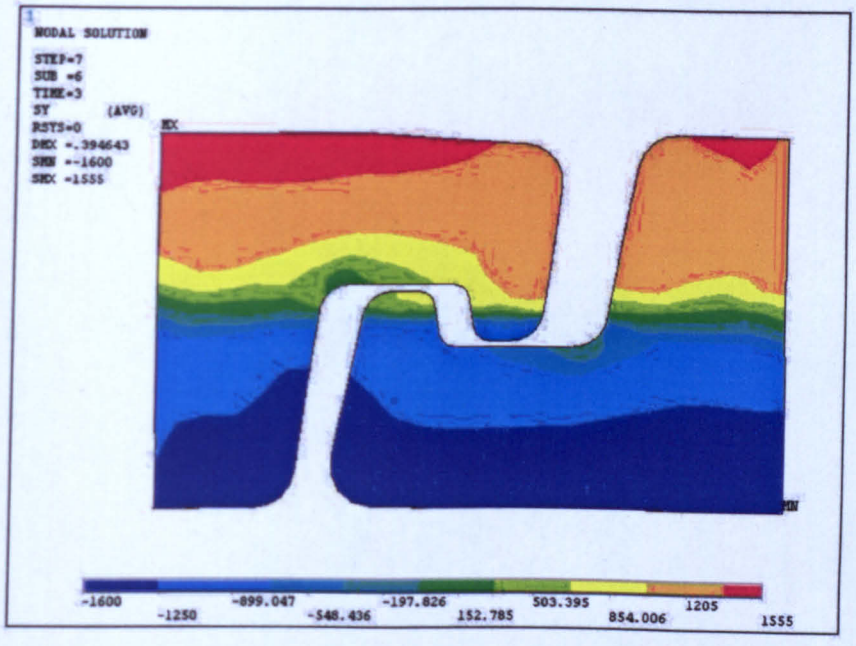

FIGURE 6.5: Seventh bend of radius 116 mm to pipe radius (final stage in pipe manufacturing) stresses in MPa

applied internal pressure is below FAT pressure, the wire deforming would be elastic during subsequent pressure loadings. In conclusion there would be no cyclic plastic deformation in the wire; the pipe would be safe under this condition [54, 55].

At the inner wire surface compressive hoop stress is expected at the end of the forming processes. When the FAT pressure is applied, the inner surface will be stretched. Since the material strain hardening has already occurred during forming, the stress and strain deformation follows the elastic relationship as the hoop stress increase. When the FAT pressure is withdrawn, the stress returns by following the same elastic relationship to a similar level as seen at the end of forming. The same process is also expected during subsequent pressure loading. The results indicate that the compressive hoop stress does not exceed the maximum hoop stress level observed at the end of the forming. Therefore, no plastic deformation is expected after FAT depressurisation.

Furthermore, the results indeed show that the subsequent pressure load stretches

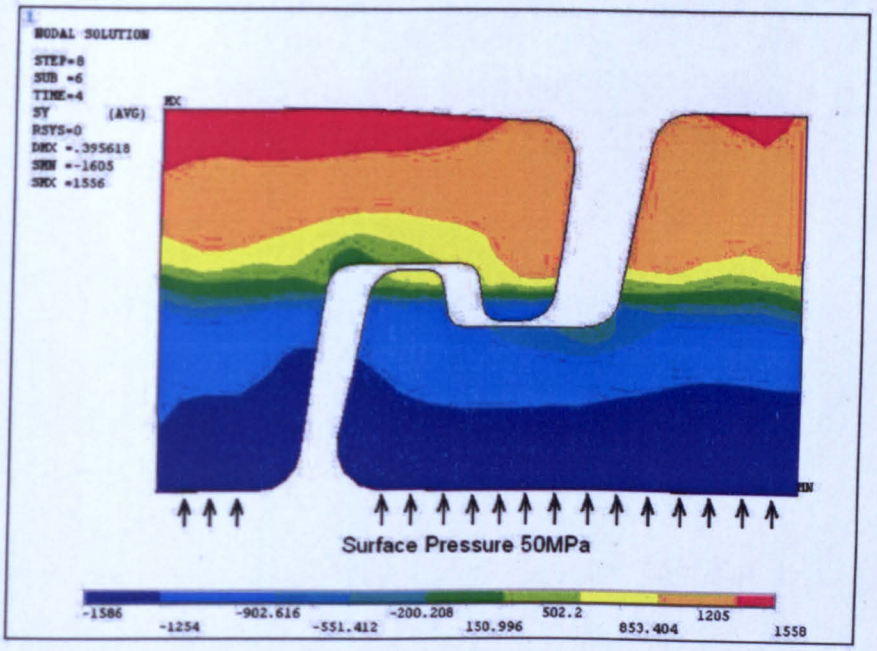

FIGURE 6.6: Eighth stage, surface pressure of 50 MPa applied on inner radius; stress in MPa

the wire cross-section quite uniformly after FAT depressurisation. Such uniform deformation is governed by elastic deformation as a result of the material strain hardening resulting from the cold forming and FAT pressurisation. It should be noted that a slight spring-back in the wrapped wire would result in a significant reduction in the magnitude of stress. The nature of stress (tensile /compressive) obtained from the x-ray diffraction method compared well with the predictions of the FE analyses.

The metallic layers in a typical flexible riser are separated by polymer sheaths to avoid abrasion, however there is no non metallic material in the interlocking mechanism within the pressure armour wire which cause friction and fretting damage. This degradation is coupled with high amount of residual stresses in outer fibres of wire and can drastically reduce the fatigue life. As mentioned in the literature survey, there are many cases of riser failures ranging from separation of layers, over bend, birdcaging, to end fitting failures. Ovalization and kink formation roughly accounts 11% of total failures. Disarray of tensile armour wires over time has been a reasonably significant mode of failure in risers. It seems to occur mainly when

the pipe is constrained in a tight radius and the disarray tends to be local rather than through the whole length of pipe. Such examples of this include a pipe upheaval buckle, or tight constraint within a drag chain structure. High lay angle of the tensile armours also contribute to the failure mode. The high amount residual stress in wires may contribute to such failures. It is recommended to consider residual stresses while designing flexible risers.

The method consists of FE analysis using a 3D wire model which allows evaluation of the residual stress introduced in the wire during manufacturing of the pipe. The 3D stress analyses performed during this study show that conventional elastic axisymmetric stress analyses could underestimate the local stress in the wire during FAT pressurisation. Moreover the maximum hoop stress in the wire would occur in the outer surface and not in the inner surface as shown by the axisymmetric results. Due to the presence of high tensile stress in the outer surface and high compressive stress in the inner surface of the wire, the section average hoop stress in the wire may be relatively small although the actual maximum stresses in the wire are high. The present study also shows that significant residual stress relaxation occurs in the material after FAT depressurisation.

The difficulty in assessing the local plastic deformation in different layers of the pipe, considering fabrication deformation effects (residual stresses) throws a real challenge to the analyst. Further stress analysis becomes cumbersome due to the external loads which the pipe undergoes in service [56, 57, 58]. Residual stresses are self-equilibrating internal stresses existing in a free body when no external loads are applied. At equilibrium the integral of this stress in the volume of the body must be null as well as the integral over any plane thought the specimen [44, 59]. By accurately determining the local plastic deformation in pipes, it is possible to predict fatigue life more reliably [60, 61]. Fatigue testing of risers [62, 63, 64] has shown that pipes failed due to fatigue of the tensile armour, but at different locations. In one pipe, the primary failures were in the inner layer of armour, in an approximately 2 m long section of pipe from the tapered end of the bend stiffener. The failures were due to contact fatigue, where the fretting took place at metal-to-metal contact points between the two layers of armour, and in two

cases, between armour tendons in the same layer. In the other pipe, the primary failures were in the end termination, at a location where the tendons were bent outwards to be anchored in the epoxy. These failures were due to fatigue, possibly influenced by built in stresses and wear between tendons and epoxy.

Chapter 7

Conclusions & Suggestions for Further Work

Designing a riser system is an iterative process. A number of preliminary steps have to be taken before it can be optimized into a final design. The existing procedure of FE analysis is envisioned to handle more general problems encountered in design of submarine cables, umbilicals as well as flexible pipes. The finite element method is employed to assess the overall plastic deformation and subsequent residual stresses considering contact within the layer. Accurate boundary conditions are imposed to simulate cyclic bending of wires during fabrication. Experiments are carried out to measure actual residual stress state in wires using X-Ray diffraction method and results are in good agreement with FE calculations. The following conclusions were made from the work done:

1. The residual stress in the pressure armour wire material observed in the FEM simulation of the roller bending process is close to the values measured by X-ray diffraction.

2. The equivalent stress and the principal stresses are reliable to the residual stress determination of materials that present plastic deformation caused by metalworking process.

3. The results met by X-ray diffraction and by finite elements are very close, evidencing the method effectiveness, to cyclic bending of pressure armour and tensile armour wires as well as the pipes pressurization operation.

4. The enclave of the plastic region, the deformed geometry and the distribution of the bending load were well predicted according to the finite-element model. This information may be applied to improve both the manufacturing process and the design of tools.

5. The calculation demonstrated clearly the efficiency of the code in simulating successive roller-bending processes that proceed under complicated deformation and contact conditions. The calculated results agree satisfactorily with the results of experiment.

6. As the tools are depicted by functional relationships, the finite-element model can accommodate any arbitrary tool used in the workshop for general bending processes.

7. This work has provided an improved understanding of the residual stress state in flexible pipes.

8. The method proposed in this work is user-friendly because it does not require high operational costs.

The current work bridges the gap in knowledge of effect of manufacturing process on the flexible pipes performance in service, particularly during operation, factory acceptance test and maximum burst pressures. Hence fabrication and testing methods can be improved to enhance the life of flexible risers.

Future work involves study of the current model/procedure and modification to effectively analyze loads while the pipe is in service such as:

1. Effect of tensile load in wire during roller cyclic bending

2. Inter-wire friction and fretting damage

3. Bending of pipe during transportation.

4. Deformation due to torsion.

5. Bending due to dynamic boundary conditions such as ocean currents, movement of vessel, buoys, etc.

It is clear from the results of the present study that suitable methods exist for predicting the structural response of a flexible pipe subject to service loads and manufacturing effects. This is extremely encouraging when one considers the complexity of these flexible structures. A key feature of the suitability of these models is the ability to take into account the interaction between the component layers. Models which do not take this interaction into account may give erroneous results for some load cases which the user must be aware of. Apart from this factor it is extremely encouraging to see the convergence of the results predicted from the parametric studies of different models. However, a note of caution should be issued. These models demand significant input in terms of material properties and geometry which are not always clearly known and a key factor relating to the reliability of the results is the experience of the engineer in the structural modelling of flexible pipes. In the case of flexural loading, some of the advanced models performed reasonably well when one compares the results with the measurements. However, it is clear that more research is needed in this area to establish the structural behaviour of flexible pipe under combined axial, torsional and flexural loading. This case study has also illustrated the difficulties associated with interpretation of test results. Further research is needed to understand complete structural behaviour of flexible pipes under different types of loads.

Appendix A

Pressure armour wire stress plots

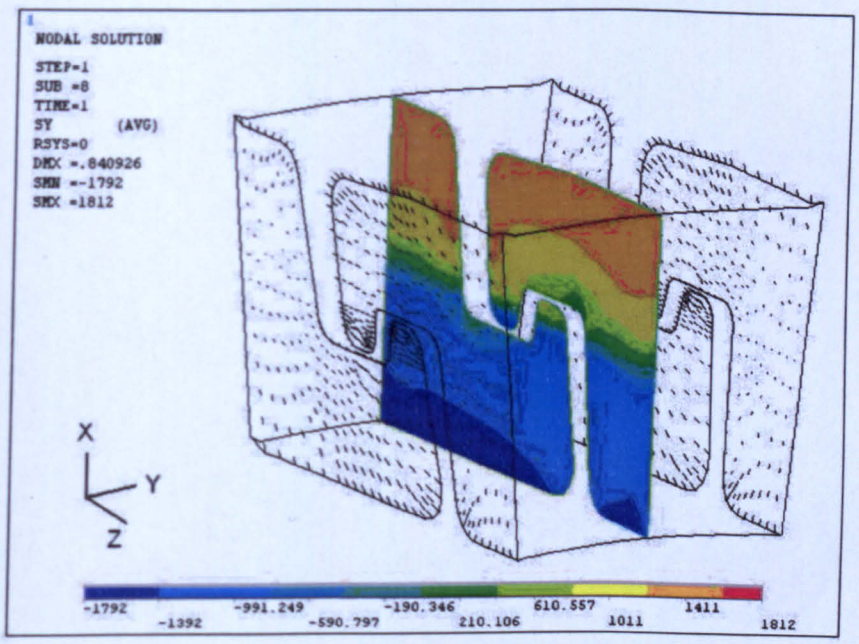

FIGURE A.1: Stress plot of PA wire and mid-section shows Stress in Y-direction in MPa

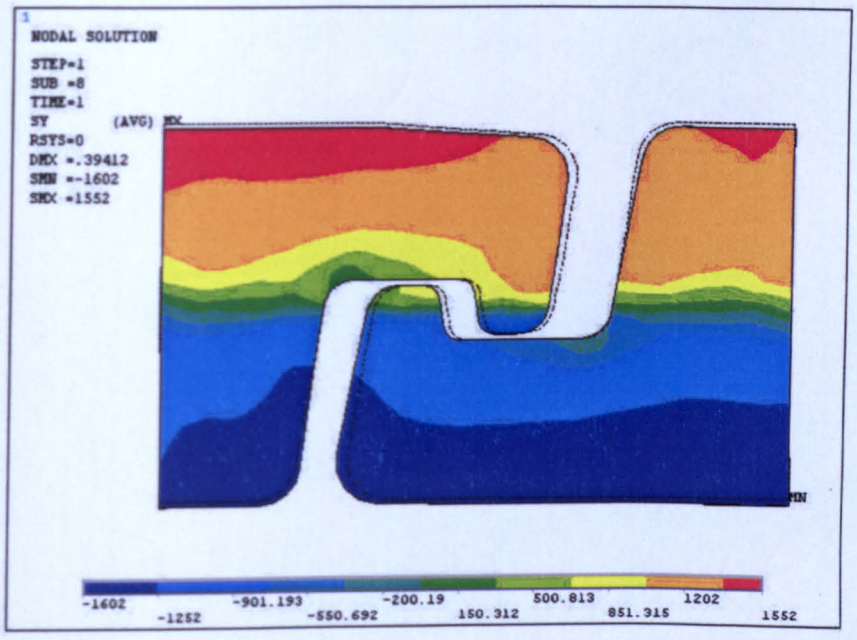

FIGURE A.2: First bend of radius 75 mm bending stress in MPa

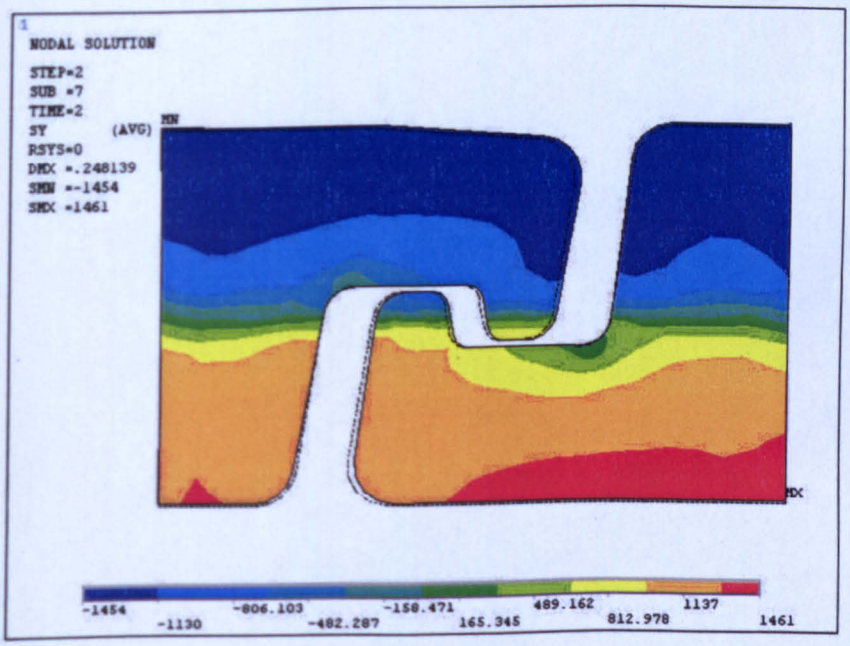

FIGURE A.3: Second bend of radius 110 mm bending stress in MPa

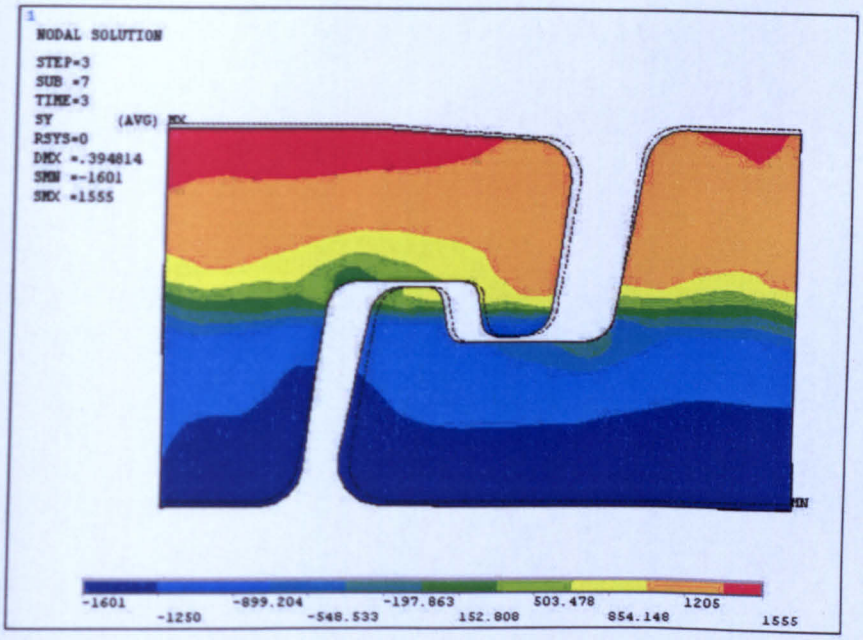

FIGURE A.4: Third bend of radius 75 mm bending stress in MPa

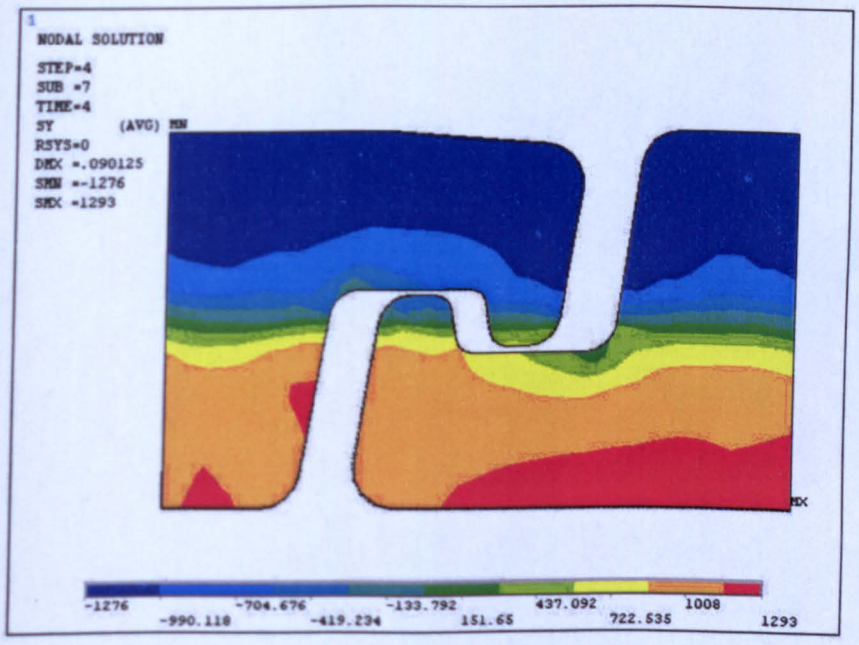

FIGURE A.5: Fourth bend of radius 300 mm bending stress in MPa

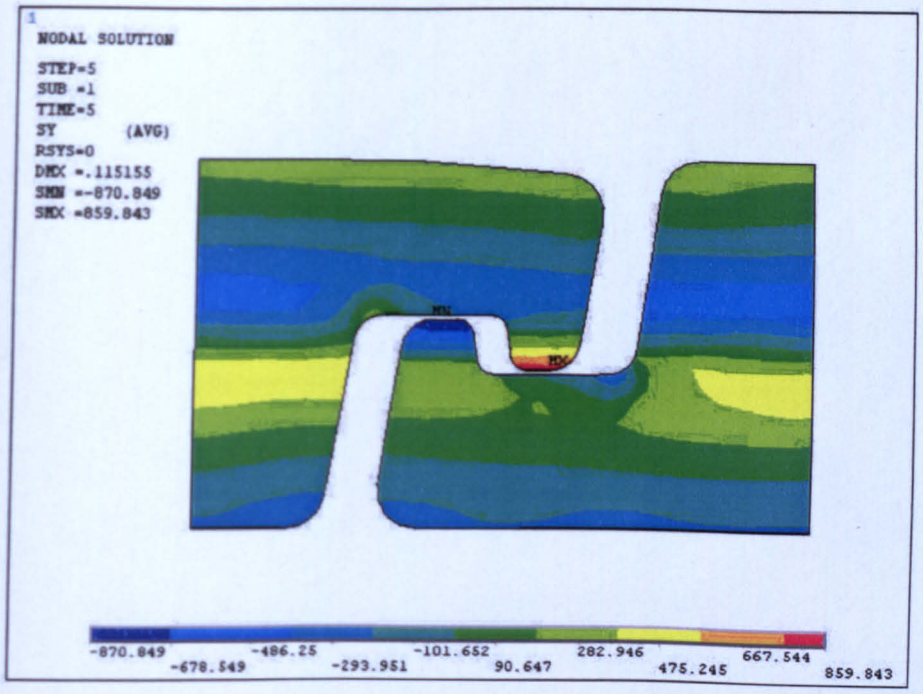

FIGURE A.6: Fifth displacements released and residual stress in MPa

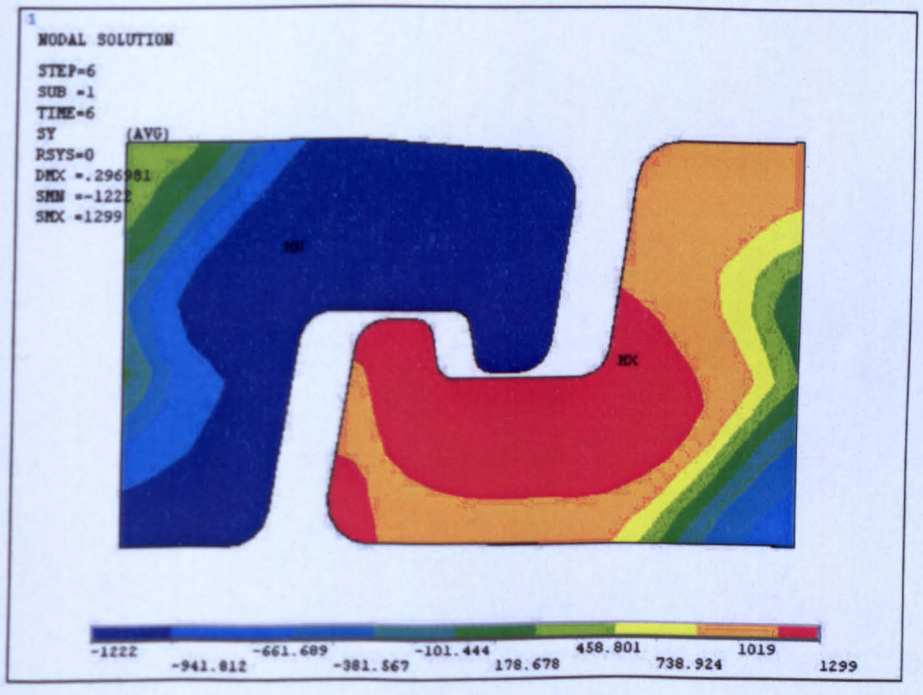

FIGURE A.7: Sixth bend of radius 300 mm side (off plane) bending stress in MPa

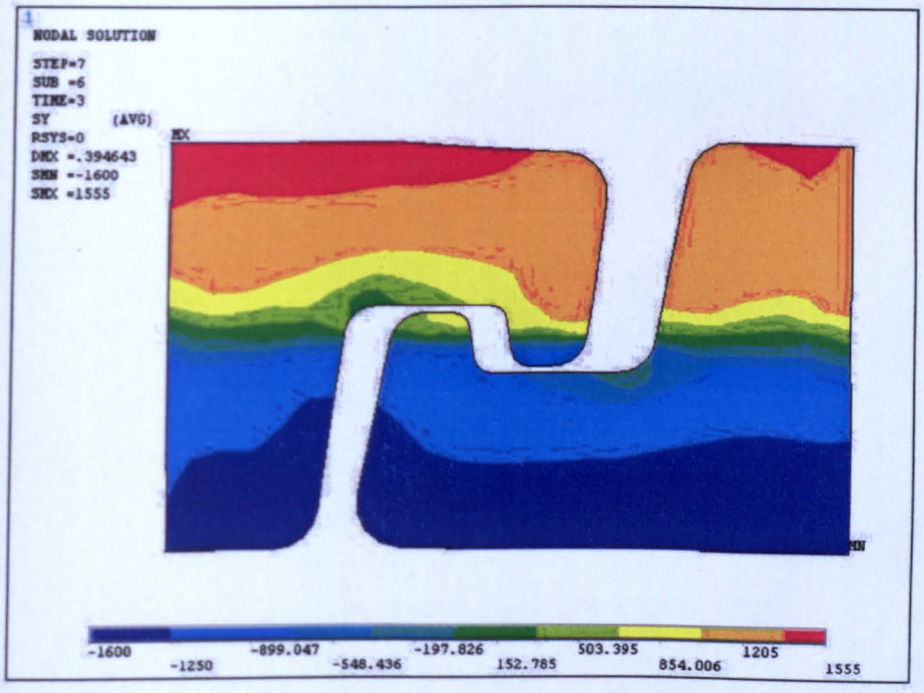

FIGURE A.8: Seventh bend of radius 116 mm to pipe radius (final stage in pipe manufacturing) stresses in MPa

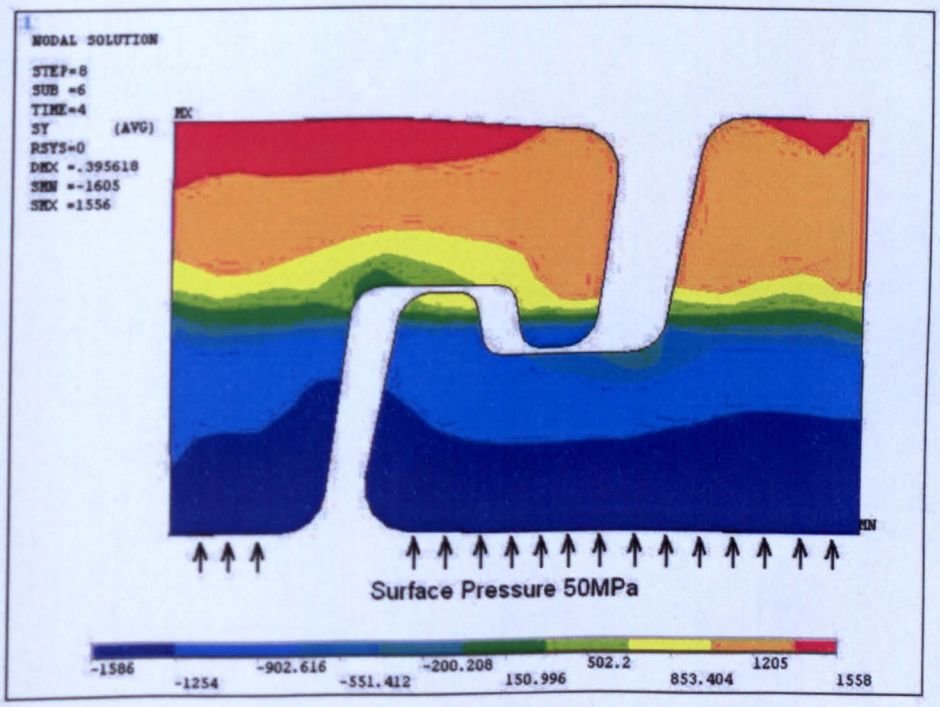

FIGURE A.9: Eighth stage, surface pressure of 50 MPa applied on inner radius stress in MPa

Appendix B

Tensile armour wire stress plots

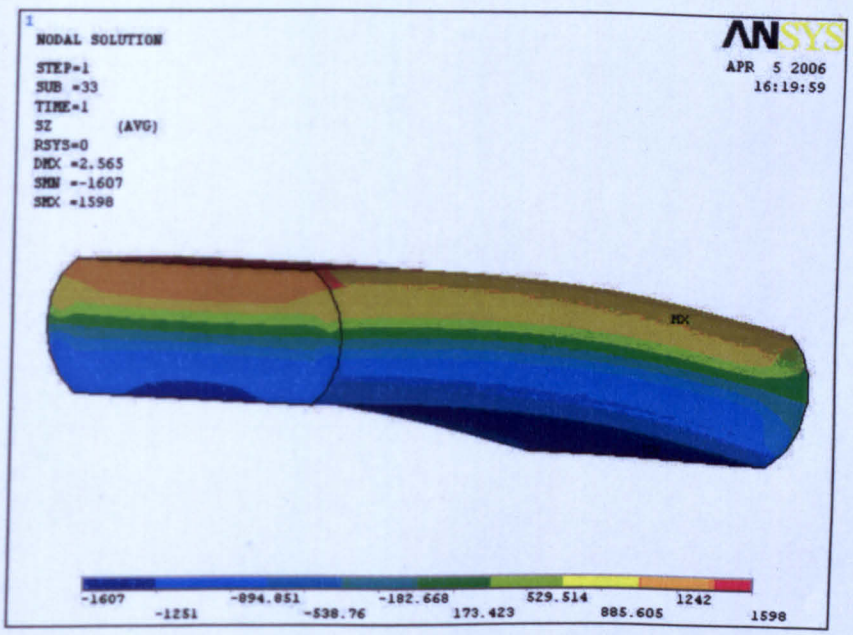

FIGURE B.1: First bend of radius 75 mm; bending stress in MPa

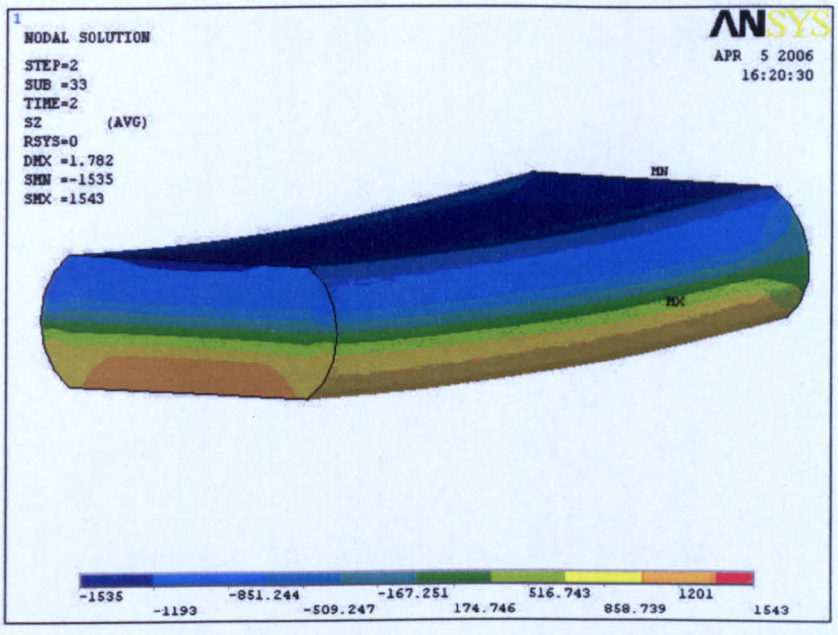

FIGURE B.2: Second bend of radius 110 mm; bending stress in MPa

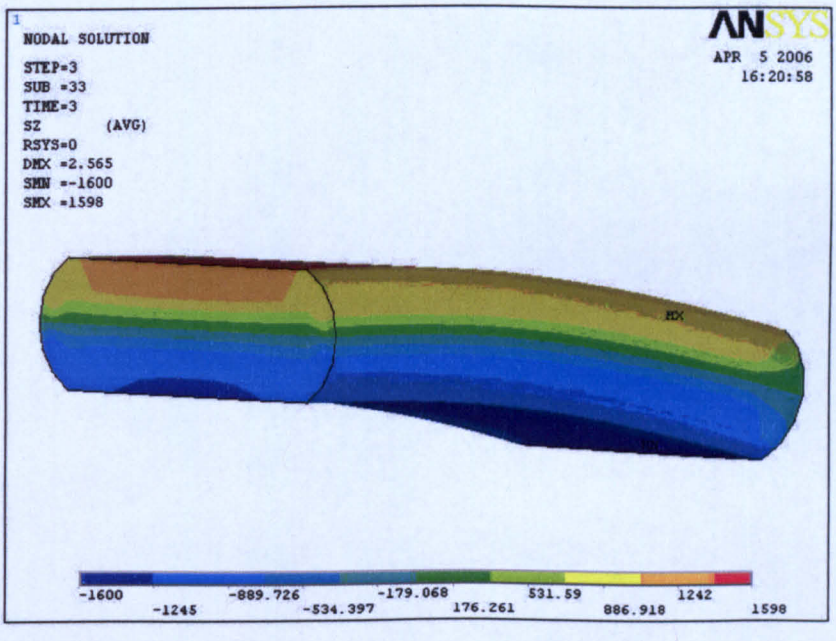

FIGURE B.3: Third bend of radius 75 mm; bending stress in MPa

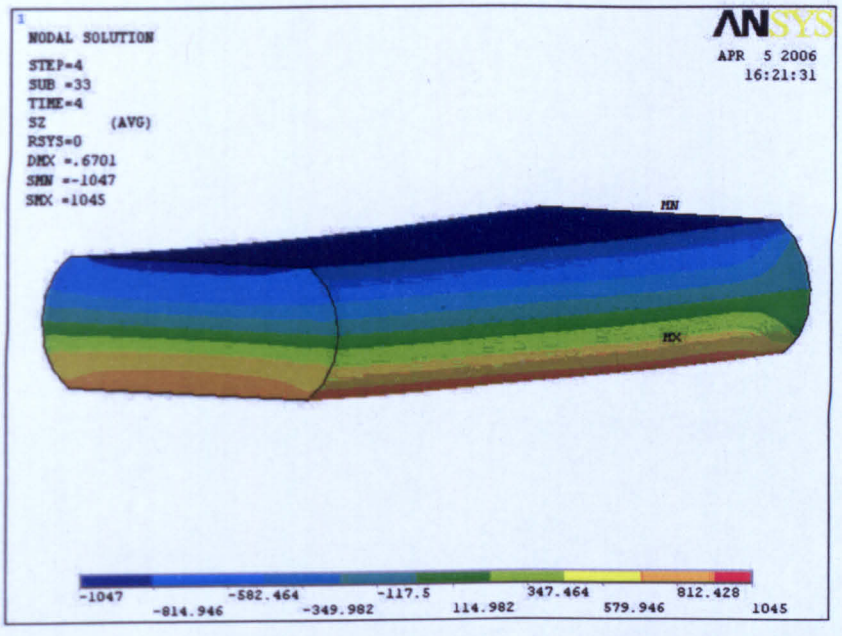

FIGURE B.4: Fourth bend of radius 300 mm; bending stress in MPa

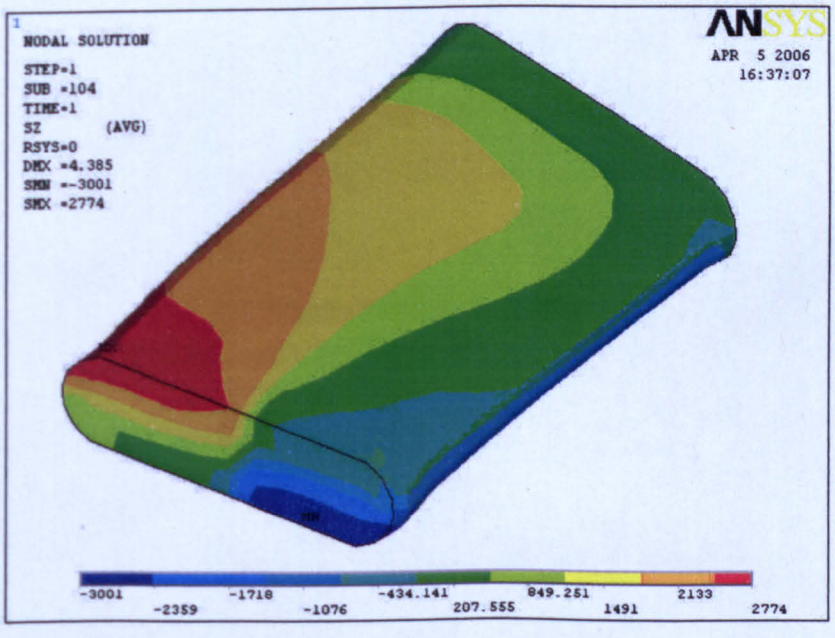

FIGURE B.5: Fifth bend of radius 300 mm; side (off plane) bending stress in MPa

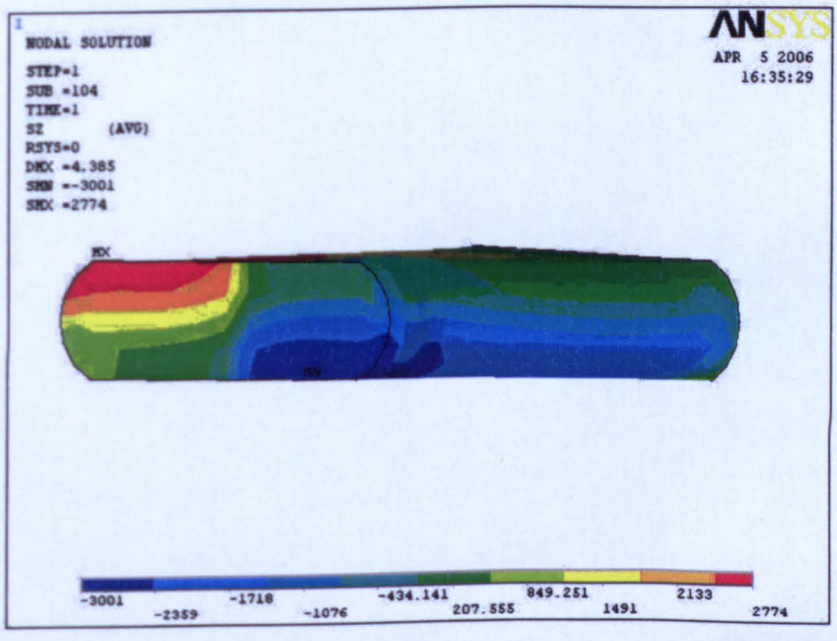

FIGURE B.6: Fifth bend of radius 300 mm; side (off plane) bending stress in MPa

Appendix C

Software Input Listing

```
RESIDUAL STRESS ANALYSIS OF PRESSURE & TENSILE ARMOUR WIRES OF FLEXIBLE RISERS
A 3D FE MODEL BY S ALAVANDIMATH
ANSYS INPUT FILE; ALL RIGHTS RESERVED
RESEARCH CONDUCTED AT SHEFFIELD HALLAM UNIVERSITY

!*************** INPUT DATA ********************

FINI
/CLEAR

/TITLE, CYCLIC BENDING OF PA WIRE; S ALAVANDIMATH
/FILENAM,PABEND
/UNITS,SI
GRAV=9.81
PI=ACOS(-1)

AN_TYPE=2                    ! 1=ELASTIC ;   2=ELASTIC-PLASTIC

!****************** GEOMETRY **************
```

```
!ALL DIMENSIONS ARE IN MM

OD=240          !PA OUTER DIAMETER
WT=12           !PA WIRE THICKNESS
ZL=2            !GEOMETRY START Z-LOCATION MUST BE ALWAYS >0

/PREP7

ET,1,MESH200,6    !2D ELEMENT DEFINITION FOR AREA MESH
ET,2,SOLID185     !3D SOLID ELEMENT DEFINITION
ET,3,SOLID185     !3D SOLID ELEMENT DEFINITION

K,1,OD/2-WT,,ZL
K,2,OD/2-WT,,ZL*3.09
K,3,(OD/2-WT)*1.06363,,ZL*3.67
K,4,(OD/2-WT)*1.06363,,ZL*4.878
K,5,(OD/2-WT)*1.06363,,ZL*5.288
K,6,(OD/2-WT)*1.06363,,ZL*6.05
K,7,(OD/2-WT)*1.047,,ZL*6.2
K,8,(OD/2-WT)*1.047,,ZL*7.2
K,9,(OD/2-WT)*1.059,,ZL*7.31
K,10,(OD/2-WT)*1.104,,ZL*7.7
K,11,(OD/2-WT)*1.1081,,ZL*5.838
K,12,(OD/2-WT)*1.1091,,ZL*4.45
K,13,(OD/2-WT)*1.1091,,ZL
K,14,OD/2-WT/2,,ZL

*GET,KMAX,KP,,NUM,MAX
*DO,LK,1,KMAX-1,1
L,LK,LK+1
*ENDDO
```

```
L,1,KMAX

LFILLT,1,2,1.01
LFILLT,2,3,1.01
LFILLT,5,6,0.5
LFILLT,6,7,0.5
LFILLT,7,8,1.01
LFILLT,9,10,1.27

L,14,17
L,18,12
L,19,11
L,20,9

AL,6,18,7,19,8,24
AL,17,24,9,20,10,23
AL,3,4,5,23,11,22
AL,16,22,12,13,21
AL,1,15,2,21,14

!***********MESHING AREA 1 ***************

LESIZE,6,,,5
LESIZE,19,,,5
LESIZE,18,,,3
LESIZE,8,,,3
LESIZE,7,,,4
LESIZE,24,,,6

MSHAPE,0,2D
MSHKEY,2
```

```
ALLS

TYPE,1
AMESH,1
ALLS

!***********MESHING AREA 2 ***************

LESIZE,23,,,7
LESIZE,17,,,3
LESIZE,9,,,4
LESIZE,20,,,5
LESIZE,10,,,3

MSHAPE,0,2D
MSHKEY,2
ALLS
TYPE,1
AMESH,2
ALLS

!***********MESHING AREA 3 ***************

LESIZE,22,,,9
LESIZE,3,,,3
LESIZE,4,,,4
LESIZE,5,,,3
LESIZE,11,,,6

MSHAPE,0,2D
MSHKEY,2
```

```
ALLS

TYPE,1
AMESH,3
ALLS

!***********MESHING AREA 4 ***************

LESIZE,13,,,6
LESIZE,21,,,9
LESIZE,16,,,5
LESIZE,12,,,7

MSHAPE,0,2D
MSHKEY,2
ALLS

TYPE,1
AMESH,4
ALLS

!***********MESHING AREA 5 ***************

LESIZE,14,,,6
LESIZE,1,,,6
LESIZE,15,,,4
LESIZE,2,,,7

MSHAPE,0,2D
MSHKEY,2
ALLS
```

```
TYPE,1
AMESH,5

!************** SECOND SECTION *************

K,27,OD/2-WT,,ZL*3.89
K,28,(OD/2-WT)*1.04925,,ZL*4.33617
K,29,(OD/2-WT)*1.0618,,ZL*4.45
K,30,(OD/2-WT)*1.0618,,ZL*5.5
K,31,(OD/2-WT)*1.045,,ZL*5.65
K,32,(OD/2-WT)*1.045,,ZL*6.41175
K,33,(OD/2-WT)*1.045,,ZL*6.77462
K,34,(OD/2-WT)*1.045,,ZL*8.15
K,35,(OD/2-WT)*1.1091,,ZL*8.65
K,36,(OD/2-WT)*1.1091,,ZL*11
K,37,OD/2-WT/2,,ZL*11
K,38,(OD/2-WT),,ZL*11
K,39,(OD/2-WT),,ZL*7.712
K,40,(OD/2-WT),,ZL*5.8617

*GET,KMAX2,KP,,NUM,MAX
*DO,LM,27,KMAX2-1,1
L,LM,LM+1
*ENDDO
L,27,KMAX2

LFILLT,25,38,1.27
LFILLT,26,27,1.01
LFILLT,27,28,0.5
LFILLT,28,29,0.5
```

```
LFILLT,31,32,1.01
LFILLT,32,33,1.01

L,28,47
L,40,48
L,39,49
L,50,37

AL,26,40,27,41,28,45
AL,25,45,42,46,38,39
AL,46,29,30,31,47,37
AL,47,43,48,35,36
AL,32,44,33,34,48

!***********MESHING AREA 6 ***************

LESIZE,40,,,5
LESIZE,28,,,5
LESIZE,41,,,3
LESIZE,26,,,3
LESIZE,27,,,4
LESIZE,45,,,6

MSHAPE,0,2D
MSHKEY,2
ALLS

TYPE,1
AMESH,6
ALLS
```

```
!***********MESHING AREA 7 ***************

LESIZE,46,,,7
LESIZE,42,,,3
LESIZE,25,,,4
LESIZE,39,,,5
LESIZE,38,,,3

MSHAPE,0,2D
MSHKEY,2
ALLS

TYPE,1
AMESH,7
ALLS

!***********MESHING AREA 8 ***************

LESIZE,47,,,9
LESIZE,31,,,3
LESIZE,30,,,4
LESIZE,29,,,3
LESIZE,37,,,6

MSHAPE,0,2D
MSHKEY,2
ALLS

TYPE,1
AMESH,8
ALLS
```

```
!***********MESHING AREA 9 ***************

LESIZE,35,,,6
LESIZE,48,,,9
LESIZE,43,,,5
LESIZE,36,,,7

MSHAPE,0,2D
MSHKEY,2
ALLS

TYPE,1
AMESH,9
ALLS

!***********MESHING AREA 10 ***************

LESIZE,34,,,6
LESIZE,33,,,6
LESIZE,44,,,4
LESIZE,32,,,7

MSHAPE,0,2D
MSHKEY,2
ALLS

TYPE,1
AMESH,10
/VIEW,1,,1
/ANG, 1
```

```
GPLO

!---------------------

/VIEW,1,,,-1
/ANG,1,-90


YMX=10
R=80
H=6

ND_=0
KALE=0
KOODU=0
!=======================
!EXTRUSION IN Y-DIRE'TN

ALLS
EXTOPT,ESIZE,20
EXTOPT,ACLEAR,0
TYPE,3
VEXT,1,5,1,,YMX
TYPE,4
VEXT,6,10,1,,YMX

ALLS
EPLO

ALLS
NUMMRG,KP
```

```
NUMMRG,NODE
NUMMRG,MAT

!------------
!KINH PROPERTIES

ALLS
TB,KINH,1,1,10
TBTEMP,20
TBPT,,0.00175,350
TBPT,,0.0027,500
TBPT,,0.0035,600
TBPT,,0.0055,815
TBPT,,0.008,1000
TBPT,,0.0145,1070.6
TBPT,,0.04,1180
TBPT,,0.1,1400
TBPT,,0.2,1800
TBPT,,0.3,2200

MPTEMP,1,20
MPDATA,EX,1,1,200000
MPDATA,PRXY,1,1,0.3
ALLS

!-------------------
!NODE COUPLING

ALLS
NSEL,S,LOC,Z,2,2
NSEL,A,LOC,Z,22,22
```

```
CM,COUPLE,NODE
ALLS

CMSEL,S,COUPLE,NODE
!CPCYC,UX,0.3,,,,20.00
!CPCYC,UY,0.3,,,,20.00
!CPCYC,UZ,0.3,,,,20.00
ALLS

!************************************
!MPC 184 ELEMENTS

ALLS
NSEL,S,LOC,Y,YMX,YMX
!NSEL,R,LOC,Z,2,21.8
CM,FREENODE,NODE
ALLS

CMSEL,S,FREENODE
*GET,INPLT_NUM,NODE,,COUNT
*DIM,FPILOT,ARRAY,INPLT_NUM
*GET,N_TOPACTIVE,NODE,,NUM,MIN
  FPILOT(1)=N_TOPACTIVE

*DO,I,2,INPLT_NUM
  *GET,N_NEXT,NODE,N_TOPACTIVE,NXTH
   FPILOT(I)=N_NEXT
   N_TOPACTIVE=N_NEXT
*ENDDO

ALLS
```

```
CMSEL,S,FREENODE
NWPAVE,ALL
CSYS,4
*GET,DX,CDSY,4,LOC,X
*GET,DY,CDSY,4,LOC,Y
*GET,DZ,CDSY,4,LOC,Z
NSEL,ALL
*GET,N_MAX,NODE,,NUM,MAX
PLT_NODE=N_MAX+1
CSYS,0
N,PLT_NODE,DX,DY+5,DZ
ALLS

*GET,MAX_ET,ETYP,,NUM,MAX
ET,MAX_ET+1,MPC184,1
TYPE,MAX_ET+1
MAX_MAT=MPINQR(0,0,14)
MP,DENS,MAX_MAT+1,0
MP,ALPX,MAX_MAT+1,0
MAT,MAX_MAT+1
REAL

CMSEL,S,FREENODE
NSEL,A,NODE,,PLT_NODE

*DO,I,1,INPLT_NUM
E,PLT_NODE,FPILOT(I)
*ENDDO

/PBC,CE,1
ALLS
```

```
!
!STOP FLYING

ALLS
NSEL,S,LOC,Y
D,ALL,UY
ALLS

NSEL,S,LOC,X,109.98,110
NSEL,R,LOC,Y
D,ALL,UX
ALLS

NSEL,S,LOC,Z,2,2
NSEL,R,LOC,Y
D,ALL,UZ
ALLS

!------------------------------
!BOTTOM FACE DISPS---1ST BENDCW

ALLS
*DO,I,0,19,0.5
NSEL,S,LOC,X,109.98,110.05
NSEL,R,LOC,Y,I,I
YDISP=((R-H)*(SIN(I/R)))-I
XDISP=(R-H)*(COS(I/R)-1)
!D,ALL,UY,YDISP
!D,ALL,UX,XDISP
*END DO
```

```
ALLS

!------------------------------
!TOP FACE DISPS---1ST BENDCW

ALLS
*DO,I,0,19,0.5
NSEL,S,EXT
NSEL,R,LOC,X,122.1,122
NSEL,R,LOC,Y,I,I
YDISP=((R+H)*(SIN(I/R)))-I
XDISP=(R+H)*(COS(I/R)-1)
!D,ALL,UY,YDISP
!D,ALL,UX,XDISP
*END DO
ALLS

!--------------------------------
!SIDE END DISPLACEMENTS---1ST BENDCW

ALLS
NSEL,S,LOC,Y,YMX,YMX
NSEL,R,LOC,Z,2,21.8

*GET,CAR1,NODE,,COUNT
ND_=0
*DO,K,1,CAR1,1
ND_=NDNEXT(ND_)

*GET,CAR3,NODE,ND_,LOC,X
```

```
*IF,CAR3,LE,116.00,THEN

KALE=116.00-CAR3
YD=((R-KALE)*(SIN(YMX/R)))-YMX
XD=(R-KALE)*(COS(YMX/R)-1)

*ELSE
KOODU=CAR3-116.00
YD=((R+KOODU)*(SIN(YMX/R)))-YMX
XD=(R+KOODU)*(COS(YMX/R)-1)
*ENDIF

!D,ND_,UY,YD
!D,ND_,UX,XD

*ENDDO
ALLS

F,PLT_NODE,MZ,1000E3

ALLS
OUTRESS,ALL,ALL
LSWRITE,1

/SOLU
SOLVE
!--------------------
!SECOND BEND RADIUS 115MM

R=115
```

```
DDELE,ALL,ALL

ALLS
NSEL,S,LOC,Y
D,ALL,UY
ALLS

NSEL,S,LOC,X,109.98,110
NSEL,R,LOC,Y
D,ALL,UX
ALLS

NSEL,S,LOC,Z,2,2
NSEL,R,LOC,Y
D,ALL,UZ
ALLS

!-----------------------
!BOTTOM FACE DISPS---2CCW

ALLS
*DO,I,0,20,0.5
NSEL,S,LOC,X,109.98,110.05
NSEL,R,LOC,Y,I,I
YDISP=((R+H)*(SIN(I/R)))-I
XDISP=(R+H)*(1-COS(I/R))
D,ALL,UY,YDISP
D,ALL,UX,XDISP
*END DO
ALLS
```

```
!----------------------
!TOP FACE DISPS---2CCW
ALLS
*DO,I,0,20,0.5
NSEL,S,EXT
NSEL,R,LOC,X,122.1,122
NSEL,R,LOC,Y,I,I
YDISP=((R-H)*(SIN(I/R)))-I
XDISP=(R-H)*(1-COS(I/R))
D,ALL,UY,YDISP
D,ALL,UX,XDISP
*END DO
ALLS

!--------------------
!SIDE END DISPS--2CCW

ALLS
NSEL,S,LOC,Y,YMX,YMX
NSEL,R,LOC,Z,2,21.8

*GET,CAR1,NODE,,COUNT
ND_=0
*DO,K,1,CAR1,1
ND_=NDNEXT(ND_)

*GET,CAR3,NODE,ND_,LOC,X

*IF,CAR3,LE,116.00,THEN

KALE=116.00-CAR3
```

```
YD=((R+KALE)*(SIN(YMX/R)))-YMX
XD=(R+KALE)*(1-COS(YMX/R))

*ELSE
KOODU=CAR3-116.00
YD=((R-KOODU)*(SIN(YMX/R)))-YMX
XD=(R-KOODU)*(1-COS(YMX/R))

*ENDIF

D,ND_,UY,YD
D,ND_,UX,XD

*ENDDO
ALLS

ALLS
OUTRESS,ALL,ALL
LSWRITE,2

!--------------------
!THIRD BEND RADIUS 80MM

R=80

DDELE,ALL,ALL

ALLS
NSEL,S,LOC,Y
D,ALL,UY
ALLS
```

```
NSEL,S,LOC,X,109.98,110
NSEL,R,LOC,Y
D,ALL,UX
ALLS

NSEL,S,LOC,Z,2,2
NSEL,R,LOC,Y
D,ALL,UZ
ALLS

!------------------------
!BOTTOM FACE DISPS---3-CW

ALLS
*DO,I,0,20,0.5
NSEL,S,LOC,X,109.98,110.05
NSEL,R,LOC,Y,I,I
YDISP=((R-H)*(SIN(I/R)))-I
XDISP=(R-H)*(COS(I/R)-1)
D,ALL,UY,YDISP
D,ALL,UX,XDISP
*END DO
ALLS

!----------------------
!TOP FACE DISPS---3-CW
ALLS
*DO,I,0,20,0.5
NSEL,S,EXT
NSEL,R,LOC,X,122.1,122
```

```
NSEL,R,LOC,Y,I,I
YDISP=((R+H)*(SIN(I/R)))-I
XDISP=(R+H)*(COS(I/R)-1)
D,ALL,UY,YDISP
D,ALL,UX,XDISP
*END DO
ALLS

!-------------------------
!SIDE END DISPLACEMENTS--3-CW
ALLS
NSEL,S,LOC,Y,YMX,YMX
NSEL,R,LOC,Z,2,21.8

*GET,CAR1,NODE,,COUNT
ND_=0
*DO,K,1,CAR1,1
ND_=NDNEXT(ND_)

*GET,CAR3,NODE,ND_,LOC,X

*IF,CAR3,LE,116.00,THEN

KALE=116.00-CAR3
YD=((R-KALE)*(SIN(YMX/R)))-YMX
XD=(R-KALE)*(COS(YMX/R)-1)

*ELSE
KOODU=CAR3-116.00
YD=((R+KOODU)*(SIN(YMX/R)))-YMX
XD=(R+KOODU)*(COS(YMX/R)-1)
```

```
*ENDIF

D,ND_,UY,YD
D,ND_,UX,XD

*ENDDO
ALLS

ALLS
OUTRESS,ALL,ALL
LSWRITE,3
!--------------------
!FOURTH BEND RADIUS 305MM

R=305

ALLS
DDELE,ALL,ALL

ALLS
NSEL,S,LOC,Y
D,ALL,UY
ALLS

NSEL,S,LOC,X,109.98,110
NSEL,R,LOC,Y
D,ALL,UX
ALLS

NSEL,S,LOC,Z,2,2
NSEL,R,LOC,Y
```

```
D,ALL,UZ
ALLS

!-----------------------
!BOTTOM FACE DISPS---4CCW

ALLS
*DO,I,0,20,0.5
NSEL,S,LOC,X,109.98,110.05
NSEL,R,LOC,Y,I,I
YDISP=((R+H)*(SIN(I/R)))-I
XDISP=(R+H)*(1-COS(I/R))
D,ALL,UY,YDISP
D,ALL,UX,XDISP
*END DO
ALLS

!-----------------------
!TOP FACE DISPS---4CCW
ALLS
*DO,I,0,20,0.5
NSEL,S,EXT
NSEL,R,LOC,X,122.1,122
NSEL,R,LOC,Y,I,I
YDISP=((R-H)*(SIN(I/R)))-I
XDISP=(R-H)*(1-COS(I/R))
D,ALL,UY,YDISP
D,ALL,UX,XDISP
*END DO
ALLS
```

```
!--------------------
!SIDE END DISPS--4CCW

ALLS
NSEL,S,LOC,Y,YMX,YMX
NSEL,R,LOC,Z,2,21.8

*GET,CAR1,NODE,,COUNT
ND_=0
*DO,K,1,CAR1,1
ND_=NDNEXT(ND_)

*GET,CAR3,NODE,ND_,LOC,X

*IF,CAR3,LE,116.00,THEN

KALE=116.00-CAR3
YD=((R+KALE)*(SIN(YMX/R)))-YMX
XD=(R+KALE)*(1-COS(YMX/R))

*ELSE
KOODU=CAR3-116.00
YD=((R-KOODU)*(SIN(YMX/R)))-YMX
XD=(R-KOODU)*(1-COS(YMX/R))

*ENDIF

D,ND_,UY,YD
D,ND_,UX,XD

*ENDDO
```

```
ALLS

ALLS
OUTRESS,ALL,ALL
LSWRITE,4

!------------------------
!************************
!WIRE STRAIGHTENING-- 5TH BEND
!REVERSAL OF 4TH BCS

ALLS
DDELE,ALL,ALL

ALLS
NSEL,S,LOC,Y
D,ALL,UY
ALLS

NSEL,S,LOC,X,109.98,110
NSEL,R,LOC,Y
D,ALL,UX
ALLS

NSEL,S,LOC,Z,2,2
NSEL,R,LOC,Y
D,ALL,UZ
ALLS

ALLS
OUTRESS,ALL,ALL
```

```
LSWRITE,5

!-----------------------
!SIXTH SIDE BEND CCW-TV

*SET,R,305

DDELE,ALL,ALL

ALLS
NSEL,S,LOC,Y
D,ALL,UY
ALLS

NSEL,S,LOC,X,109.98,110
NSEL,R,LOC,Y
D,ALL,UX
ALLS

NSEL,S,LOC,Z,2,2
NSEL,R,LOC,Y
D,ALL,UZ
ALLS

NSEL,S,LOC,Z,1.98,2.1
NSEL,R,LOC,X,109.98,110
D,ALL,UX
ALLS

!----------------------
!TOP FACE SIDE BEND CCW-TV
```

```
ALLS
*DO,I,0,20,0.5
NSEL,S,LOC,Z,1.98,2.1
NSEL,R,LOC,Y,I,I
YDISP=((R+0)*(SIN(I/R)))-I
ZDISP=(R+0)*(1-COS(I/R))
D,ALL,UY,YDISP
D,ALL,UZ,ZDISP
*END DO
ALLS

!--------------------------------
!SIDE END DISPLACEMENTS---1ST BENDCW

ALLS
ESEL,S,TYPE,,3
NSLE,R,ALL
NSEL,R,LOC,Y,YMX,YMX

*GET,CAR1,NODE,,COUNT
ND_=0
*DO,K,1,CAR1,1
ND_=NDNEXT(ND_)

*GET,CAR3,NODE,ND_,LOC,Z

RHUN=CAR3-2.00
YD=((R-RHUN)*(SIN(YMX/R)))-YMX
ZD=(R-RHUN)*(1-COS(YMX/R))
```

```
D,ND_,UY,YD
D,ND_,UZ,ZD

*ENDDO
ALLS

ALLS
ESEL,S,TYPE,,4
NSLE,R,ALL
NSEL,R,LOC,Y,YMX,YMX
NSEL,R,LOC,Z,1.8,21.9

*GET,BUS1,NODE,,COUNT
ND_=0
*DO,K,1,BUS1,1
ND_=NDNEXT(ND_)

*GET,BUS3,NODE,ND_,LOC,Z

DHAN=22.00-BUS3
YD=((R+DHAN)*(SIN(YMX/R)))-YMX
ZD=(R+DHAN)*(1-COS(YMX/R))

D,ND_,UY,YD
D,ND_,UZ,ZD

*ENDDO
ALLS

ALLS
OUTRESS,ALL,ALL
```

```
LSWRITE,6

!------------------
!FINAL PIPE BENDING--7CW

ALLS
*SET,R,116

DDELE,ALL,ALL

ALLS
NSEL,S,LOC,Y
D,ALL,UY
ALLS

NSEL,S,LOC,X,109.98,110
NSEL,R,LOC,Y
D,ALL,UX
ALLS

NSEL,S,LOC,Z,2,2
NSEL,R,LOC,Y
D,ALL,UZ
ALLS
!------------------------------
!BOTTOM FACE DISPS--7TH BEND CW

ALLS
*DO,I,0,20,0.5
NSEL,S,LOC,X,109.98,110.05
NSEL,R,LOC,Y,I,I
```

```
YDISP=((R-H)*(SIN(I/R)))-I
XDISP=(R-H)*(COS(I/R)-1)
D,ALL,UY,YDISP
D,ALL,UX,XDISP
*END DO
ALLS

!----------------------------
!TOP FACE DISPS--7TH BEND CW

ALLS
*DO,I,0,20,0.5
NSEL,S,EXT
NSEL,R,LOC,X,122.1,122
NSEL,R,LOC,Y,I,I
YDISP=((R+H)*(SIN(I/R)))-I
XDISP=(R+H)*(COS(I/R)-1)
D,ALL,UY,YDISP
D,ALL,UX,XDISP
*END DO
ALLS

!-------------------------------
!SIDE END DISPLACEMENTS--7TH BEND CW

ALLS
NSEL,S,LOC,Y,YMX,YMX
NSEL,R,LOC,Z,2,21.8

*GET,CAR1,NODE,,COUNT
ND_=0
```

```
*DO,K,1,CAR1,1
ND_=NDNEXT(ND_)

*GET,CAR3,NODE,ND_,LOC,X

*IF,CAR3,LE,116.00,THEN

KALE=116.00-CAR3
YD=((R-KALE)*(SIN(YMX/R)))-YMX
XD=(R-KALE)*(COS(YMX/R)-1)

*ELSE
KOODU=CAR3-116.00
YD=((R+KOODU)*(SIN(YMX/R)))-YMX
XD=(R+KOODU)*(COS(YMX/R)-1)
*ENDIF

D,ND_,UY,YD
D,ND_,UX,XD
*ENDDO
ALLS

ALLS
OUTRESS,ALL,ALL
LSWRITE,7

/SOLU
ALLS
!SOLCONTROL,ON
NSUBST,100,200,30
LSSOLVE,1,7
```

```
/POST1
UPCOORD,1,ON

FINI

/PREP7
!************* PRESSURE ANALYSIS ************
!--------------------
!PRESSURE COMPMONENTS

NSEL,S,LOC,X,109.98,110.05
CM,INPRE,NODE
ALLS

NSEL,R,LOC,X,122.1,122
CM,EXPRE,NODE
ALLS

ALLS
NSEL,S,LOC,X,109.98,110.05
NSEL,A,LOC,X,122.1,122
DDELE,ALL,ALL
ALLS

CSYS,1
NROTAT,ALL,ALL

D,ALL,UY

CMSEL,S,INPRE,NODE
```

```
SF,ALL,PRES,50
ALLS

ALLS
OUTRESS,ALL,ALL
LSWRITE,8

/SOLU
ALLS
KUSE,-1
SOLVE

/POST1
/DSCALE,,1
RSYS,1
SET,8
PLNSOL,S,Y

!------------------
!GRAPHING
ALLS
/GTHK,CURVE,0
/GTHK,AXIS,1
/GTHK,GRID,1
PATH,SHIVA44,2,30,20,
PPATH,1,412
PPATH,2,147
PDEF,,S,Y,NOAV
PLPATH,SY
```

Appendix D

Offshore Operations and Riser Installation

D.1 Oil Platforms

The flexible risers are used to connect the seabed production flow lines to oil platforms or FPSOs when the hydrocarbons are pumped vertically up from sea beds. An oil platform or oil rig is a large structure used to house workers and machinery needed to drill and or extract oil and natural gas through wells in the ocean bed. Depending on the circumstances, the platform may be attached to the ocean floor, consist of an artificial island or be floating as shown in Figure D1. Generally, oil platforms are located on the continental shelf, though as technology improves, drilling and production in deeper waters becomes both feasible and profitable.

A typical platform may have around thirty wellheads located on the seabed and directional drilling allows reservoirs to be accessed at both different depths and at remote positions up to 5 miles (8 kilometers) from the platform. Many platforms also have remote wellheads attached by umbilical connections, these may be single wells or a manifold centre for multiple wells.

FIGURE D.1: Different kinds of offshore oil platforms (Source: U.S. Minerals Management Service, Gulf of Mexico Region, Offshore Information, October 1999)

D.2 Fixed Platforms

These platforms are built on concrete and/or steel legs anchored directly onto the seabed, supporting a deck with space for drilling rigs, production facilities and crew quarters. Such platforms are, by virtue of their immobility, designed for very long term use (for instance the Hibernia platform). Various types of structure are used, steel jacket, concrete caisson, floating steel and even floating concrete. Steel jackets are vertical sections made of tubular steel members, and are usually piled into the seabed

Concrete caisson structures, pioneered by the Condeep concept, often have in-built oil storage in tanks below the sea surface and these tanks were often used as a flotation capability, allowing them to be built close to shore (Norwegian fjords and Scottish firths are popular because they are sheltered and deep enough) and then floated to their final position where they are sunk to the seabed. Fixed platforms are economically feasible for installation in water depths up to about 1,700 feet (520 m).

D.3 Compliant Towers:

These platforms consist of narrow, flexible towers and a piled foundation supporting a conventional deck for drilling and production operations. Compliant towers are designed to sustain significant lateral deflections and forces, and are typically used in water depths ranging from 1,500 and 3,000 feet (450 and 900 m).

D.4 Semi-submersible Platform:

These platforms have legs of sufficient buoyancy to cause the structure to float, but of weight sufficient to keep the structure upright. Semi-submersible rigs can be moved from place to place; can be ballasted up or down by altering the amount of flooding in buoyancy tanks; they are generally anchored by chain, wire rope and/or polyester rope during drilling operations, though they can also be kept in place by the use of dynamic positioning. Semi-submersibles can be used in water depths from 200 to 10,000 feet (60 to 3,050 m).

D.5 Jack-up Platforms:

Jackups, as the name suggests, are platforms that can be jacked up above the sea using legs which can be lowered like jacks. These platforms are typically used in water depths up to 400 feet (120 m), although some designs can go to 550 feet (170 m) depth. They are designed to move from place to place, and then anchor themselves by deploying the legs to the ocean bottom using a rack and pinion gear system on each leg.

D.6 Drillships

A drillship is a maritime vessel that has been fitted with drilling apparatus. It is most often used for exploratory drilling of new oil or gas wells in deep water but can also be used for scientific drilling. Early versions were built on a modified tanker hull, but purpose-built designs are used today. Most drillships are outfitted with a dynamic positioning system to maintain position over the well. They can drill in water depths up to 12,000 feet (3,660 m).

D.7 Floating production systems

FPSOs are large ships equipped with processing facilities and moored to a location for a long period. The main types of floating production systems are FPSO (floating production, storage, and offloading system), FSO (floating storage and offloading system), and FSU (floating storage unit). These ships do not actually drill for oil or gas. A typical FPSO is shown in Figure D2.

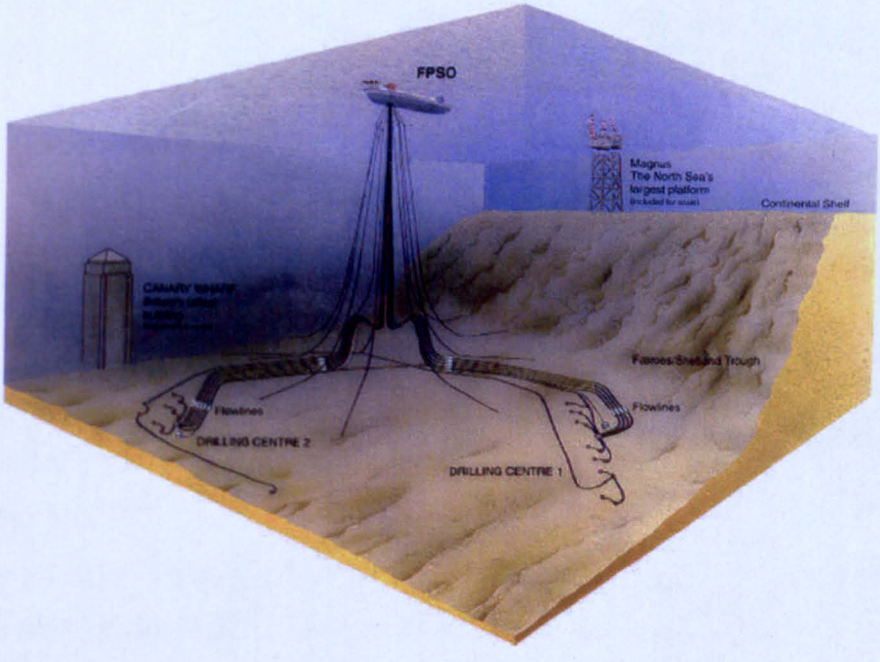

FIGURE D.2: Risers connected to seabed flow lines and a FPSO

D.8 Tension-leg platform

TLPs consist of floating rigs tethered to the seabed in a manner that eliminates most vertical movement of the structure. TLPS are used in water depths up to about 6,000 feet (2,000 m). The "conventional" TLP is a 4-column design which looks similar to a semisubmersible. Proprietary versions include the Seastar and MOSES mini TLPs; they are relatively low cost, used in water depths between 600 and 4,300 feet (200 and 1,300 m). Mini TLPs can also be used as utility, satellite or early production platforms for larger deepwater discoveries.

D.9 Spar Platforms

Spars are moored to the seabed like the TLP, but whereas the TLP has vertical tension tethers the Spar has more conventional mooring lines. Spars have been designed in three configurations: the "conventional" one-piece cylindrical hull, the "truss spar" where the midsection is composed of truss elements connecting the upper buoyant hull (called a hard tank) with the bottom soft tank containing permanent ballast, and the "cell spar" which is built from multiple vertical cylinders.

The Spar may be more economical to build for small and medium sized rigs than the TLP, and has more inherent stability than a TLP since it has a large counterweight at the bottom and does not depend on the mooring to hold it upright. It also has the ability, by use of chain-jacks attached to the mooring lines, to move horizontally over the oil field. The first production spar was Kerr–McGee's Neptune, which is a floating production facility anchored in 1,930 feet (588 m) in the Gulf of Mexico, however spars (such as Brent Spar) were previously used as FSOs. Eni's Devil's Tower is located in 5,610 feet (1,710 m) of water, in the Gulf of Mexico, and is currently the world's deepest spar; however, when Shell's Perdido Spar is installed, it will be the deepest at 8,000 feet (2,438 m).

A vessel for exploration of hydrocarbons includes one or more risers extending from the vessel to the seabed, a hydrocarbon processing unit connected to the one

or more risers and to a storage or transport structure for storing the processed hydrocarbons. The vessel is anchored to the seabed; the vessel includes a lifting member for lowering risers vertically towards the sea bed. The lower end of the riser is connected to a subsea structure which is in turn connected to a long flow line where the hydrocarbons (either oil or gas or mixture of both) are transported from a well. The subsea structure is specially designed to allow the expansion and contraction of the long flow lines as well as risers due to operating temperature and pressure. The expansion and contraction of the flow lines is also due to slugging where in the oil flows as discontinues mixture of liquid and gas resulting in shocks when it passes through bends and restrictions. This creates repeated axial compressive and tensile forces leading to cyclic movement of risers. Apart from this the risers are also subjected to vibration due to ocean currents and waves.

D.10 Installation of risers in deep waters

Operators developing offshore oil and gas reserves, face the increasing challenge of reducing costs when the developments move into deeper water. The riser system cost is particularly sensitive to any increase in water depth; this is true also of the riser installation costs. The majority of current deepwater riser systems are based on a welded construction. High specification vessels are required to install these welded risers, incurring high day rates and mobilisation costs. An alternative to welded construction is the use of threaded and coupled (T&C) connections, T&C connections are a reliable, low cost method of joining pipe and have been used extensively in applications such as well casings and down hole tubing strings, and have recently been used successfully on top tensioned risers for dry tree production platforms in deepwater.

D.11 Flexible Catenary Risers

Flexible pipe is built up of a number of independent spiral laid steel and thermoplastic layers, and has been used for many years for both riser and flow line applications worldwide. The beneficial feature of flexible pipe is its ability to accommodate high curvature, allowing ease of installation and accommodation of dynamic motions. Flexible risers are used in a simple or wave catenary arrangement, as shown in Figure D3.

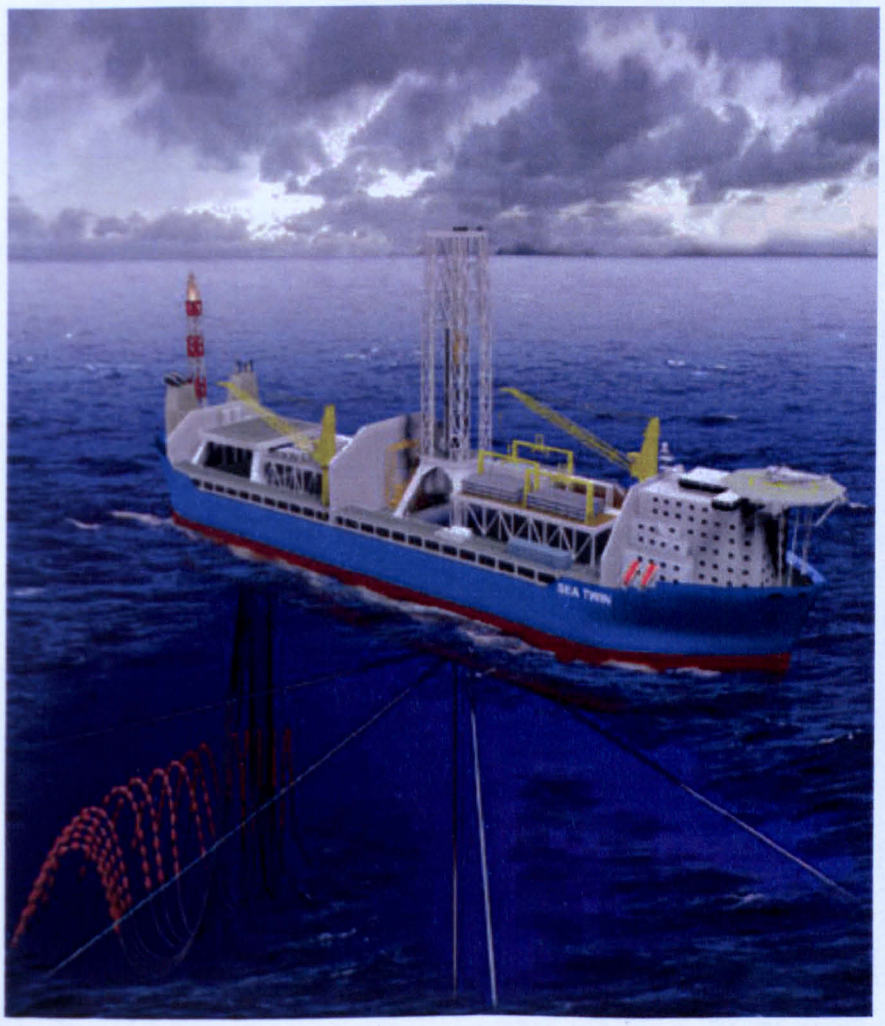

FIGURE D.3: Risers are connected to typical FPSO as wave catenary

The installation of flexible risers in deepwater is often limited by the collapse resistance of the pipe as it may be installed empty to keep the riser weight within the pipe lay vessel's tensioning capacity. As the external hydrostatic pressure increases

with water depth, the maximum riser diameter is thus limited by the practicality of strengthening the flexible pipe structure to resist the external pressure.

Flexible risers and flow lines are normally designed, procured and installed from a single vendor. There are only a small number of companies worldwide which manufacture flexible pipes for riser systems.

The flexibility of these pipes allows them to be spooled continuously on to a reel for efficient and quick transportation and installation. Installation speeds can average 500 metres per hour. Flexible risers can be installed from a large number of reel lay vessels, however for larger pipe diameters and deeper water the number of capable vessels is reduced. Special reels may have to be built in the case of large diameter flexible risers.

The installation weather window is mainly determined by the vessel response to environmental loading. In mild environments riser installation can be conducted almost year round and so installation schedules are generally quite flexible. For harsh environments suitable weather windows are small and risers are often pre-installed in the summer months. The risers are wet stored, and simply lifted from the seabed and connected to the host vessel when it is brought on station.

D.12 Steel Catenary Risers

Steel Catenary Risers (SCRs) have emerged as a major alternative to flexible risers in recent years for mild to moderate deepwater environments, such as Gulf of Mexico, West Africa, Brazil and Indonesia. The main advantage of the SCR is that steel pipe costs significantly less than flexible pipe, and is "flexible" in a long length.

The SCR consists primarily of a steel pipe string free hanging from the vessel to form a simple catenery. SCRs are typically used with tension leg platforms or spars where heave motions are small, or with semi-submersibles or FPSOs where the environment is mild.

A SCR is made up of a series of welded pipe joints. The fatigue performance of the welds is highly dependant on several inter related factors including pipe and weld material properties, joint dimensional tolerances, welding processes, welding procedure and inspection criteria. Good quality offshore welds are required in order to achieve sufficient fatigue lives for SCRs. As such, high specification vessels are required to perform these critical offshore welds, even if these vessels command high day rates and mobilisation costs. The installation window is determined by the vessel response whilst the riser joints are fixed during welding.

Unlike flexible risers, SCRs do not lend themselves to being wet stored before arrival of the host vessel, so they are generally installed in one campaign to avoid additional vessel mobilisation costs. Several installation methods are possible including:

J-Lay – The majority of SCRs installed to date use the J-lay technique. Riser stalks of up to 6 joints (hex-joint) are prefabricated onshore, reducing the number of welds that need to be made during offshore installation. J-lay collars used to support the pipe during installation are welded around the pipe and can act as buckle arrestors. The number of vessels capable of deeper water J-lay installation is limited. The current maximum tension limit is around 1000Te for high-end installation vessels, with several more vessels with capacities of over 500Te.

S-Lay – Installation of a riser by the S-lay method is similar to the J-lay method except the pipes are handled in the horizontal attitude. The technique is generally not suited to deepwater due to the very high back tensions required to prevent over stressing of the sag bend and over bend. This high back tension also makes dynamically positioning the installation vessel difficult. Consequently increased water depths reduce the number of capable installation vessels.

D.13 Single Line Offset Risers

Although relatively new in the market, the single line offset riser (SLOR) design has been proven or is planned on a number of projects. The SLOR employs a vertical steel riser section that is linked to the host vessel via a flexible pipe jumper. The key advantage of this hybrid arrangement is that the vertical riser response is largely decoupled from the vessel motions and hence becomes less susceptible to fatigue damage.

The vertical riser section is tensioned by steel buoyancy cans positioned at a distance below the water surface to minimize wave and current loading. It is offset from the host vessel such that a suitable length of flexible pipe jumper joining the top of the steel riser to the vessel can be fitted to accommodate the vessel motions. The SLOR can be used with any floating vessels and is suitable for deepwater and ultra-deepwater applications in all environments.

The SLOR can be either single pipe or pipe-in-pipe facilitating gas lift. Designs of both systems are available for depths up to 3000m and these can be installed from a wide range of installation vessels. The SLOR is developed with full consideration to dynamic response, thermal requirements, hardware selection, installation, and field development flexibility. A key feature is that it has low fatigue sensitivity and can be used with vessels which exhibit large dynamic motions and excursions.

Bibliography

[1] WITZ, J. A. and ZHIMIN, Tan (1992). On the flexural structural behaviour of flexible pipes, umbilical and marine cables. *Marine structures*, 5 (2–3), 229–249.

[2] A B CUSTODIO and M A VAZ, A Nonlinear formulation for the axisymmetric response of umbilical cables and flexible pipes, March 2002, Journal of Applied Ocean Research, 21–29.

[3] WITZ, J. A. and ZHIMIN, Tan (1992). On the axial-torsional structural behaviour of flexible pipes, umbilical and marine cables. *Marine structures*, 5 205–227.

[4] LOVE, A. E. H. (1893). A treatise on the mathematical theory of elasticity, Chapter 18, Cambridge University Press.

[5] COSTELLO, G. A. (1977). Large deflections of helical spring due to bending. *Engineering mechanics*, ASCE (103), 481-7.

[6] LECLAIR, R. A. and COSTELLO, G. A. (1986). Axial bending and torsional loading of a strand with friction. In: 550-5.

[7] BLANCO, J. A. and COSTELLO, G. A. (December 1974), Cylindrical constraint of helical springs. *Journal of applied mechanics div.*, 1138-40.

[8] OLIVEIRA, J. G., GOTO, Y. and OKAMOTO, T. (1985). Theoretical and methodological approaches to flexible pipe design & application. In: 517–26.

[9] GOTO, Y., et al. (1987). Analytical study of the mechanical strength of flexible pipes. *Offshore mechanics and arctic engineering*, 109 249–53.

[10] MCNAMARA, J. F. and HARTE, A. M. (March 1989). Three dimensional analytical simulation of flexible pipe wall structure. In: 477–82.

[11] FERET, J. J. and BOURNAZEL, C. L. (1987). Calculation of stresses and slip in structural layers of unbonded flexible pipes. *Offshore mechanics and arctic engineering*, 109 263–9.

[12] LUTCHANSKY, M. (August 1969). Axial stresses in armored wires of bent submarine cables. *Engineering for industry*, (ASME), 687–693.

[13] SPILLERS, W. R., et al. (1983). A helical tape on the cylinder subjected to bending. *Journal of engineering mechanics*, 109 1124–33.

[14] VINOGRADOV, O. G. and ATATEKIN, I. S. (1986). Internal friction due to wire twist in bent cable. *Journal of engineering mechanics*, 112 859–73.

[15] CARDOU, A. and JOLICOEUR, C. (1997). Mechanical models of helical strands. *Applied mechanics reviews*, 50 (1), 1–14.

[16] RAOOF, M. AND KRAINCANIC. I (1994). Critical examination of various approaches used for analyzing helical cables. *Journal of strain analysis for engineering design*, 29 (1), 43–55.

[17] RAMSEY, H. (1990). Analysis of inter-wire friction in multilayered cables under uniform extension and twisting. *International journal of mechanical sciences*, 32 (8), 709–716.

[18] MCIVER, D. B. (1995). A method of modelling the detailed component and overall structure of flexible pipe sections. *Engineering structures*, 17 (4), 254–266.

[19] FERNANDO, U. S. (January 2003). *Stress analysis of 10 mm and 12 mm FLEXLOK wires wrapped on to wellsteam flexible pipes.*

[20] FERNANDO, U. S., et al. (2004). The stress analysis and residual stress evaluation of pressure armour layers in flexible pipes using 3D finite element models. In: *23rd International Conference on Offshore Mechanics and Arctic Engineering, Jun 20–25 2004*, Vancouver, BC, Canada, American Society of Mechanical Engineers, New York, NY 10016-5990, United States, 57–65.

[21] JIANG, W. G., HENSHALL, J. L. and WALTON, J. M. (2000). A concise finite element model for three layered straight wire rope strand. *International journal of mechanical sciences*, 42 63–86.

[22] JIANG, W. G., YAO, M. S. and WALTON, J. M. (1999). A concise finite element model for simple straight wire rope strand. *International journal of mechanical sciences*, 41 143–161.

[23] HUH, H. and KIM, S. H. (2000). Stress evaluation with numerical integration schemes in finite element analysis of elasto-plastic bending. *Communications in numerical methods in engineering*, 16 (11), 755–66.

[24] FARHOOD NOWZARTASH and MAGDI MOHAREB, An elasto-plastic finite element for steel pipelines, May 2004, Journal of International Journal of Pressure Vessels and Piping, 919–930.

[25] R B WATERHOUSE, International Material Reviews, A Joint Publication of The Institute of Materials and ASM International, Vol. 37, No. 2, pp. 77–97.

[26] *MCS, Advanced Sub sea Engineering, MCS report on riser.* (April 2001), 2-1-4-181.

[27] SCHLEINZER, G. and FISCHER, F. D. (2000). Residual stresses in rails. Materials science and engineering, A288 280–283.

[28] JEFF GORDON and A BENJAMIN PERLMAN, Estimation of Residual Stresses In Railroad Commuter Car Wheels Following Manufacture.

[29] S L SRIMANI and J BASU, An investigation for control of residual stress in roller-straightened rails,

[30] K J MILLER "Educating the design engineer in materials technology" Dept. of Mechanical Engineering University of Sheffield.

[31] K J MILLER. "Material science perspective of metal fatigue resistance" The institute of Materials, Manuscript received 13 April 1993: in final form 28 May 1993 Author is at the Structural Integrity Research Institute, University of Sheffield (SIRIUS).

[32] S W WEN, P HARTLEY, I PILLINGER, and C E N STURGESS, Finite element analysis of four-pass cold rolling.

[33] HKDH Bhadeshia, Material Factor, Handbook of Residual stress and deformation of steel, ASM, 2002.

[34] J.LU, LASMIS, Prestress Engineering of structural materials: A global design approach to residual stress problem, Handbook of Residual stress and deformation of steel, ASM, 2002.

[35] JAIRO APARECIDO MARTINS, LISANDRO PAVIO CARDOSO, JOSE ALFREDO FRAYMANN, SERGIO TONINI BUTTON, Journal of Materials Processing Technology, pp. 30–35.

[36] Z BARSOUM, Residual Stress Analysis and Fatigue of Multi-pass Welded Tubular Structures.

[37] A D TRIM, Extreme responses of flexible risers, Marine Structures, Volume 5, Issue 5, 1992, pp. 367–385.

[38] A J WATTERS, I C SMITH, and D L GARRETT, The lifetime dynamics of a deep water riser design, Journal of Applied Ocean Research, 69–81.

[39] P A BROWN, A SOLTANAHMADI, R CHANDWANI, Problems encountered in detailed design of flexible riser systems, Engineering Structures, Volume 11, Issue 4 , October 1989, pp. 234–241.

[40] D.LOHE, K.H.LONG, VOHRINGER, Residual stresses and fatigue behaviour, University of Karlsruhe, Germany, Handbook of Residual stress and deformation of steel, ASM, 2002.

[41] LOHE AND O.VOHRINGER, Stability of residual stresses, Institute of Werkstoffkunde I, University of Karlsruhe, Germany. Handbook of Residual stress and deformation of steel, ASM, 2002.

[42] H HUH and S M KIM, Stress evaluation with numerical integration schemes in finite element analysis of elastic-plastic bending, April 2000.

[43] S J BARKER, Residual Stresses In Normal Grade Rails, British Railways Board, March 1994.

[44] B WANG, Residual Stress Distribution in Pure Bending Beam Subjected to Tensile Failure on One Side.

[45] HOBBS R.E., RAOOF M., Mechanism of Fretting Fatigue in Steel Cables, Internal Journal of Fatigue, 1994, Vol. 16, pp. 273–280, ISSN: 0142-1123.

[46] W KERR WILSON, Effect on fatigue strength, Institute of Mechanical Engineers, Nov. 1944.

[47] JANG-PING WANG, WEI-CHEN KAO, and JAMES WANG, Analysis of 3-D Rolling Forming with Generalized Rigid-Plastic Boundaries Approach.

[48] SEUNG-EOCK KIM, and DONG-HO LEE, Second-order distributed plasticity analysis of space steel frames, December 2001, Journal of Engineering Structures, 735–744.

[49] YOU-MIN HUANG, and DAW-KWEI LEU, An elasto-plastic finite-element simulation of successive UO-bending processes of sheet metal, March 1994, Journal of Materials Processing Technology 643-661.

[50] D. HORROCKS1 AND W. JOHNSON, "On anticlastic curvature with special reference to plastic bending" A literature survey and some experimental investigations, 1967, International Journal of Mechanical Sciences, Volume 9, Issue 12, December 1967, pp. 835–844.

[51] FATEMI AND L. YANG "Cumulative fatigue damage and life prediction theories: a survey of the state for the art of homogeneous materials" International Journal Fatigue Vol. 20. No. 1 pp. 9–34 1998.

[52] ANSYS Inc. *ANSYS multi-physics Documentation, Release. 9.0* [Computer Program].

[53] RAOOF M, HOBBS R.E., Torsional stiffness and Hysteresis in Spiral Strands, P.I. Civil Engineering, Pt-2, 1989, Vol. 87, pp. 501–514.

[54] M H PATEL, F B SYED, Review of flexible riser modelling and analysis techniques, Engineering Structures, Vol. 17, Issue 4, May 1995, pp. 293–304.

[55] KNAPP R H, Derivation of a new stiffness matrix for helically armoured cables considering tension and torsion, International Journal of Numerical Methods in Engineering, Volume 14, Issue 4, 1979, pp. 515–529.

[56] WANG ZHIQUN, Elastic-plastic fracture analysis of a thick-walled cylinder, June 1994,

[57] WILLIAM E BOWERS CAMESA, The Gap in Cable Technology.

[58] J A WITZ, A Case Study in the Cross-section Analysis of Flexible Risers, August 1995,

[59] J M LEROY and P ESTRIER, Calculation of Stresses and Slips in Helical Layers of Dynamically Bent Flexible Pipes.

[60] STEVEN A VELINSKY, GRANT L ANDERSON and GEORGE A COSTELLO, Wire Rope With Complex Cross Sections, Engineering Structures.

[61] F W GREALISH, A BLIAULT and K P CAVENY, New Standards in Flexible Pipe Technology Including API Spec 17J, May 1996.

[62] JOSE A G BOGARIN and NELSON F F EBECKEN, Integration of knowledge Sources for Flexible Pipe Evaluation and Design.

[63] S SAEVIK and S BERGE, Fatigue testing and theoretical studies of two 4 in flexible pipes, Engineering Structures.

[64] MICHAEL M BERNITSAS, JOHN E KOKARAKIS and ASJHAR IMRON, Large deformation three-dimensional static analysis of deep water marine risers, Engineering Structures.

[65] FERNANDO, U. S. (January 2002). *Wellstream B502 riser failure analysis report.* ENG/F3/C0/5816.

[66] PALMGREN. A Die Lebensdauer von Kugellagern. *Verfahrenstechinik. Berlin* 1924. Vol. 68, pp. 339–341.

[67] J M ALEXANDER, An Analysis Of The Plastic Bending Of Wide Plate, And The Effect Of Stretching On Transverse Residual Stresses. Engineering Structures.

[68] J F MCNAMARA and A M HARTE, Three Dimensional Analytical Simulation Of Flexible Pipe Wall Structure, Engineering Structures.

[69] WILLIAM R SPILLERS, EDWARD D EICH, ALLAN N GREENWOOD and RUSSELL EATON, A Helical Tape On Cylinder Subjected To Bending, Engineering Structures.

[70] J A GRAHAM, SAE Fatigue Design Handbook, Society of Automotive Engineers, Warrendale, 1986.

[71] API Specification 17J, Specification for Unbounded Flexible Pipe, Second Edition, November 1999.

[72] API Recommended Practice 17B, Recommended Practice for Flexible Pipe, Second Edition, July 1998.